# MODELS OF THE TRAPPE

# RADIATION ENVIRONMENT

## Volume VII: Long Term Time Variations



NATIONAL AERONAUTICS AND SPACE ADMINISTRATION

NASA SP-3024

# MODELS OF THE TRAPPED RADIATION ENVIRONMENT

## Volume VII: Long Term Time Variations

W. L. Imhof, C. O. Bostrom, D. S. Beall
J. C. Armstrong, H. H. Heckman, P. J. Lindstrom,
G. H. Nakano, G. A. Paulikas, and J. B. Blake

*Prepared at NASA Goddard Space Flight Center*

*Scientific and Technical Information Office* 1971
NATIONAL AERONAUTICS AND SPACE ADMINISTRATION
*Washington, D.C.*

For sale by the National Technical Information Service, Springfield, Virginia 22151 — Price $3.00

# PREFACE

During the International Association of Geomagnetism and Aeronomy (IAGA) General Scientific Assembly in Madrid, 1–12 September 1969, Commission V (Solar-Magnetosphere Relations) held a one-and-a-half day Scientific Session on Models of the Earth's Radiation Environment. This was organized by the undersigned at the suggestion of the Chairman of Commission V, Dr. J. G. Roederer. In addition to quantitative models of the radiation environment, long-term time variations and average behavior of magnetospheric particles were emphasized. The following papers were presented by the authors whose names are in italics.

*Imhof, W. L.*: "The Low Altitude Radiation Environment" (invited),

*Bostrom, C. O.*, Beall, D. S., and Armstrong, J. C.: "Time Variations in the Inner Radiation Zone,"

*Rosen, A.* and Sanders, N. L.: "The Temporal Behavior of Inner Zone Electrons During 1965, 1966 and 1967,"

*Heckman, H. H.* and Nakano, G. H.: "Long-Term Behavior of Energetic Inner Belt Protons,"

Filz, R. C. and *Bellew, W. F.*: "Comparison of Trapped Radiation Models with Nuclear Emulsion Measurements at Low Altitudes,"

*Rothwell, P.*: "Energetic Particles and Plasma Inside the Earth's Plasmasphere" (invited),

*Frank, L.*: "Spatial Distributions of Low Energy Protons and Electrons in the Earth's Magnetosphere" (invited),

*Davis, L. R.*: "Spatial and Temporal Characteristics of 100 KeV to 1700 KeV Outerbelt Protons" (invited),

*Webb, V. H.*, Rothwell, P. L., and Katz, L.: "Quiescent and Disturbed Proton and Electron Distributions,"

Sanders, N. L. and *Rosen, A.*: "Study of the Response of $E > 0.3$ MeV and $E > 0.5$ MeV Electrons in the Inner Zone to Magnetic Activity,"

*Vette, J. I.* and Singley, G. W.: "An Outer Zone Electron Model Environment" (invited),

*Paulikas, G. A.* and Blake, J. B.: "The Particle Environment at Synchronous Altitude" (invited),

*White, R. S.*, Wilson, J., Martina, F., and Stevens, J. R.: "Proton Energy Distributions from 0.065 to 3.6 MeV at 6.6 Earth Radii,"

*Pruett, R. G.* and Lucero, A. B.: "The Impact of the Charged Particle Space Radiation Environment on Spacecraft Design and Mission Analysis,"

*Nishida, A.*, Lyon, E. F., and Ness, N. F.: "Plasma Sheet at Lunar Distance,"

*Anderson, K. A.*: "High Energy Particles in the Earth's Magnetotail " (invited),
and
*Masley, A. J.*: "Solar Cosmic Ray Activity Near Sunspot Maximum."

A number of these papers were solicited for publication in this series of Models of the Trapped Radiation Environment because they contained an excellent description of the long-term behavior of several components of the radiation belts. The four papers presented here are the result of that effort. I wish to thank all the contributors to the sessions in Madrid and especially the authors who have provided their manuscripts for publication herein. The Outer Zone Electron Model Environment by G. W. Singley and myself will form the main body of the next volume in this series.

James I. Vette
National Space Science Data Center
Goddard Space Flight Center
Greenbelt, Maryland

CONTENTS

# THE LOW-ALTITUDE RADIATION ENVIRONMENT

W. L. Imhof
Physical Sciences Laboratory
Lockheed Palo Alto Research Laboratory
3251 Hanover Street
Palo Alto, California 94304

## ABSTRACT

Observations of electrons and protons at low altitudes have provided valuable information relating to the source and loss mechanisms of particles trapped in both the inner and outer radiation belts. In the various latitude regions, the radiation environment is quite different in character. At the lower edge of the inner radiation belt the flux gradients of both electrons and protons are typically quite steep and the lifetimes rather short. Accordingly, this region of space has been important for evaluating the cosmic-ray albedo-neutron decay source of trapped protons. Observations of redistributions of trapped electrons associated with magnetic storms and measurements of the long-term decay of the Starfish radiation belt have indicated the occurrence of $L$-shell diffusion. Throughout the inner radiation belt the fluxes of trapped electrons having minimum altitudes below sea level are seen to vary with longitude, indicating the continual action of precipitation processes. In the slot region and the outer radiation belt the rates of buildup with longitude drift of the quasi-trapped electrons have been found to be consistent with the assumption that the dominant loss mechanism for trapped electrons is pitch-angle diffusion. More detailed information on the precipitation mechanisms has been obtained from direct observation of electrons having pitch angles within the loss cone. In the polar-cap regions, low-altitude observations of the incident particle fluxes have revealed a great complexity in the parameters associated with energetic electrons, protons, and alpha particles. The foregoing topics are reviewed with emphasis on the long-term average behavior.


## INTRODUCTION

The low-altitude radiation environment encompasses many regions: the inner and outer radiation belts, the auroral zones, and the polar caps. In any of these regions, at heights up to a few hundred kilometers, the atmosphere strongly influences trapped and precipitating particles. As a result, the spatial flux gradients are often very steep and the trapping lifetimes quite short. These features, when measured in detail, can provide unique clues to the important source and loss mechanisms for particles trapped in the earth's radiation belts. The purpose of this paper is to present some of the more important low-altitude measurements and to attempt to summarize the environment and related geophysical characteristics obtained from these observations. In order to cover the subject with any reasonable degree of completeness, the discussion is restricted primarily to those characteristics related to the higher energy ($\gtrsim$40 keV) electrons and ($\gtrsim$40 MeV) protons, for which more complete data are available than for the lower energy fluxes. Even under such restrictions a complete review of all experiments at low altitudes is clearly not possible within the scope of this paper.

## INNER RADIATION BELT

The distinction between the earth's inner and outer radiation belts (with a slot region in between) is not precisely defined. The change in character with position depends strongly upon the energy and type of particle. A definite slot region exists for MeV electrons but it tends to disappear at lower energies. High-energy protons, on the other hand, exist only in the inner radiation belt. These general features for both electrons and protons are summarized in Figure 1, where the equatorial fluxes are plotted as a function of McIlwain's (1961) $L$-parameter. In order to discuss the low-altitude portion of each of these regions in some logical order, we start with the inner belt, progress outward through the outer belt, and finally consider the polar-cap regions. In starting with the inner belt, much of the initial attention is devoted to what is perhaps the most distinctive low-altitude region of the radiation belts, the South Atlantic anomaly. Here the earth's magnetic field is distorted so that trapped particles dip to the lowest altitude in their longitude drifts around the world.

### Trapped Protons

Much of our knowledge of inner-zone protons has come from measurements performed at relatively low altitudes. Some of the earliest and most significant of these measurements were made with nuclear emulsions carried by recoverable rockets or

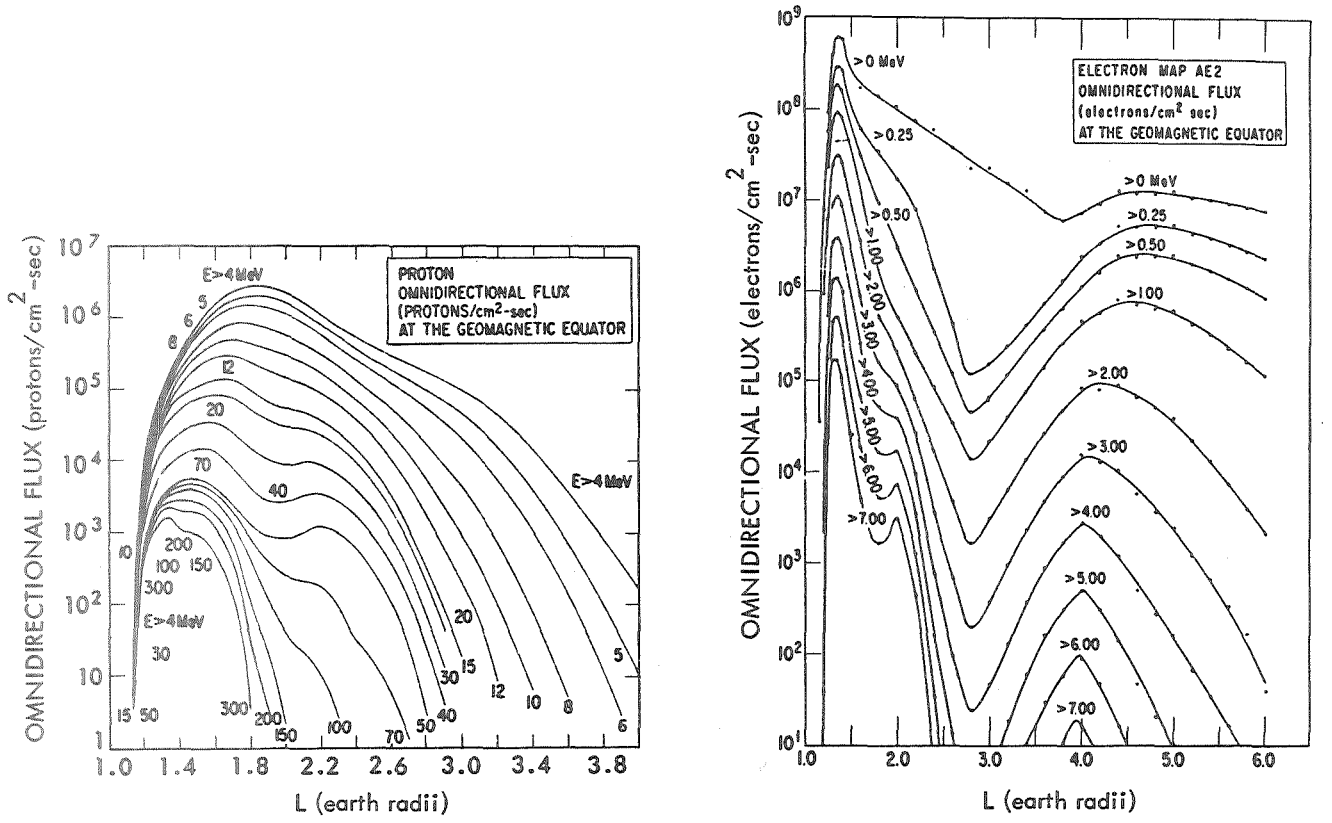


a—Protons.

b—Electrons.

Figure 1—Omnidirectional fluxes of protons and electrons at the equator plotted as a function of $L$ (from Vette, 1966 and Vette, Lucero, and Wright, 1966).

satellites. For example, the first identification of protons in the inner belt resulted from the emulsion experiment of Freden and White (1959). The energy spectra obtained from this and similar flights are shown in Figure 2a. The shape, which agrees rather well with subsequent measurements is consistent with the expectation for injection of trapped protons by the CRAND (cosmic-ray albedo-neutron decay) process. The agreement in spectral shape becomes less valid at lower proton energies, particularly for $L$-shells above about 1.4.

At low altitudes, pronounced changes with solar-cycle period in the energy spectrum of high-energy protons have been predicted by Blanchard and Hess (1964). Thus, one should expect the low-altitude trapped proton environment to be very complex and interesting in regard to spectral and intensity variations. However, as shown in Figure 2b (Heckman and Nakano, 1969), observations have indicated a lack of pronounced time variations (through June 1966) in the proton spectrum, perhaps due to the small atmospheric changes which have taken place during this period.

One of the more dramatic characteristics of the trapped proton environment at low altitudes is the existence of an east-west asymmetry, shown schematically in Figure 3. The asymmetry, first predicted by Lenchek and Singer (1962), arises because (at the point of observation) protons arriving from the east have guiding centers at lower altitudes than those arriving from the west. Conclusive observations of this asymmetry were first reported by Heckman and Nakano (1963). In their experiment protons above 57 MeV were recorded in nuclear emulsions placed on a low-altitude oriented satellite. The angular distributions of protons stopping in an emulsion stack displayed unequal numbers of protons entering from the east and west. This effect has also been observed with emulsions by Filz and Holeman (1965); and with counters by Garmire (1963), Galperin and Temny (1965), and Reagan and Imhof (1969a). Overall, these various observations show general agreement with the assumption that the dominant loss mechanism is atmospheric interactions. However, in detail certain deviations are observed. Heckman and Nakano (1969) have found that the asymmetries differ significantly from calculations for the Harris and Priester model atmosphere. For such comparisons with theory the asymmetry measurements provide information similar to that derived from omnidirectional flux contours, the latter being used more widely. The east-west asymmetry has yet to be measured in great detail as a function of position in space.

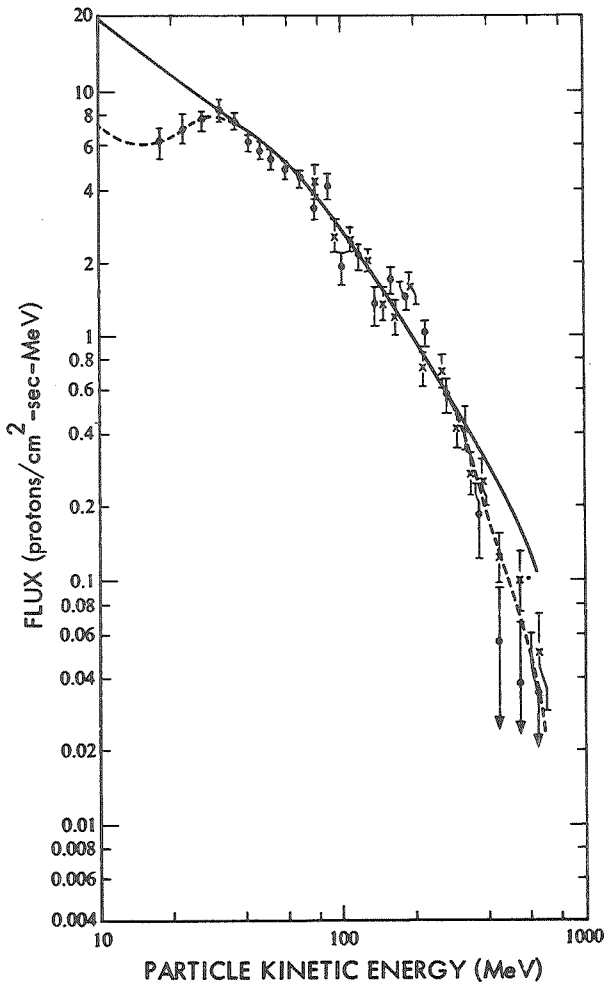


a—The solid curve is a theoretical spectrum expected from cosmic-ray albedo-neutron decay. (Data from Freden and White, 1960.)

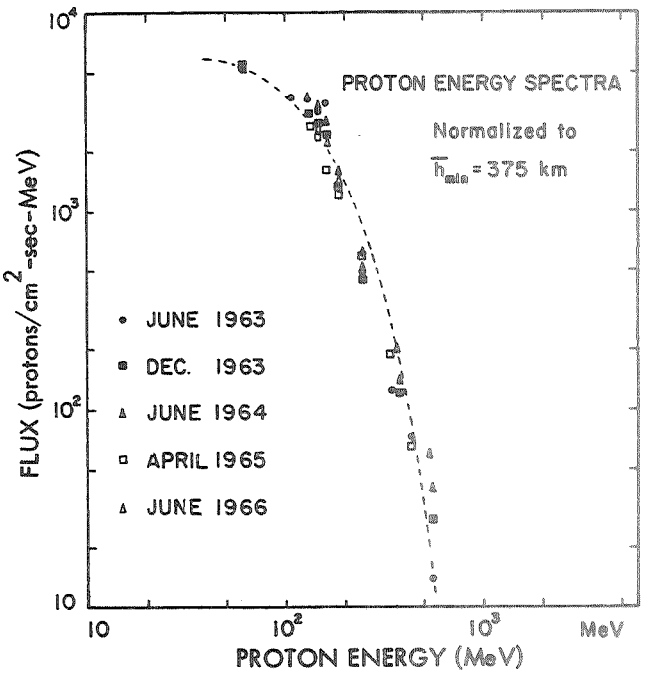


b—(Data from Heckman and Nakano, 1969.)

Figure 2—Energy spectra of inner-zone protons.

The absolute intensities of protons trapped in the inner radiation belt have been compared by several authors (Haerendel, 1964; Hess and Killeen, 1966; Dragt et al., 1966; and Imhof and Reagan, 1969a) with calculations of the CRAND source strength and atmospheric losses. The calculated CRAND source strength appears to be too weak throughout the inner belt by factors ranging from 6.5 to 50. It has been argued that the ideal positions for comparing the measured fluxes with the CRAND expectations are at lower altitudes where any diffusion effects should be small. Accordingly, Dragt et al. (1966) compared their calculated profiles of flux versus $B$ at $L = 1.4$ with low-altitude emulsion measurements performed by Filz and Holeman (1965). As is shown in Figure 4, a discrepancy of a factor of 50 between CRAND and the measured fluxes resulted. In an attempt to reduce further any pitch-angle and/or $L$-shell diffusion contributions, Imhof and Reagan (1969a) have considered the lower edge of the inner radiation belt. At $L \leqslant 1.15$ the slopes of the spatial flux profiles were found to be in reasonable agreement with the predictions of an injection rate nearly independent of position over this narrow region of space and a loss rate due to atmospheric interactions, as shown in Figure 5. However, the measured fluxes were higher by about a factor of 20 than those expected for CRAND.

Effects of atmospheric variations on trapped-proton fluxes have been observed by Nakano and Heckman (1968). Between November 1962 and June 1966, the omnidirectional proton flux at 63 MeV remained constant to within ±7.6%, as shown in Figure 6. Then, between August 1966 and November 1967, the proton flux decreased by about a factor of two. A drop in flux at this time in the solar cycle was predicted by Blanchard and Hess (1964), but a much larger decrease was expected. However, this

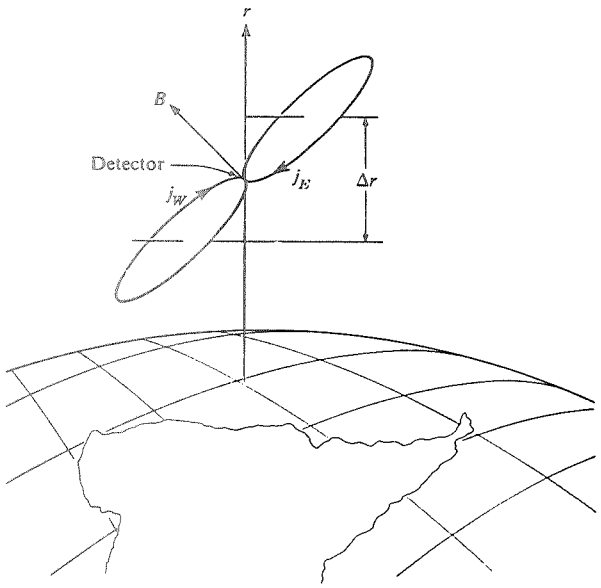


Figure 3—Schematic representation of the east-west asymmetry. Due to the atmospheric density gradient, the fluxes of protons traveling toward the west are lower than those traveling toward the east (Heckman and Jakano, 1965).

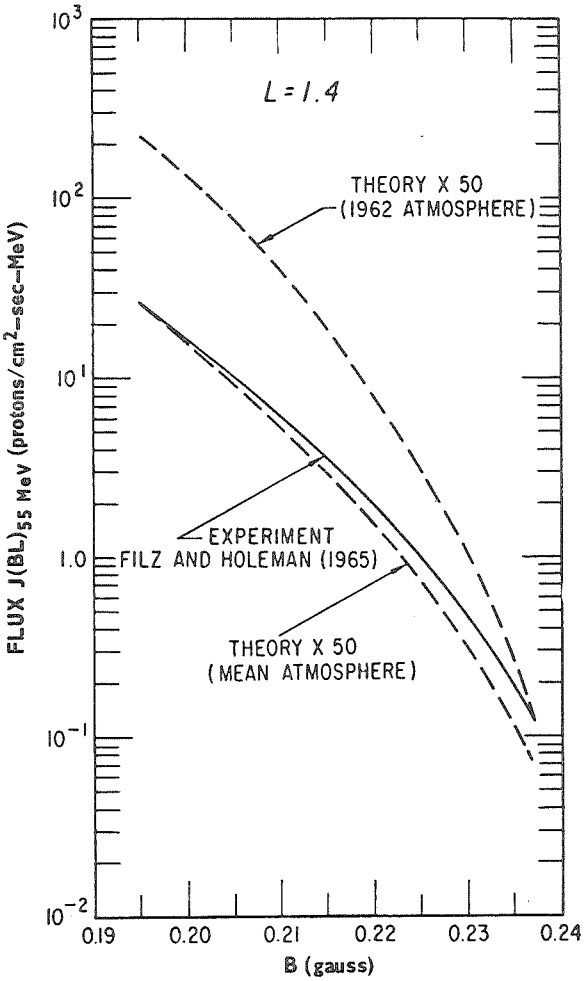


Figure 4—Comparison of the proton fluxes measured by Filz and Holeman with the calculated fluxes for cosmic-ray albedo-neutron decay (Dragt et al., 1966).

apparent discrepancy may not be significant since the actual solar-cycle variations of the 10.7-cm flux have been considerably less than those used in the calculations of Blanchard and Hess. Equatorial fluxes of protons were measured over the range $1.15 \leqslant L \leqslant 1.21$ by Achtermann et al. (1969). Their measured profiles of flux versus $L$ displayed variations at different proton energies, and hence different lifetimes, which they attribute to changes in the atmosphere shortly before the flight on June 17, 1967.

Many of the fundamental questions relating to the sources of protons in the inner belt and possible redistribution mechanisms are more properly considered elsewhere. Here some of the effects unique to the low-altitude regions have been outlined. Several classes of experiments have shown the dominance of atmospheric effects. The east-west asymmetry, the spatial flux profiles, and the variations of the trapped-proton fluxes with periods in the solar cycle are generally consistent with the assumption that the loss rate is determined by atmospheric collisions. However, significant deviations have been observed. Perhaps more serious discrepancies exist in the absolute fluxes; even at the lower edge of the inner radiation belt the intensities of high-energy protons are much larger than predicted for the CRAND source mechanism.

## Trapped Electrons

Very few measurements of electrons in the inner radiation belt were made before the artificial injection of electrons by the Starfish nuclear detonation on July 9, 1962. In particular, the energy spectrum was not well established. The available pre-Starfish electron spectrum measurements, as illustrated in Figure 7, display a large degree of inconsistency. Intensity profiles are available only for limited spatial regions. It is clear that our knowledge of the naturally trapped electrons in the inner belt will remain meager until the Starfish electrons no longer dominate. Fortunately, the emergence of the natural electron belt may be just around the corner; recent experiments have indicated the appearance of naturally trapped electrons in the inner belt (Marbach et al., 1968); Pfitzer and Winckler, 1968; and Vampola, 1968). But at present our knowledge of the behavior of electrons in the inner belt is derived mostly from measurements of Starfish electrons.

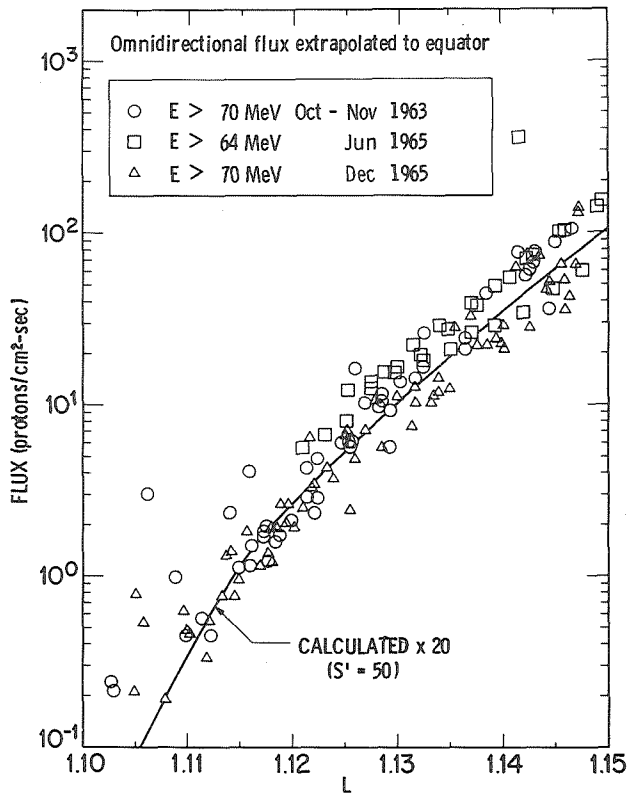


Figure 5—Equatorial omnidirectional fluxes plotted as a function of $L$. The points represent measured values with $h_{min} >$ 150 km normalized to the equator on the basis of the calculated flux variations with $B$. The curve represents the fluxes calculated for the CRAND source strength arbitrarily increased by a factor of 20 (Imhof and Reagan, 1969a).

The sudden injection of many electrons from the Starfish detonation presented a unique opportunity to measure trapping lifetimes. The early lifetime observations performed on Injun 1 (Van Allen, 1963) and Explorer 15 (McIlwain, 1963) have been compared with those calculated by Walt (1964) for losses of electrons due to collisions with atmospheric constituents. For $L \gtrsim 1.25$, the measured lifetimes were considerably shorter than the theoretical values, suggesting the dominance of other loss processes. However, as is shown in Figure 8, for $L \lesssim 1.25$ there was good agreement between theory and experiment, indicating that atmospheric scattering is the dominant loss mechanism in this region of space. The lifetime measurements were extended down to an $L$-value of 1.145 by Imhof and Smith (1966). They observed the decay of electron intensities following two different energy-selective redistributions of electrons at 1.34 and 0.74 MeV. Each of the two groups of electrons decayed at a rate that was in agreement with the atmospheric scattering calculations of Walt.

During a somewhat later period (October 1963 through December 1965) the decay of the Starfish radiation belt at low altitudes was followed in detail with instruments aboard the satellite 1963 38C (Beall et al., 1967). The long-term averages displayed a systematic dependence on energy, time, and position, which for $L \approx 1.25$ was in general agreement with Walt's calculations at relatively early times when a $B$-dependence in decay rate was expected. However, the observed decrease in lifetime with increasing $B$ was relatively weak. Despite the overall average agreement with atmospheric scattering calculations, the observed decay was somewhat irregular; significant short-term variations in the decay constant were observed.

Electrons trapped on low $L$-shells have been observed to undergo significant variations in intensity. Measurements from the Pegasus 1 satellite (Rosen et al., 1968) in 1965 revealed an

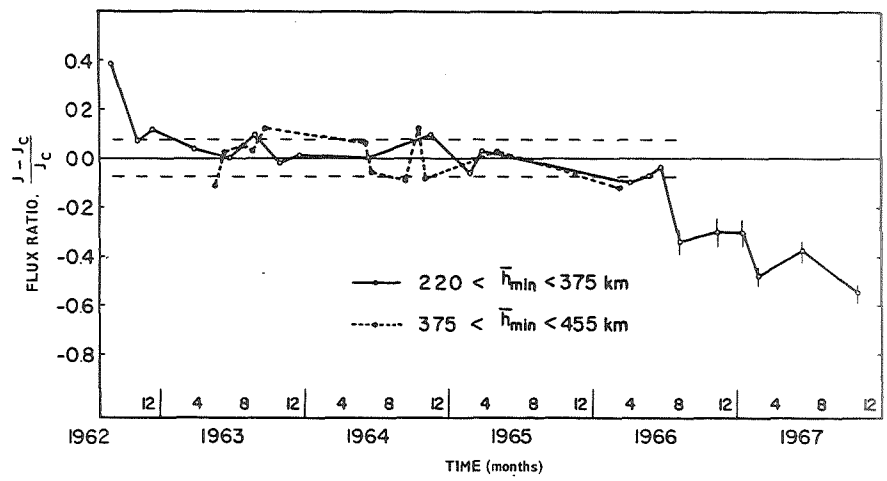


Figure 6—Time behavior of the proton flux between September 1962 and November 1967. The fractional deviations are plotted as a function of time for $220 < h_{min} < 375$ km and $375 < h_{min} < 455$ km (Nakano and Heckman, 1968).

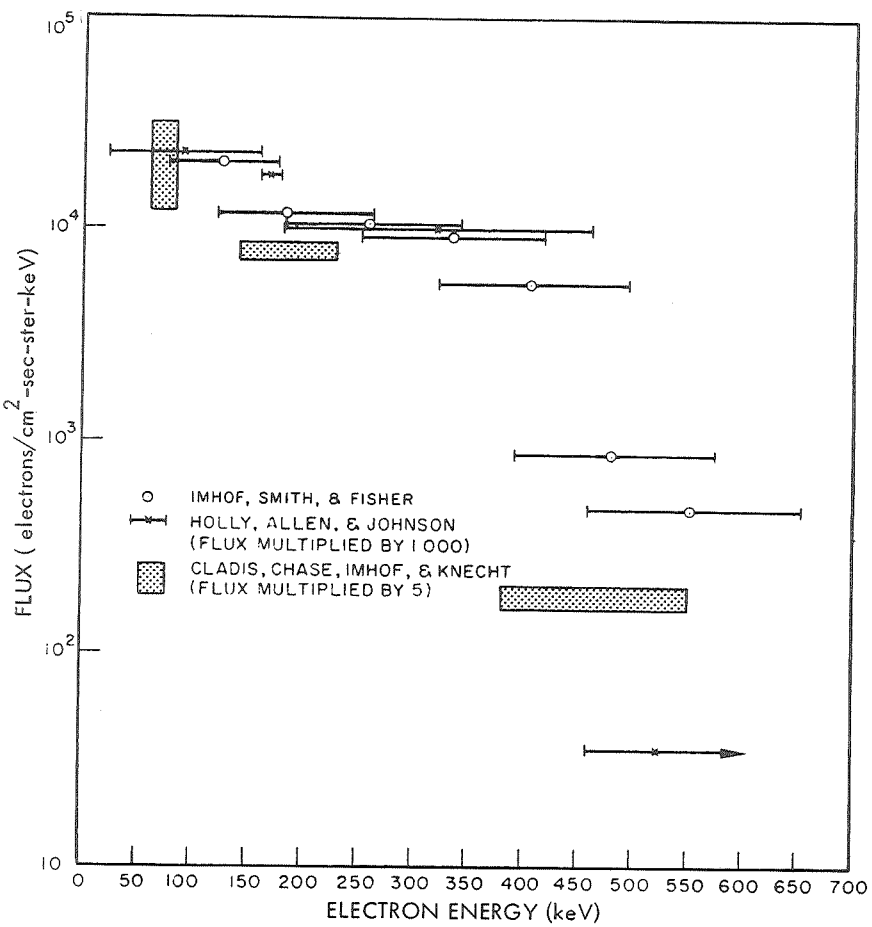


Figure 7—Pre-Starfish electron energy spectra (Imhof et al., 1963).

enhancement of 0.5-MeV electron fluxes at $L$-shells less than 1.2. This enhancement was related to, but not clearly correlated with, magnetic activity. Measurements on a polar-orbiting satellite with an instrument having high-energy resolution and sensitivity have shown, on two different occasions, the appearance of nearly monoenergetic groups of electrons (Imhof and Smith, 1965b and 1966) on low $L$-shells. One of the sets of observations is illustrated in Figure 9. Data from the satellite measurements and from ground magnetogram records suggest that the observed onset of nearly monoenergetic electrons was the result of a redistribution of electrons trapped on somewhat higher $L$-shells (Imhof et al., 1966). The responsible mechanism has been explored by Cladis (1966). He has suggested that the electrons were accelerated by fluctuations in the intensity of the equatorial electrojet that had periods comparable to the azimuthal drift periods of the electrons. The energies imparted to the electrons were small but sufficient to account for the observed redistributions. For this acceleration mechanism the energy spectra computed by Cladis were in good agreement with the measurements.

It is evident that in the absence of any sources of new electrons the lower $L$-shells should eventually become completely vacated due to atmospheric scattering. However, measurements (Imhof et al., 1967 and Rosen et al., 1968) have indicated that three years after Starfish, electrons were still trapped on $L$-shells $\leqslant 1.18$. The persistence of trapped electrons at the lower edge of the inner radiation belt has been interpreted by Newkirk and Walt (1968) in terms of diffusion across $L$-shells. Empirical values for the diffusion coefficients at low $L$-shells have been obtained by Newkirk and Walt (1968) and by Farley (1969a and b). Both of these calculations were based on the measured radial-flux profiles and long-term decay rates. The values of the diffusion coefficients were found to increase monotonically with decreasing $L$, a trend which is opposite to the variation of diffusion rates higher in the magnetosphere. The physical interpretation of this unique characteristic of the very low $L$-shell region is still an open question.

From the collection of observations at low $L$-shells, it appears that the trapping lifetimes at $L \leqslant 1.25$ are consistent with the assumption that the dominant loss mechanism is atmospheric scattering. On much higher $L$-shells, clearly other loss mechanisms

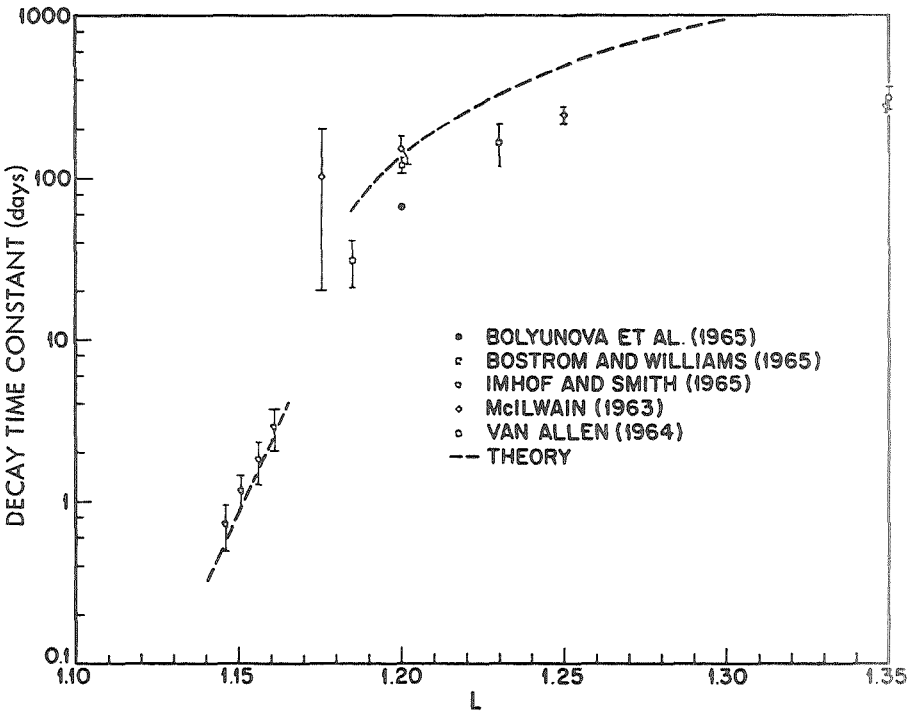


Figure 8—Electron decay rate as a function of $L$. The time constant is the time required for the electron flux to decrease by a factor of $1/e$. The theoretical curve for $L = 1.185$ was calculated for an initial fission energy spectrum; the theoretical curve near $L = 1.15$, for a nearly monoenergetic group of electrons at 1.3 MeV (Walt, 1966).

are dominant. On very low $L$-shells the behavior of the electrons is rather complex. Atmospheric scattering appears to dominate at times but other perturbing effects play an important role. Significant redistributions have been reported at times of magnetic disturbances. Overall, there appears to be a significant radial movement of electrons from one $L$-shell to another.

One of the outstanding features unique to the low-altitude environment is the existence of electrons with mirror points at positions where the longitude trace dips to an altitude below sea level. Such electrons may appear to be trapped, but are doomed to precipitate into the atmosphere as a result of their longitude drift. Accordingly, these fluxes of quasi-trapped electrons mirroring at a given $B$-, $L$-value are seen to display pronounced variations with longitude. The combination of the flux buildup with longitude drift and the subsequent dumping is often referred to as the windshield-wiper effect. This phenomenon has been reported over a very wide range of $L$-values (Paulikas and Freden, 1964; Imhof and Smith, 1965a; Vernov et al., 1965; Williams and Kohl, 1965; Blake et al., 1966; Rosen et al., 1968; and Imhof, 1968). As an illustrative example, the fluxes of electrons above 50 keV measured by Vernov et al. (1965) on Cosmos 17 in mid-1963 are shown in Figure 10. On various $L$-shells the intensities are plotted as a function of $h_{min}$. As might be expected for electrons drifting eastward, the fluxes are greater to the west of the Brazilian anomaly than to the east. The appearance of particles at low values of $h_{min}$ appears to be more prevalent for electrons than protons; however, Vernov et al. (1966) have reported a longitude dependence of protons on magnetic shells $L = 1.2$ to 1.4 in the region of the South Atlantic anomaly.

It can be seen from Figure 10 that in the inner belt the fluxes fall off very rapidly with decreasing $h_{min}$ in the vicinity of $h_{min} \approx 100$ km. Whereas the electrons at $h_{min} \approx 100$ km may represent an appreciable fraction of those being lost by atmospheric scattering from the belt, the intensities at $h_{min} \leqslant 0$ km are considerably lower. It has been shown (Imhof and Smith, 1965a) that in late 1963 on a given $L$-shell in the inner belt, the buildup and subsequent precipitation of electrons at $h_{min} < 0$ km can be sustained by an influx considerably less than the total loss rate of trapped electrons from that shell. Consequently, the fluxes appearing at high $B$-values may be associated with a small effect which is perhaps not representative of the primary loss mechanism(s). Atmospheric scattering calculations by Roederer et al. (1967) for low $L$-shells have shown that multiple coulomb scattering can account for the electron fluxes observed at $h_{min} \gtrsim 0$ km, but that an additional mechanism is needed to explain the fluxes observed at $h_{min} < 0$ km.

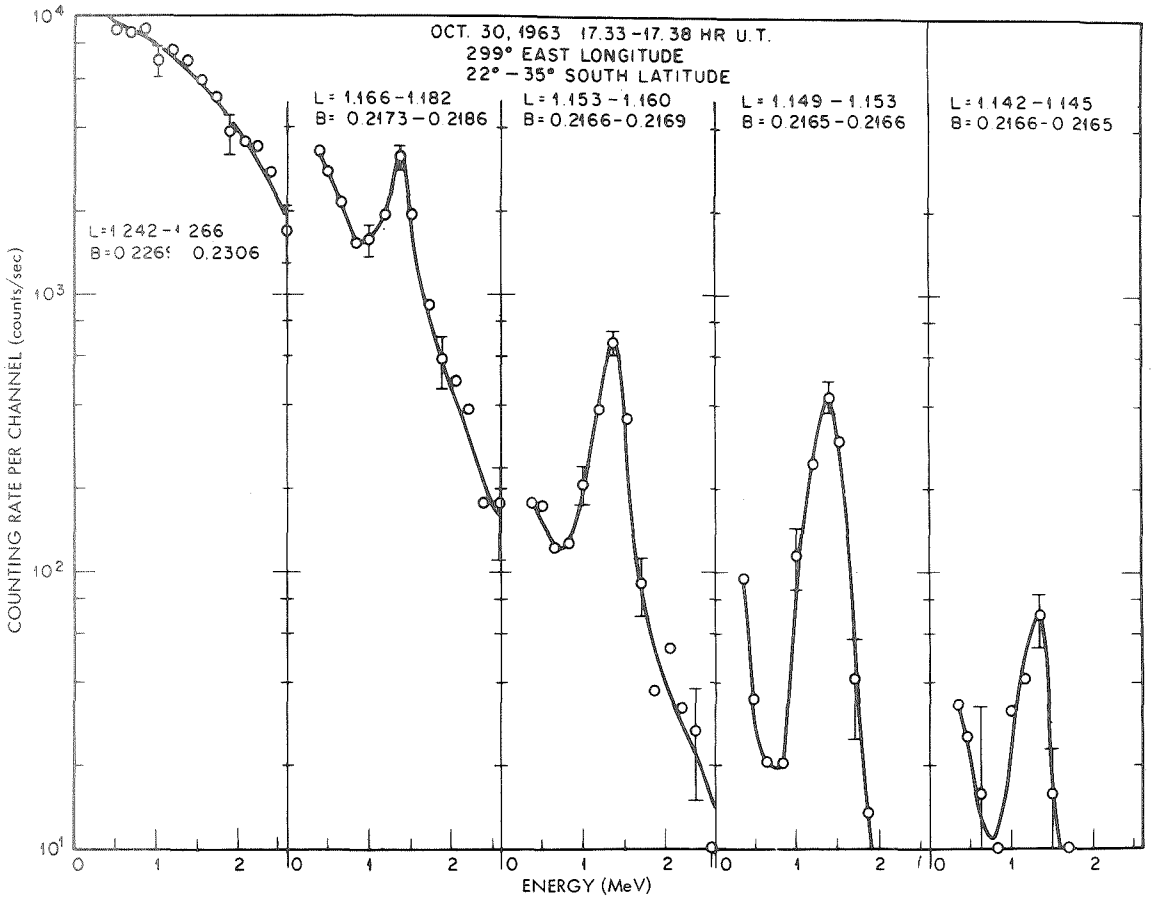


Figure 9—Output of an electron spectrometer on different $L$-shells for one pass through the South Atlantic anomaly (Imhof and Smith, 1965b).

Various processes have been suggested to account for the electrons observed at minimum altitudes below sea level, but for any of these mechanisms detailed comparisons between theory and experiment are still lacking. On the basis of the intensities measured in September 1962 and in October to November 1963, it has been suggested (Imhof and Smith, 1965a) that inner-belt electrons at $h_{min} < 0$ km originate from the trapped-radiation belt. An important redistribution process was postulated to be single large-angle coulomb scatterings in the atmosphere. Such scatterings surely occur, but more extensive calculations and comparisons with the measured intensities and longitude variations are needed to firmly establish the importance of this process. Other non-atmospheric precipitation mechanisms have been suggested, particularly to account for the high-$B$ fluxes in the slot region and outer belt where the atmosphere clearly cannot play an important role. The scattering of trapped electrons by whistlers was first investigated by Dungey (1963) and by Cornwall (1964). Cornwall calculated that the conditions for a resonance interaction lead to a pronounced dependence on $L$, the maximum interactions occurring near $L = 1.2$ and $L = 2$. Subsequently, Roberts (1968) has performed calculations to support the suggestion of a dual mechanism to account for the precipitation of trapped electrons. He proposed that bounce-resonant scattering accounts for the pitch-angle diffusion of electrons mirroring near the equator, whereas those mirroring at lower altitudes are perturbed by cyclotron-resonant scattering. Insufficient data, particularly on the magnetic and electric field fluctuations in the magnetosphere are presently available to evaluate definitively this dual mechanism.

## OUTER RADIATION BELT

Many satellite measurements of electrons in the outer radiation belt have been made at low altitudes. Perhaps one of the most notable sets of measurements in regard to long-term coverage has been performed from 1963 38C (October 1963 to present). In this paper, processes such as precipitation phenomena that are more characteristic of the low-altitude regions are emphasized.

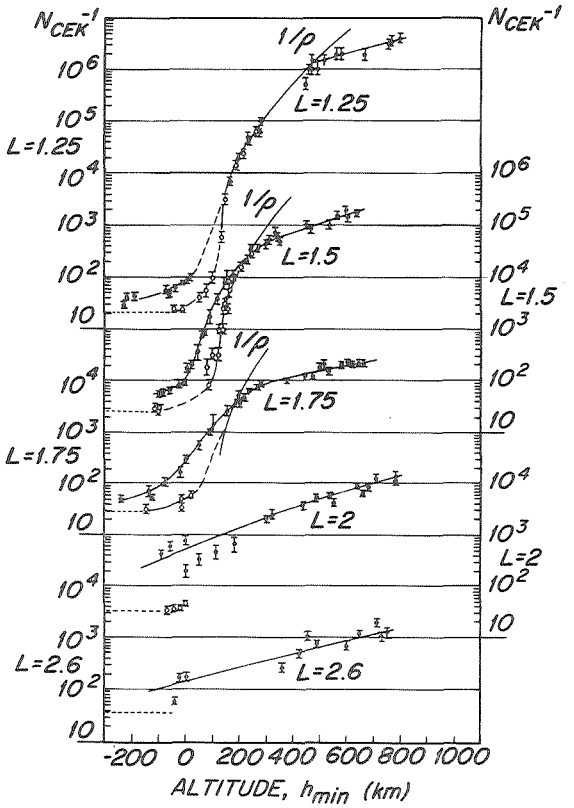


Figure 10—Intensities on various magnetic shells plotted as a function of minimum altitude of the mirror points. The open circles represent measurements performed at positions east of the South Atlantic anomaly (Vernov et al., 1965).

As already mentioned in the discussion on the inner radiation belt, quasi-trapped electrons doomed to precipitate upon drift in longitude have been regularly observed throughout the radiation belts. Paulikas et al. (1966) have noted that such electrons appear in three broad peaks in $L \sim 1.5$, $\sim 2.5$, and 4 to 7. In the slot region and the outer belt, the character of the electron precipitation is in distinct contrast to that measured in the inner belt. On low $L$-shells significant fluxes of electrons at low altitudes are generally limited to the immediate vicinity of the South Atlantic anomaly. On the other hand, in the outer belt appreciable fluxes of precipitating electrons are observed to exist on a worldwide basis (Paulikas and Freden, 1964 and Imhof, 1968), as is shown in Figure 11. In the inner belt the energy spectrum of electrons with $h_{min} < 0$ km has been observed to be much softer than that of the more stably trapped electrons. However, in the outer belt the spectra display only minor variations, with $h_{min}$ being somewhat softer for the precipitating electrons (Imhof, 1968). In the inner belt the intensities of the quasi-trapped electrons at any given region of space have been observed to be reasonably steady. Williams and Kohl (1965) have noted in the inner-belt and slot regions that a relatively stable longitudinal intensity distribution exists during periods of magnetic quiet. However, significant fluctuations have been observed in the slot and outer-belt regions (Paulikas and Freden, 1964 and Imhof et al., 1969). Despite the scatter in fluxes of precipitating electrons, both the findings of Williams and Kohl (1965) and of Imhof (1968) have indicated a general flux buildup with eastward drift in longitude.

To date, studies of the flux variations with longitude have been quite limited in number and scope. From a series of flux measurements at several longitudes in the northern hemisphere, Williams and Kohl (1965) concluded that for $1.45 \leq L \leq 2.8$ electrons are injected into the depleted regions at all longitudes. They also obtained measurements of the fractional electron transmission through the South Atlantic anomaly as a function of $h_{min}$. The transmissions were found to be 100% for electrons with $h_{min} \geq 350$ km, about 10% for $h_{min} = 100 \rightarrow 250$ km, and 0% for $h_{min} \leq 100$ km.

The buildup of electron flux with longitude drift has been investigated with data taken in 1963 on a polar-orbiting satellite that had complete worldwide coverage through use of an onboard tape recorder (Imhof, 1968). The longitude variations of the intensities and spectra were found to be consistent with a continual buildup and, in the outer-belt regions, with the rapid achievement of a state of near equilibrium. The rates of flux buildup were compared with calculations of pitch-angle diffusion, yielding empirical values for the diffusion coefficients. These coefficients were found to vary by only a factor of four over a rather wide range of magnetic latitudes covering the outer radiation belt and slot regions. The diffusion coefficients were also found to be consistent with the assumption that the dominant loss mechanism for trapped electrons is pitch-angle diffusion. Pitch-angle diffusion coefficients for electrons in the outer belt have also been obtained (Theodoridis and Paolini, 1967) by measuring the pitch-angle distribution near and within the loss cone. The diffusion coefficients derived by this method were considerably larger than those obtained by Imhof from the buildup of the trapped flux with longitude drift.

The observations of electrons in the loss cone are most conveniently performed at low altitudes since here the loss cone is relatively large. Some of the earliest detailed studies of the precipitation of electrons at high latitudes were performed with instruments onboard the satellites Injun 1 and Injun 3 by O'Brien (1964). He studied in detail the variations in the intensities of the trapped and precipitating electrons above 40 keV. During precipitation events, the angular distributions tended to approach isotropy over the upper hemisphere, as is illustrated in Figure 12. Strong energy dependences were observed. O'Brien found that electrons $\geq 1$ MeV can be trapped and unperturbed on a field line along which fresh electrons are being precipitated with energies above 40 keV.

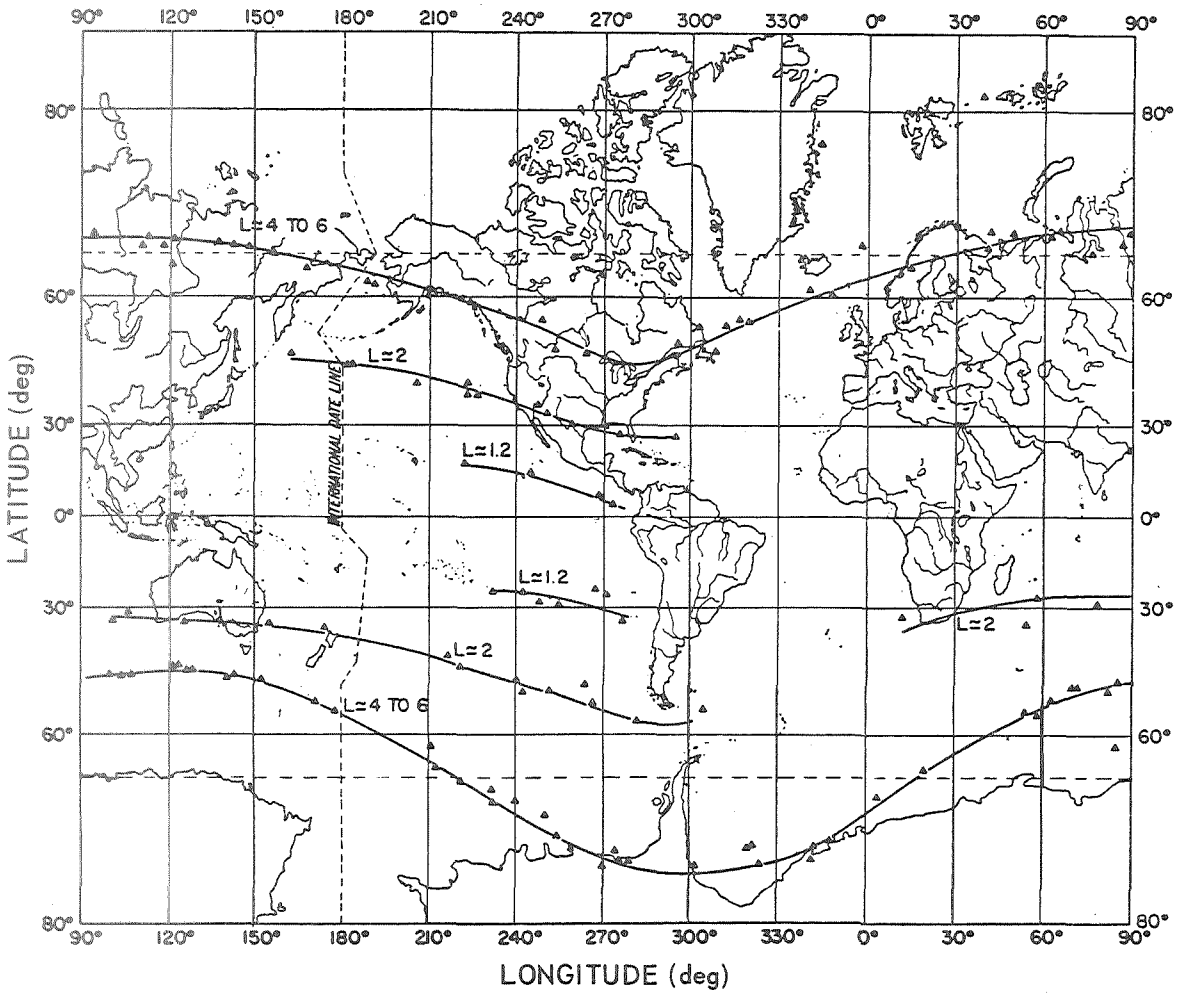


Figure 11—Locus of peaks of electron flux above 0.9 MeV for September 1962 as observed at altitudes of 300 to 690 km. Measurements near the center of the South Atlantic anomaly are not included (Paulikas and Freden, 1964).

Further evidence for the tendency to favor the precipitation of low-energy electrons has come from the observations of Mozer (1968). From high-energy (>65 keV) electron measurements on rockets flown into auroras at times near local midnight, Mozer found that the variations were generally greatest for electrons with energies between 65 and 200 keV. However, fluctuations occasionally occurred exclusively in the electrons above 400 keV. During five well-defined magnetic storms, Williams et al. (1968) compared simultaneous flux measurements of electrons at low altitudes and in near-equatorial regions, as is shown in Figure 13. The behavior of electrons of about 300-keV, mirroring near the equator and at low altitudes is very similar; the ≥300-keV electron intensities on a given $L$-shell generally come quickly to equilibrium. On the other hand, for electrons ≥1-MeV such a rapid attainment of equilibrium is not achieved, suggesting that the mechanisms of major importance in pitch-angle diffusion apparently act more effectively for electrons ≥300-keV.

Energy dependences of the overall loss rates of trapped electrons can be obtained from the measured time variations in the intensities of the trapped population. Vernov et al. (1969) have concluded from all available measurements that in the 40- to 500-keV energy range the lifetime depends little on energy, but that above 500 keV it increases rapidly with increasing energy. From all of these classes of experiments one concludes that on the average low-energy electrons precipitate at a somewhat greater rate.

The foregoing evidence for some energy selectivity in the precipitation of electrons leads to the interesting considerations of the existence at high latitudes of nearly monoenergetic groups of electrons, as observed at the lower edge of the inner radiation belt. Observations show that the lower energy auroral electrons do display monoenergetic groups. McIlwain (1960) first suggested the presence of a monoenergetic peak at about 6 keV in interpreting some of his auroral zone measurements. More recently, nearly monoenergetic groups of electrons at a few keV have been observed by Evans (1968), Albert (1967a and b), and by Westerlund

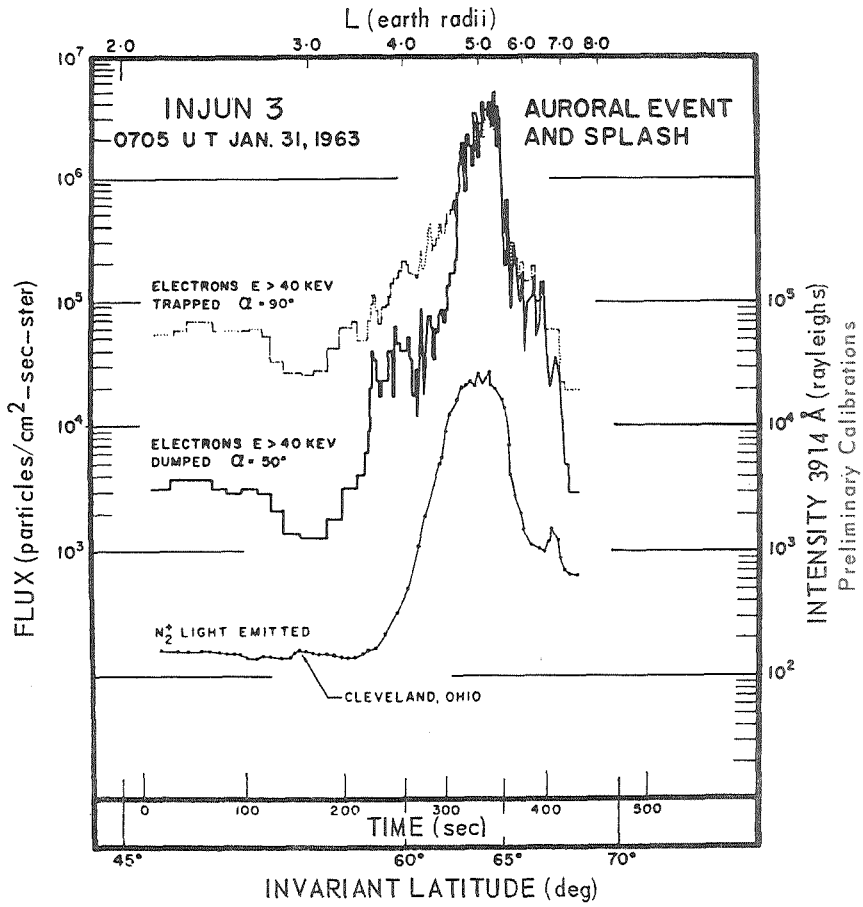


Figure 12—Fluxes of trapped and precipitating electrons plotted as a function of invariant latitude for one pass. The outputs of a photometer onboard the satellite are also shown (O'Brien, 1964).

(1969). High-altitude observations in the slot region of spectra peaked at energies of several hundred keV have been reported by West (1969).

Overall, the measurements of high-energy electrons at high latitudes have been rather limited in spatial and temporal coverage, sensitivity, and in energy and angular resolution. These deficiencies can be attributed to the need for fast-time resolution and to the relatively low flux levels present. Greater intensities are generally present at lower energies, but until recently the much greater experimental difficulties associated with measuring low-energy particles have severely limited the coverage. Now with significant advances in experimental techniques, this situation has changed somewhat, but there still exist very few systematic studies of the overall morphology as measured from satellites. These measurements are summarized in recent review articles (Sharp and Johnson, 1968 and Johnson and Sharp, 1969).

Some of the most interesting and important features of the low-altitude radiation environment involve the outer trapping boundary. Several studies of the high-latitude boundary have revealed the complexities of this region. The boundary is not only dependent upon various parameters such as the local magnetic time and the magnetic activity, but at any one time its location is strongly dependent upon the precise definition being used. Perhaps the simplest definition of a boundary in terms of data analysis is the position at which a given detector reaches a specified counting rate. Such a prescription is convenient for long-term studies with a given set of instruments but is clearly dependent upon the response of the detector and does not necessarily correspond to a sudden change in the physical character of the radiation environment.

Williams and Mead (1965) have studied diurnal variations of the electron-trapping boundary using absolute electron intensities as a latitude criterion. The diurnal variations of the boundaries for electrons above 280 keV and above 1.2 MeV were found to be similar and consistent with the drift of the particles through a distorted magnetosphere. By comparing the calculations with

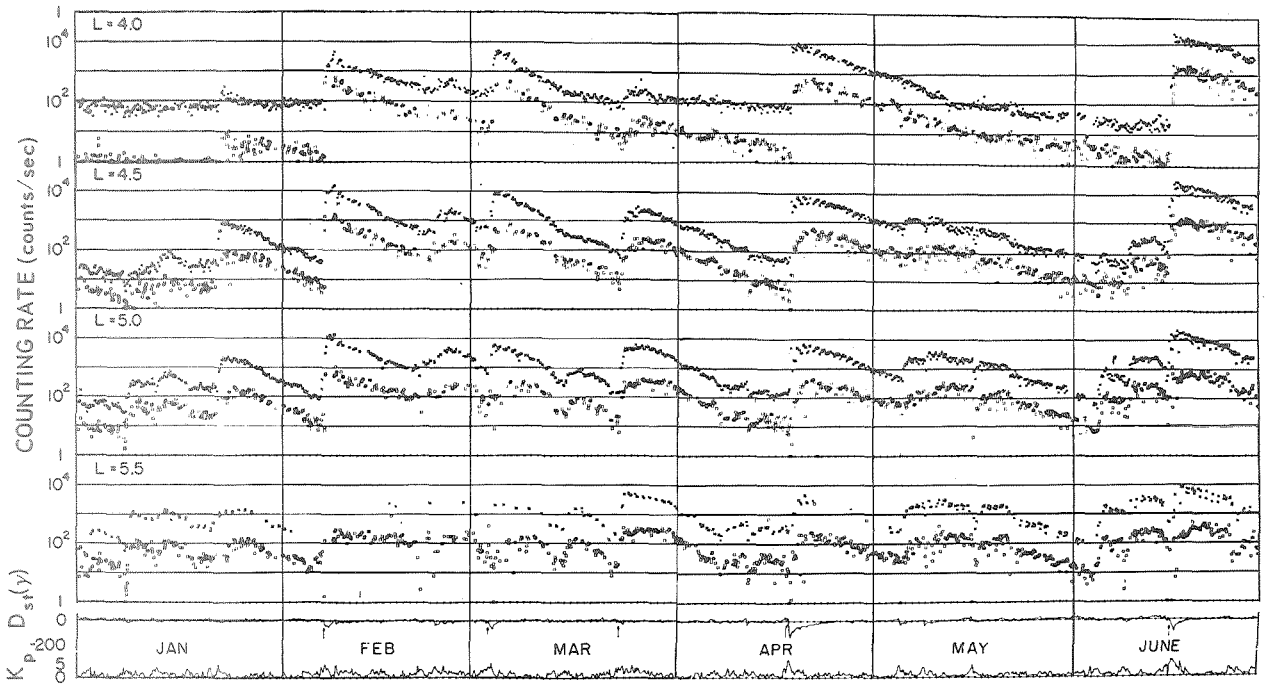


a—Electrons above 280 keV and 300 keV for the low- and high-altitude satellites, respectively.

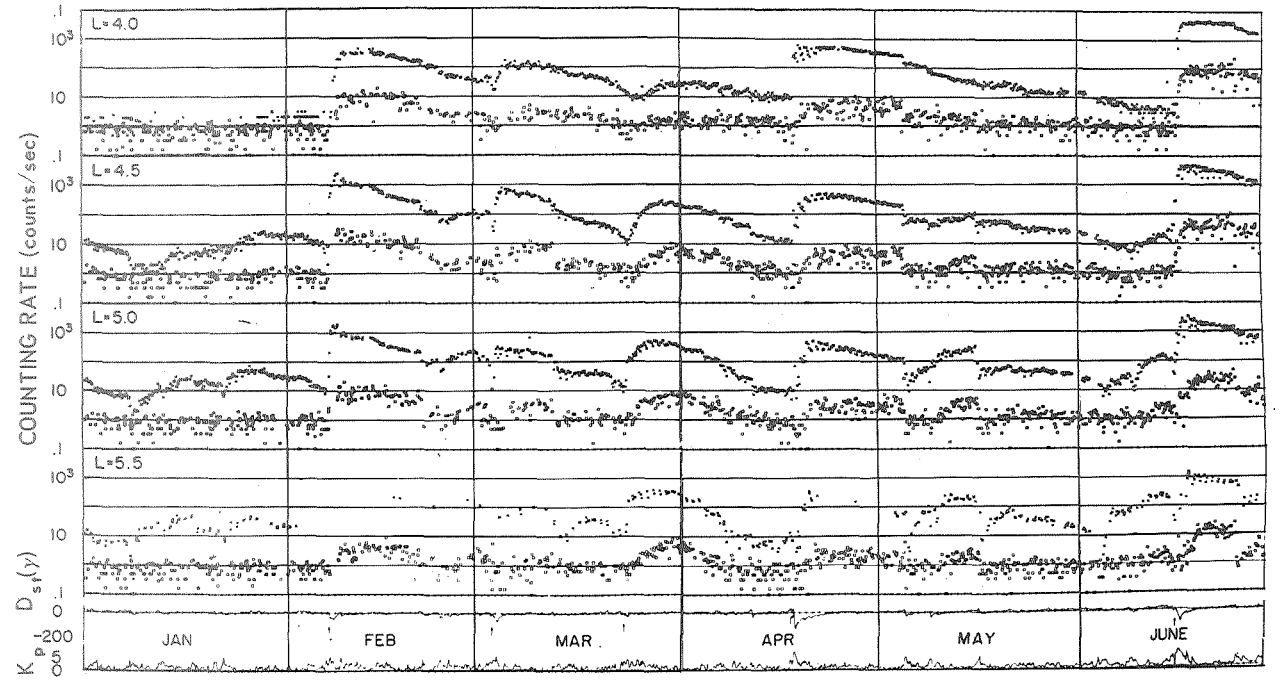


b—Electrons above 1.2 MeV and 1.0 MeV for the low- and high-altitude satellites, respectively.

Figure 13—Simultaneous electron data from the low-altitude polar-orbiting satellite 1963 38C, denoted by □, and the near-equatorial satellite Explorer 26, denoted by *X* (Williams et al., 1968).

experiment they obtained an empirical nightside magnetic field configuration. From comparisons with similar measurements of electrons >40-keV by Frank et al. (1964), they found that the midnight boundaries were nearly independent of electron energy but that the dayside boundary for the low-energy electrons extended to significantly higher latitudes than was the case for the higher energy electrons. Williams and Mead interpreted the larger diurnal shifts for electrons >40-keV to imply a daytime source mechanism. More recently, Taylor (1966) has accounted for the differences in daytime latitudes of the boundaries >40-keV and >280-keV by invoking magnetospheric electric fields.

With data acquired on the Alouette 2 satellite the Canadian group has examined a variety of high-latitude boundaries (Burrows and McDiarmid, 1968 and McDiarmid and Burrows, 1968). Each of these boundaries is defined in terms of the absolute counting rates of a 35-keV detector or a 3.9-MeV counter, or in terms of the marked change in character usually observed at the outer edge, or by the requirement that the flux change by more than a decade in a latitude interval of less than 0.5°. These four boundaries are plotted in Figure 14 as a function of local magnetic time. Physical interpretations have been given for the various boundaries. For example, comparisons with the auroral oval as given by Feldstein (1969) have shown that the boundary of the auroral oval coincides rather well with the so-called smooth boundary of Burrows and McDiarmid.

A more sophisticated boundary definition has been used by Fritz (1968) in his analysis of Injun 3 data. His boundary is based on the degree of isotropy in the fluxes of electrons above 40 keV as measured with two detectors, one parallel to and one perpendicular to the local magnetic field line. The boundary between the high-latitude occurrence of isotropy and the lower latitude region of anisotropy was usually sharply defined at local night but was rather broad or nonexistent at local afternoon during days of little geomagnetic activity. Fritz's isotropic boundary was found to be in rather good agreement with the smooth boundary of McDiarmid and Burrows. The measurements of both McDiarmid and Burrows and of Fritz have indicated a narrow spike in the electron flux associated with the sharp boundary on the nightside. As the measurements of Imhof et al. (1969) indicate, the energy spectrum associated with this spike may be much softer than that of electrons at slightly lower latitudes. Burrows and McDiarmid point out that the spike seems to represent an unstable region inside the nighttime sharp boundary.

## POLAR-CAP REGIONS

Satellite-borne observations of solar protons at low altitudes over the earth's polar caps have been reported by several groups of experimenters (Pieper et al., 1962; Akasofu et al., 1963; Stone, 1964 and 1969; Krimigis and Van Allen, 1967; Bostrom et al.,

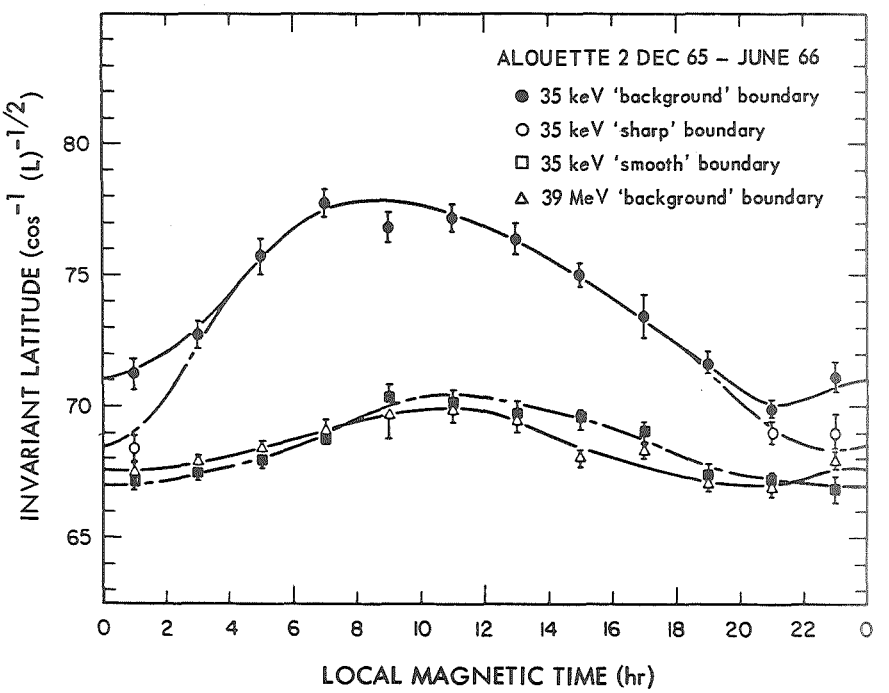


Figure 14—A comparison of different outer radiation zone boundaries, as measured from Alouette 2 satellite (Burrows and McDiarmid, 1968).

1967; Paulikas et al., 1968; Blake et al., 1968; Katz and Rothwell, 1968; and Williams and Bostrom, 1969). Examples of energy spectra and intensities (Paulikas et al., 1968 and Reagan and Imhof, 1969b) for the precipitating protons are shown in Figure 15.

For several years it has been known that the latitudes of magnetic cutoff for solar protons deviate significantly from the predictions of Stormer for a dipole field. Pieper et al. (1962) noted that the cutoff geomagnetic latitudes were of the order of 61° during the prestorm period; during the main phase of the storm the protons were detectable down to latitudes as low as 53° or to an $L$-value of 3.0. Even the higher of these cutoff latitudes is lower than that of the classical Stormer theory. Stone (1964) observed 1.5-MeV protons over the polar caps during a geomagnetically quiet period. The cutoff latitudes were 65° and 67° on the night and day sides, respectively, compared with a theoretical Stormer cutoff of 76°. Paulikas et al. (1968) have similarly observed lower latitude cutoffs than those predicted by Stormer. As is shown in Figure 16, the nightside cutoffs for protons of various energies in the 1 to 100-MeV interval were at lower latitudes than calculated for a dipole field and in rather good agreement with the calculations of Reid and Sauer (1967) for a magnetic field model with the permanent existence of a geomagnetic tail.

Solar protons have been observed to display pronounced spatial/temporal variations in flux over the polar caps (Reid and Sauer, 1967; Williams and Bostrom, 1967 and Blake et al., 1968). This latitude structure greatly complicates the description of a given solar-flare event. As pointed out by Blake et al., a polar-cap average may not be an easily interpretable quantity.

The simultaneous observations of solar particles from a low-altitude satellite in one of the polar regions and from a spacecraft in interplanetary space have been reported in several instances. Simultaneous observations have involved Explorer 7 and Pioneer 5, Injun 1 and Explorer 12, Mariner 4 and Injun 4, and Injun 4 and Explorer 33. In the latter set of measurements performed on the satellites Injun 4 and Explorer 33, located inside and outside the magnetosphere, respectively, Krimigis et al. (1967) found that 0.5-MeV solar protons have access to the polar caps with a delay of 0.5 hour or less, as shown in Figure 17. These results were interpreted in terms of an open magnetospheric model with essentially immediate access from interplanetary space to the polar caps of the earth. Williams and Bostrom (1969) have reported general similarities between the flux-time profiles from Explorer 33 and from the low-altitude satellite 1963 38C, but have noted that significant differences in their time histories did occur. They have interpreted their observations in terms of the low-energy proton access to the polar caps being controlled by a diffusion process. North-south asymmetries in the access of protons have been reported. Perhaps the most pronounced is the event

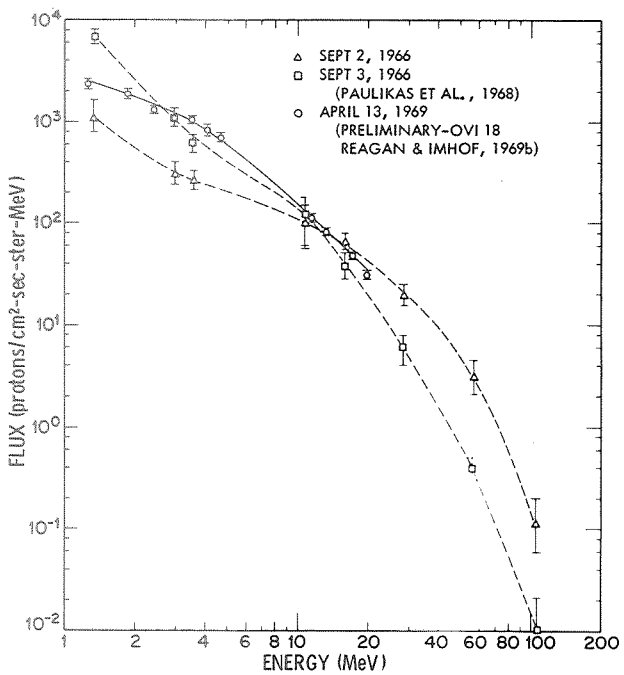


Figure 15—Energy spectra of protons observed over the polar caps at times of selected solar events.

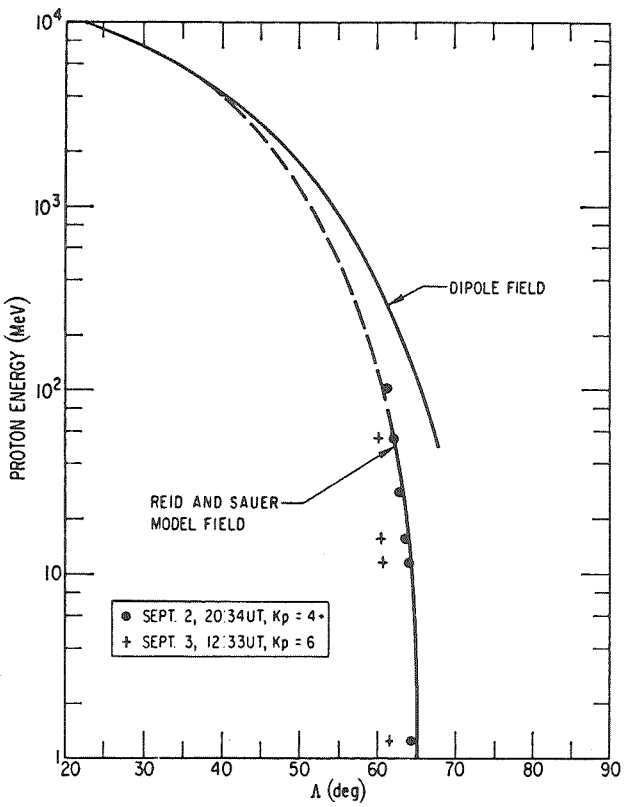


Figure 16—Nightside cutoffs as a function of energy. Calculations of Reid and Sauer and of the classical Stormer theory are also shown (Paulikas et al., 1968).

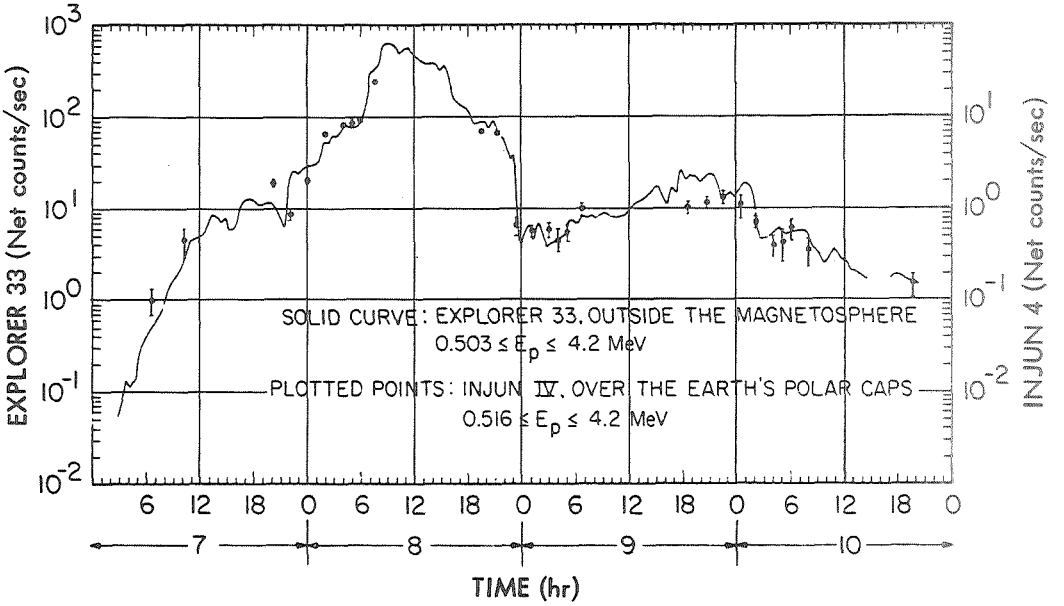


Figure 17—Counting rates obtained with similar detectors onboard the Explorer 33 and Injun 4 satellites. Each of the points for Injun 4 represents the average counting rate during a polarcap pass (Krimigis et al., 1967).

of November 2, 1967, reported by Stone (1969), in which the access delay to the northern cap was about 20 hours compared with less than one hour in the southern region.

The interpretation of the access of solar protons to the polar caps as a function of time, latitude, and energy, in terms of the various magnetosphere models is still an open question. The subject has been introduced primarily to emphasize the importance of low-altitude measurements of solar events. Here the term low-altitude applies to a much broader altitude range than considered in the radiation belts. In particular, for an isotropic influx of solar protons as often observed over the upper hemisphere (Paulikas et al., 1968) the low-altitude region is distinguished primarily by its location within the magnetosphere rather than by the presence of the atmosphere. However, at very low satellite altitudes, the proton environment may also be sensitive to steep flux variations with altitude for nonisotropic pitch-angle distributions. Such angular distributions have often been observed at positions near the magnetic cutoff. For studies of quasi-trapping phenomena, measurements at very low altitudes can indeed provide unique and important information. There is clearly a great need for more extensive low-altitude coverage with instrumentation possessing substantially greater sensitivity and better temporal and spatial resolution.

In addition to isotropic and trapped pitch-angle distributions, the observation of energetic protons on magnetic field lines from the earth has been reported by Katz and Rothwell (1968). These protons were observed over the northern polar cap at an altitude of about 4800 km but not over the South Pole where the satellite altitude was 500 km. They have interpreted the surprising existence of such protons in terms of very large electric fields (~0.14 volts/meter) parallel to the magnetic field lines. More pitch-angle measurements are probably needed before such phenomena can be well understood.

In addition to protons, alpha particles and electrons have been observed over the polar caps in conjunction with certain solar events. The lack of experimental attention to these particles can be attributed partly to the lower intensities at comparable energies in the case of alpha particles and in the case of energetic electrons to the fact that they appear to be accompanied always by energetic protons, but not vice versa (Vampola, 1969). According to Vampola, electrons of energy above 200 keV do not appear to be a common feature of the polar-cap region. However, at the time of certain solar events, electrons may appear with a reasonably hard spectrum, as is shown in Figure 18. In addition to the spectral measurements of Vampola, the figure also includes some recent observations on April 13, 1969 by the Lockheed group (Imhof and Reagan, 1969b) from the polar-orbiting satellite OV1 18.

From the limited observations to date the minority-group particles appear to behave differently than protons in several respects. Solar alpha particles in the polar-cap regions have given no evidence of durable trapping (Blake et al., 1968). In contrast to

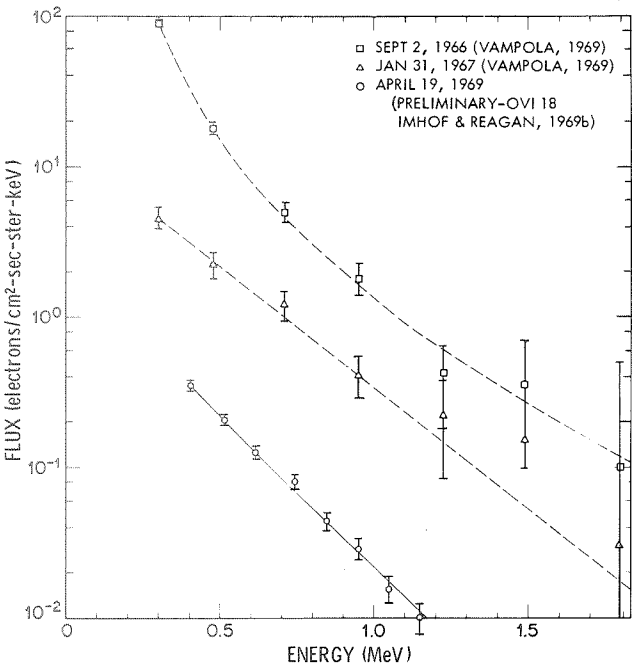


Figure 18—Energy spectra of electrons observed over the polar caps at times of selected solar events.

the protons, energetic solar electrons have displayed no spatial structure over the entire polar zone (Vampola, 1969); that is, electrons of solar origin seem to have uniform access to the polar caps.

## CONCLUSION

Clearly, many of the types of measurements performed to date should be carried out on a more regular long-term basis. For example, the inner-belt proton population should be followed in detail over a complete solar cycle. However, with a few notable exceptions the bulk of the low-altitude measurements have been performed on rocket or short-term satellite missions. Much information on the long-term behavior of trapped protons has been obtained through the use of nuclear emulsions. However, long-term counter data are clearly needed in addition, since emulsions are integrating devices and, therefore, cannot generally provide good spatial resolution. As the Starfish population decays, it is of great importance to continue monitoring the trapped electrons, particularly at the lower edge of the inner belt. Since the outer radiation belt environment is very dynamic, there is a clear need for more complete simultaneous coverage from several satellites at different positions. Of course, there still remains an important role for vehicles other than satellites. For example, a rocket can provide nearly simultaneous coverage over a broad range of $L$-shells at their magnetic equators or over a broad interval of altitude on a given magnetic field line.

Several characteristics of the lower edge of the inner radiation belt (the short-trapping lifetimes, the low fluxes of trapped electrons, and the relatively small volume of space covered) have suggested that it may be an ideal region for increasing our knowledge of loss processes through the controlled injection of electrons by artificial means (Imhof et al., 1967). Such methods might include the placement of an accelerator (Christofilos, 1959 and Singer, 1962), reactor (Carpenter and Cohen, 1965), or radioactive source (Christofilos, 1966), onboard a satellite or rocket. In contrast to the injection of electrons by the detonation of a nuclear weapon, these techniques provide for greater control of the energy spread and positions of injection. It has been calculated that early time fluxes of about $10^2$ to $10^3$ electrons/cm$^2$-sec would be achieved during one pass of a low-altitude satellite at $L \approx 1.15$ with an accelerator having a beam energy and current of 1.35 MeV and 100 $\mu$a, respectively. Although these intensities are relatively low, they appear to be higher than naturally existing fluxes of electrons trapped at $L \approx 1.15$ and should provide adequate counting rates in a properly designed detector. By injecting a relatively small number of electrons at positions where the lifetimes are quite short, controlled trapping experiments can be performed without causing any long-term contaminations of the belts.

In addition to the needs for better coverage of the low-altitude radiation environment with the type of instrumentation previously employed, it is important to perform measurements with instruments of much greater sensitivity and higher spatial/temporal resolution. At low altitudes the fluxes are often quite small and the environment frequently changes very rapidly with position. Complete worldwide coverage with the required high-bandwidth instruments onboard the low-altitude satellites can now be achieved with improved data-handling capabilities.

## ACKNOWLEDGMENTS

Appreciation is extended to the following colleagues for their helpful discussions relating to this presentation: Drs. Martin Walt, R. G. Johnson, and G. H. Nakano and Messrs. J. B. Reagan and G. Paschmann.

## REFERENCES


Achtermann, E., Hovestadt, D., and Paschmann, G., "Atmospharische Dichteabhangigkeit des Protonenflusses am unteren Rand des Strahlungsgurtels," presented at convention of the German Physical Society, Berlin, 1969.

Akasofu, S. I., Lin, W. C., and Van Allen, J. A., "The Anomalous Entry of Low-Rigidity Solar Cosmic Rays Into the Geomagnetic Field," *J. Geophys. Res.* 68: 5327, 1963.

Albert, R. D., "Nearly Monoenergetic Electron Fluxes Detected During a Visible Aurora," *Phys. Rev. Letters* 18: 369, 1967a.

Albert, R. D., "Energy and Flux Variations of Nearly Monoenergetic Auroral Electrons," *J. Geophys. Res.* 72: 5811, 1967b.

Beall, D. S., Bostrom, C. O., and Williams, D. J., "Structure and Decay of the Starfish Radiation Belt, October 1963 to December 1965," *J. Geophys. Res.* 72: 3403, 1967.

Blake, J. B., Freden, S. C., and Paulikas, G. A., "Precipitation of 400-keV Electrons in the Auroral Zone," *J. Geophys. Res.* 71: 5129, 1966.

Blake, J. B., Paulikas, G. A., and Freden, S. C., "Latitude-Intensity Structure and Pitch-Angle Distributions of Low-Energy Solar Cosmic Rays at Low Altitude," *J. Geophys. Res.* 73: 4927, 1968.

Blanchard, R. C., and Hess, W. N., "Solar Cycle Changes in Inner-Zone Protons," *J. Geophys. Res.* 69: 3927, 1964.

Bostrom, C. O., Kohl, J. W., and Williams, D. J., "The February 5, 1965 Solar Proton Event. 1. Time History and Spectrums Observed at 1100 Kilometers," *J. Geophys. Res.* 72: 4487, 1967.

Burrows, J. R., and McDiarmid, I. B., "Local Time Asymmetries Near the High Latitude Boundary of the Outer Radiation Zone," *Earth's Particles and Fields*, ed. by B. M. McCormac, New York: Reinhold Publishing Corp., 1968, pp. 45–56.

Carpenter, D. G., and Cohen, D. A., "Trapped Electron Component From Orbiting Reactor Neutron Decay," *J. Geophys. Res.* 70: 5831, 1965.

Christofilos, N. C., "The Argus Experiment," *J. Geophys. Res.* 64: 869, 1959.

Christofilos, N. C., "Sources of Artificial Radiation Belts," *Radiation Trapped in the Earth's Magnetic Field*, Dordrecht, Holland: D. Reidel Publishing Co., 1966, pp. 565–574.

Cladis, J. B., "Acceleration of Geomagnetically Trapped Electrons by Variations of Ionospheric Currents," *J. Geophys. Res.* 71: 5019, 1966.

Cornwall, J. M., "Scattering of Energetic Trapped Electrons by Very Low-Frequency Waves," *J. Geophys. Res.* 69: 1251, 1964.

Dragt, A. J., Austin, M. M., and White, R. S., "Cosmic Ray and Solar Proton Albedo-Neutron Decay Injection, *J. Geophys. Res.* 71: 1293, 1966.

Dungey, J. W., "Loss of Van Allen Electrons Due to Whistlers," *Planet. Space Sci.* 11: 591, 1963.

Evans, D. S., "The Observation of a Near Monoenergetic Flux of Auroral Electrons," *J. Geophys. Res.* 73: 2315, 1968.

Farley, T. A., "Radial Diffusion of Electrons at Low L Values," *J. Geophys. Res.* 74: 377, 1969a.

Farley, T. A., "Radial Diffusion of Starfish Electrons," *J. Geophys. Res.* 74: 3591, 1969b.

Feldstein, Y. I., "Polar Auroras, Polar Substorms, and Their Relationships With the Dynamics of the Magnetosphere," *Rev. Geophys.* 7: 179, 1969.

Filz, R. C., and Holeman, E., "Time and Altitude Dependence of 55-MeV Trapped Protons, August 1961 to June 1964," *J. Geophys. Res.* 70: 5807, 1965.

Frank, L. A., Van Allen, J. A., and Craven, J. D., "Large Diurnal Variations of Geomagnetically Trapped and of Precipitated Electrons Observed at Low Altitudes," *J. Geophys. Res.* 69: 3155, 1964.

Freden, S. C., and White, R. S., "Protons in the Earth's Magnetic Field," *Phys. Rev. Letters* 3: 9, 1959.

Freden, S. C., and White, R. S., "Particle Fluxes in the Inner Radiation Belt," *J. Geophys. Res.* 65: 1377, 1960.

Fritz, J. A., "High-Latitude Outer-Zone Boundary Region for $\geqslant$40-keV Electrons During Geomagnetically Quiet Periods," *J. Geophys. Res.* 73: 7245, 1968.

Galperin, Yu. I., and Temny, V. V., "Atmospheric Scale Height in the 200–400 Km Range According to Radiation Belt Data," *Space Res.* 5: 769, 1965.

Garmire, G., "Geomagnetically Trapped Protons With Energies Greater Than 350 MeV," *J. Geophys. Res.* 68: 2627, 1963.

Haerendel, G., "Protonen in Inneren Strahlungsgurtel, *Fortschritte der Physik* 12: 271, 1964; "Protons in the Inner Radiation Belt," NASA Technical Translation F-8771.

Heckman, H. H., and Nakano, G. H., "East-West Asymmetry in the Flux of Mirroring Geomagnetically Trapped Protons," *J. Geophys. Res.* 68: 2117, 1963.

Heckman, H. H., and Nakano, G. H., "Direct Observations of Mirroring Protons in the South Atlantic Anomaly," *Space Res.* 5: 329, 1965.

Heckman, H. H., and Nakano, G. H., "Low-Altitude Trapped Protons During Solar Minimum Period, 1962–1966," *J. Geophys. Res.* 74: 3575, 1969.

Hess, W. N., and Killeen, J., "Spatial Distribution of Protons From Neutron Decay Trapped by the Geomagnetic Field," *J. Geophys. Res.* 71: 2799, 1966.
Imhof, W. L., "Electron Precipitation in the Radiation Belts," *J. Geophys. Res.* 73: 4167, 1968.
Imhof, W. L., Cladis, J. B., and Smith, R. V., "Observation of an Energy-Selective Redistribution of Trapped Electrons in the Inner Radiation Belt," *Planet. Space Sci.* 14: 569, 1966.
Imhof, W. L., Gaines, E. E., and Reagan, J. B., "High Resolution Studies of Electrons 25 keV–2.7 MeV Precipitating at High Latitudes," *J. Geophys. Res.* 75: 776, 1970.
Imhof, W. L., and Reagan, J. B., "Source of High-Energy Protons Trapped on Low L Shells, *J. Geophys. Res.* 74: 5054, 1969a.
Imhof, W. L., and Reagan, J. B. (to be published), 1969b.
Imhof, W. L., Reagan, J. B., and Smith, R. V., "Long-Term Study of Electrons Trapped on Low L Shells," *J. Geophys. Res.* 72: 2371, 1967.
Imhof, W. L., and Smith, R. V., "Longitudinal Variations of High-Energy Electrons at Low Altitudes," *J. Geophys. Res.* 70: 569, 1965a.
Imhof, W. L., and Smith, R. V., "Observations of Nearly Monoenergetic High-Energy Electrons in the Inner Radiation Belt," *Phys. Rev. Letters* 14: 885, 1965b.
Imhof, W. L., and Smith, R. V., "The Behavior of Trapped Electrons and Protons at the Lower Edge of the Inner Radiation Belt," *J. Geophys. Res.* 71: 4157, 1966.
Imhof, W. L., Smith, R. V., and Fisher, P. C., "Particle Flux Measurements From an Atlas Pod in the Lower Van Allen Belt," *Space Res.* 3: 438, 1963.
Johnson, R. G., and Sharp, R. D., "Satellite Measurements on Auroral Particle Fluxes," *Atmospheric Emissions*, New York: Van Nostrand Reinhold Co., 1969, pp. 219–231.
Katz, L., and Rothwell, P. L., "Evidence for a Geoelectric Field Over the Polar Cap," *Phys. Rev. Lett.* 21: 1764, 1968.
Krimigis, S. M., and Van Allen, J. A., "Observations of the February 5–12, 1965, Solar Particle Event With Mariner 4 and Injun 4," *J. Geophys. Res.* 72: 4471, 1967.
Krimigis, S. M., Van Allen, J. A., and Armstrong, J. P., "Simultaneous Observations of Solar Protons Inside and Outside the Magnetosphere," *Phys. Rev. Letters* 18: 1204, 1967.
Lenchek, A. M., and Singer, S. F., "Effects of the Finite Gyroradii of Geomagnetically Trapped Protons," *J. Geophys. Res.* 67: 4073, 1962.
Marbach, J. R., Warren, C. S., and Lindsey, R. S., "Evidence of Nonfission Electrons in the South Atlantic Anomaly," *J. Geophys. Res.* 73: 3477, 1968.
McDiarmid, I. B., and Burrows, J. R., "Local-Time Asymmetries in the High Latitude Boundary of the Outer Radiation Zone for Different Electron Energies," *Can. J. Phys.* 46: 49, 1968.
McIlwain, C. E., "Direct Measurement of Particles Producing Visible Auroras," *J. Geophys. Res.* 65: 2727, 1960.
McIlwain, C. E., "Coordinates for Mapping the Distribution of Magnetically Trapped Particles," *J. Geophys. Res.* 66: 3681, 1961.
McIlwain, C. E., "The Radiation Belts, Natural and Artificial, *Science* 142: 355, 1963.
Mozer, F. S., "Rapid Variations of Auroral Particle Fluxes," *J. Geophys. Res.* 73: 999, 1968.
Nakano, G. H., and Heckman, H. H., "Evidence for Solar-Cycle Changes in the Inner-Belt Protons, *Phys. Rev. Letters* 20: 806, 1968.
Newkirk, L. L., and Walt, M., "Radial Diffusion Coefficient for Electrons at Low L Values," *J. Geophys. Res.* 73: 1013, 1968.
O'Brien, B. J., "High-Latitude Geophysical Studies With Satellite Injun 3. 3. Precipitation of Energetic Electrons into the Atmosphere," *J. Geophys. Res.* 69: 13, 1964.
Paulikas, G. A., and Freden, S. C., "Precipitation of Energetic Electrons Into the Atmosphere," *J. Geophys. Res.* 69: 1239, 1964.
Paulikas, G. A., Blake, J. B., and Freden, S. C., "Precipitation of Energetic Electrons at Middle Latitudes, *J. Geophys. Res.* 71: 3165, 1966.
Paulikas, G. A., Blake, J. B., and Freden, S. C., "Low-Energy Solar-Cosmic-Ray Cutoffs; Diurnal Variations and Pitch-Angle Distributions," *J. Geophys. Res.* 73: 87, 1968.
Pfitzer, K. A., and Winckler, J. R., "Experimental Observation of a Large Addition to the Electron Inner Radiation Belt After a Solar Flare Event," *J. Geophys. Res.* 73: 5792, 1968.
Pieper, G. F., Zmuda, A. J., and Bostrom, C. O., "Solar Protons and Magnetic Storms in July 1961," *J. Geophys. Res.* 67, 4959, 1962.
Reagan, J. B., and Imhof, W. L., "Observations on the East-West Asymmetry of Protons Trapped at Low Altitudes," *Space Res.* (to be published), 1969a.
Reagan, J. B., and Imhof, W. L. (to be published), 1969b.
Reid, G. C., and Sauer, H. H., "The Influence of the Geomagnetic Tail on Low-Energy Cosmic-Ray Cutoffs, *J. Geophys. Res.* 72: 197, 1967.

Roberts, C. S., "Cyclotron-Resonance and Bounce-Resonance Scattering of Electrons Trapped in the Earth's Magnetic Field," *Earth's Particles and Fields*, ed. by B. M. McCormac, New York: Reinhold Publishing Corp., 1968, p. 317.

Roederer, J. G., Welch, J. A., and Herod, J. V., "Longitude Dependence of Geomagnetically Trapped Electrons, *J. Geophys. Res.* 72: 4431, 1967.

Rosen, A., Sanders, N. L., Shelton, R., Potter, R., and Urban, E., "Pegasus 1: Observations of the Temporal Behavior of the Inner Zone Electrons, 1965–1966," *J. Geophys. Res.* 73: 1019, 1968.

Sharp, R. D., and Johnson, R. G., "Satellite Measurements of Auroral Particle Precipitation," *Earth's Particles and Fields*, ed. by B. M. McCormac, New York: Reinhold Publishing Corp., 1968, p. 113.

Singer, S. F., "Nuclear Explosions in Space," *Nature* (London) 196: 307, 1962.

Stone, E. C., "Local Time Dependence on Non-Stormer Cutoff for 1.5-MeV Protons in Quiet Geomagnetic Field," *J. Geophys. Res.* 69: 3577, 1964.

Stone, E. C., Paper presented at "Earth's Particles and Fields, 1969," Summer Advanced Study Institute, Santa Barbara, Calif., Aug. 4–15, 1969.

Taylor, H. E., "Adiabatic Motion of Outer-Zone Particles in a Model of the Geoelectric and Geomagnetic Fields," *J. Geophys. Res.* 71: 5135, 1966.

Theodoridis, G. C., and Paolini, P. R., "Pitch Angle Diffusion of Relativistic Outer Belt Electrons," *Ann. Geophys.* 23: 375, 1967.

Vampola, A. L., "Electron Injection Into the Inner Zone," abstract, *Trans. Amer. Geophys. Union* 49: 719, 1968.

Vampola, A. L., "Energetic Electrons at Latitudes Above the Outer-Zone Cutoff," *J. Geophys. Res.* 74: 1254, 1969.

Van Allen, J. A., "Further Investigation of the Artificial Radiation Belts," State Univ. Iowa Report SUI 63-11, 1963.

Vernov, S. N., Chudakov, A. E., Vakulov, P. V., Gorchakov, E. V., Ignatyen, P. P., Kuznetsov, S. N., Logachev, V. I., Lubimov, G. P., Nikolaev, A. G., Okchlopkov, V. P., Sosnovets, E. N., and Ternovshya, M. V., "Preliminary Results of the Study of Radiation Carried on Board the Cosmos 17 Satellite," *Space Res.* 5: 404, 1965.

Vernov, S. N., Nesterov, V. E., Savenko, I. A., Shavrin, P. I., and Sharvina, K. N., "Discovery and Investigation of the Brazil Anomaly by Spaceships and the Cosmos Series of Satellites," *Space Res.* 6: 165, 1966.

Vernov, S. N., Gorchakov, E. V., Kuznetsov, S. N., Logachev, Yu. I., Sosnovets, E. N., and Stolpovsky, V. G., "Particle Fluxes in the Outer Geomagnetic Field," *Rev. Geophys.* 7: 257, 1969.

Vette, J. I., "Models of the Trapped Radiation Environment. Vol. I: Inner Zone Protons and Electrons," NASA SP-3024, 1966.

Vette, J. I., Lucero, A. B., and Wright, J. A., "Models of the Trapped Radiation Environment. Vol. II: Inner and Outer Zone Electrons," NASA SP-3024, 1966.

Walt, Martin, "The Effects of Atmospheric Collisions on Geomagnetically Trapped Electrons," *J. Geophys. Res.* 69: 3947, 1964.

Walt, Martin, "Loss Rates of Trapped Electrons by Atmospheric Collisions," in *Radiation Trapped in the Earth's Magnetic Field*, Dordrecht, Holland: D. Reidel Publishing Co., 1966, p. 337.

West, H. I., Private communication, 1969.

Westerlund, L. H., "The Auroral Electron Energy Spectrum Extended to 45 eV," *J. Geophys. Res.* 74: 351, 1969.

Williams, D. J., and Bostrom, C. O., "The February 5, 1965, Solar Proton Event. 2. Low-Energy Solar Protons and Their Relation to the Magnetosphere, *J. Geophys. Res.* 72: 4497, 1967.

Williams, D. J., and Bostrom, C. O., "Proton Entry Into the Magnetosphere on May 26, 1967," *J. Geophys. Res.* 74: 3019, 1969.

Williams, D. J., and Kohl, J. W., "Loss and Replenishment of Electrons at Middle Latitudes and High B Values," *J. Geophys. Res.* 70: 4139, 1965.

Williams, D. J., and Mead, G. D., "Nightside Magnetosphere Configuration as Obtained From Trapped Electrons at 1100 Kilometers," *J. Geophys. Res.* 70: 3017, 1965.

Williams, D. J., Arens, J. F., and Lanzerotti, L. J., "Observations of Trapped Electrons at Low and High Altitudes," *J. Geophys. Res.* 73: 5673, 1968.

# TIME HISTORY OF THE INNER RADIATION ZONE

## OCTOBER 1963 TO DECEMBER 1968

C. O. Bostrom
D. S. Beall*
J. C. Armstrong
The Johns Hopkins University
Applied Physics Laboratory
Silver Spring, Maryland

*Present Address:
University of Wisconsin
Department of Computer Sciences
Madison, Wisconsin

## ABSTRACT

Data from electron and proton detectors aboard satellite 1963 38C have been studied for the time period from September 1963 through December 1968. Detector energy ranges, in MeV, are $E_e \geqslant 0.28$, $E_e \geqslant 1.2$, $1.2 \leqslant E_p \leqslant 2.2$, $2.2 \leqslant E_p \leqslant 8.2$, $8.2 \leqslant E_p \leqslant 25$, and $25 \leqslant E_p \leqslant 100$. The region to be discussed is $1.2 \leqslant L \leqslant 3.0 R_e$ over the $B$-range accessible to the satellite in an 1100-km circular, polar orbit. For high-energy electrons ($\geqslant$1.2 MeV) the major feature has been the steady decay of the artificial belt. By the end of 1968, Starfish electrons had essentially disappeared and there was no indication of a natural source for electrons with energy $\geqslant$1.2 MeV. The low-energy ($\geqslant$0.28 MeV) electron flux has been near enough to the natural levels since early 1966 to reveal the effect of natural events; these electrons undergo significant changes throughout the inner zone in response to major magnetic storms. In particular, the events in September 1966, May 1967, and November 1968 produced large changes in the low-energy electrons and also in low-energy protons, although the protons responded over a more limited region of $L$-space.


## INTRODUCTION

The temporal variations in the natural charged-particle population of the inner radiation zone have been studied by many authors (Pizzella et al., 1962; Pizzella, 1963; McIlwain, 1965; Zmuda et al., 1965; Imhoff et al., 1967; Heckman and Nakano, 1969; Bostrom and Armstrong, 1966; Filz and Holeman, 1965; Filiius, 1966; and Krimigis and Burns, 1969). The major perturbation to the inner zone produced by the Starfish high-altitude nuclear explosion has also been extensively studied (Van Allen, 1966; Hess, 1963; McIlwain, 1966; Brown, 1966; Beall et al., 1967; Paulikas et al., 1967; Pfitzer, 1968; and Bostrom et al., 1968). A general summary of these observations would include the following statements. The inner radiation zone is a relatively stable region in which significant changes in the high-energy particle fluxes are rare. Energetic protons are particularly stable; the perturbations which do occur are usually small and are limited to the outer region of the inner zone. High-energy (>1 MeV) electrons have a mean lifetime ($1/e$) of $\leqslant$1 year in the inner belt but, apparently, are not a major constituent of the natural population. Low-energy electrons (<1 MeV) undergo large variations in intensity throughout the inner zone in response to major geomagnetic disturbances.

This paper presents data on inner-zone trapped electrons and protons over a 63-month period from October 1963 through December 1968, from satellite 1963 38C.

Satellite 1963 38C was launched into a circular, polar orbit at 1100-km altitude on September 28, 1963. The satellite is magnetically stabilized and contains an electron spectrometer and a proton spectrometer which measure locally mirroring particles. The instruments have been described in detail elsewhere (Williams and Smith, 1965; Bostrom et al., 1967; and Beall et al., 1967) and pertinent characteristics of selected channels are summarized in Table 1.

The coverage in $B$-, $L$-space obtained in November 1963 is shown in Figure 1 and is representative of the coverage during the lifetime of the satellite. The shape of the region is determined by the satellite orbit and the distribution of active ground stations, since there is no data-storage capability on board. The coverage, of course, goes on to very high $L$'s. All of the satellite data over its full lifetime have been scanned and 5-point (~5 sec) averages computed at 32 selected values of $L$, ranging from $L = 1.2$ to $L = 20$. Nineteen detector counting rates, time, $L$, and $B$ comprise each selected data point, and certain temperatures and voltages are retained for each pass. The passes through 1968 have been time ordered and the information presented in this paper is obtained from the selected, time-ordered data. The bars in Figure 1 show the $B$-ranges used in the time-history graphs to be shown later. The $B$-restriction is necessary to reduce the scatter in the data. The $B$-ranges associated with each $L$-value discussed herein are given in Table 2.

An example of a computer-generated time plot is shown in Figure 2 (Beall, 1969). These are data for $L = 1.25$ and $B$ between 0.16 and 0.17 gauss, during 1964. Electron spectrometer counting rates are plotted with energy thresholds as shown. At this $L$ measurements are made near the magnetic equator and the data are tightly grouped. Notice that there are two periods when the scatter in the data increases, Day 170 to 210 and from about Day 300 on. These are the times in 1964 when the satellite orbit was

Table 1
Detector Characteristics.

| Channel | Energy sensitivity (MeV) | | Geometric factor ($cm^2$-ster) |
|---|---|---|---|
| | Electrons | Protons | |
| C1 | $\geqslant 0.28$ | 1.93 to 2.28; $\geqslant 153$ | $2.8 \times 10^{-3}$* |
| C2 | $\geqslant 1.20$ | 14.4 to 14.5; $\geqslant 154$ | $2.8 \times 10^{-3}$* |
| (P1-P5) | $>0.7$ (low efficiency) | 1.2 to 2.2 | $3.0 \times 10^{-2}$ |
| (P2-P6) | nil | 2.2 to 8.2 | $3.0 \times 10^{-2}$ |
| P3 | nil | 8.2 to 25 | $1.4 \times 10^{-2}$ |
| P4 | nil | 25 to 100 | $1.4 \times 10^{-2}$ |

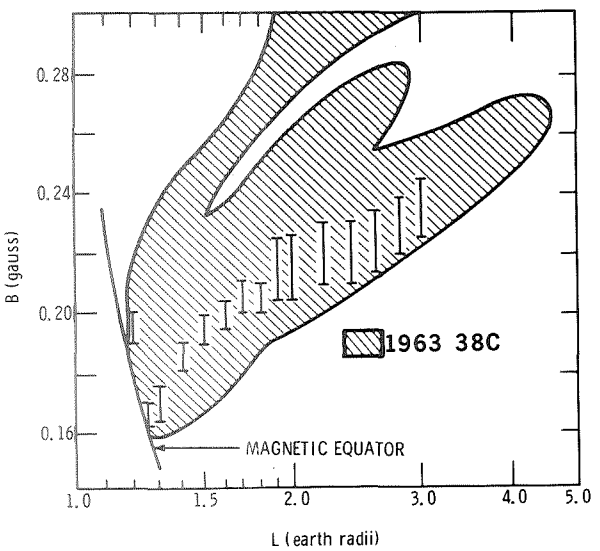


Figure 1—1963 38C ($B, L$) coverage in November 1963. This is representative of the coverage throughout the period from October 1963 through December 1968. Coverage extends to high $L$ to larger $B$.

Table 2
Range of $B$-values as a Function of $L$.

| $L$-value | Associated $B$-range |
|---|---|
| 1.20 | $0.180 \leqslant B < 0.190$ |
| 1.21 | $0.175 \leqslant B < 0.185$ |
| 1.22 | $0.175 \leqslant B < 0.185$ |
| 1.23 | $0.170 \leqslant B < 0.180$ |
| 1.25 | $0.160 \leqslant B < 0.170$ |
| 1.27 | $0.160 \leqslant B < 0.170$ |
| 1.30 | $0.165 \leqslant B < 0.175$ |
| 1.35 | $0.170 \leqslant B < 0.180$ |
| 1.40 | $0.180 \leqslant B < 0.190$ |
| 1.50 | $0.190 \leqslant B < 0.200$ |
| 1.60 | $0.195 \leqslant B < 0.205$ |
| 1.70 | $0.200 \leqslant B < 0.210$ |
| 1.80 | $0.200 \leqslant B < 0.210$ |
| 1.90 | $0.205 \leqslant B < 0.225$ |
| 2.00 | $0.205 \leqslant B < 0.225$ |
| 2.20 | $0.210 \leqslant B < 0.230$ |
| 2.40 | $0.210 \leqslant B < 0.230$ |
| 2.60 | $0.215 \leqslant B < 0.235$ |
| 2.80 | $0.220 \leqslant B < 0.240$ |
| 3.00 | $0.225 \leqslant B < 0.245$ |

in or near full sunlight, and the apparent reason for the scatter is an increase in the amplitude of the oscillation of the satellite about the magnetic field. The increased amplitude has also been observed by the onboard magnetometers. Notice that the scatter is only toward lower counting rates, as would be expected if the detectors were measuring a wide range of local pitch angles instead of a narrow range near 90°. In the following section ten-day averages of data such as these are shown. In all cases, the data were edited to remove these low points as well as some obviously noisy data.

## LONG-TERM OBSERVATIONS

In Figure 3 the 5-year and 3-month time histories of electrons with energy $\geqslant 1.2$ MeV for $L$-shells 1.2, 1.3, 1.4, 1.5, and 1.6 are shown. These are 10-day averages of the counting rates. Bad points have been removed and dead-time corrections made. The main feature in the behavior of these particles is a monotonic decrease with time to a background counting rate that is due to energetic protons. The proton background level at each $L$-value, derived from observations of the higher energy electron channels and based upon the procedure given by Beall et al. (1967) is shown. These levels differ only slightly from the values, given in the earlier paper, which were determined using only data through 1965. Of special interest is the fact that in no case is there any obvious response to the major magnetic disturbances which occurred during the satellite lifetime. This is in sharp contrast to the behavior of the lower energy electrons and implies that there is no strong natural source for 1.2-MeV electrons

*The procedure for obtaining flux from counting rate is given in Beall et al. (1967) and Bostrom (1969). The efficiencies for C1 and C2 are spectrum dependent but approximate values are $\epsilon_1 = 0.77$ and $\epsilon_2 = 0.20$ to 0.34.

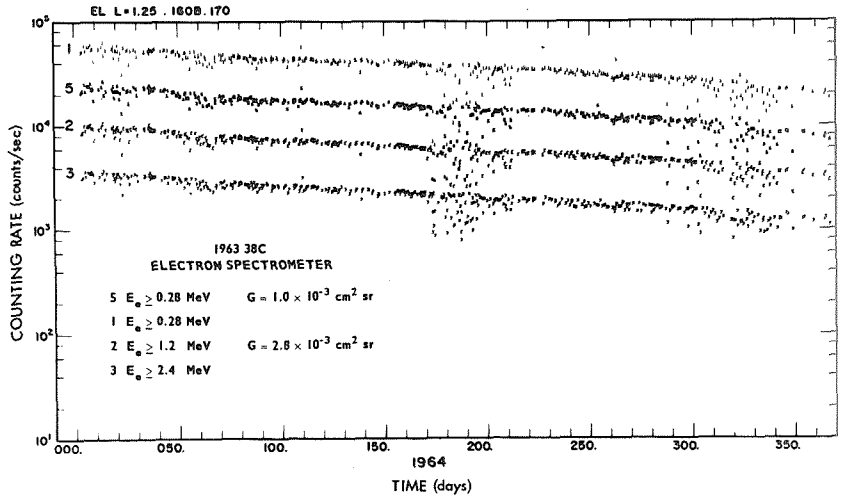


Figure 2—Electron spectrometer counting rates versus time for $L$ = 1.25 $R_e$, $0.16 \leqslant B \leqslant 0.17$ gauss in 1964.

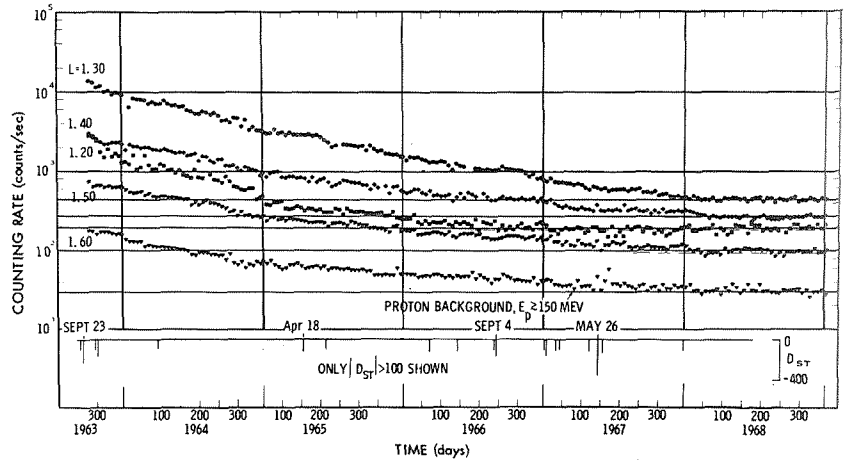


Figure 3—Ten-day average counting rates for $C_2$ ($E_e \geqslant 1.2$ MeV) from October 1963 through December 1968 at $L$ = 1.2, 1.3, 1.4, 1.5, and 1.6 $R_e$. The $D_{ST}$ scale indicates times of major magnetic storms.

in the inner zone. The effective intensity threshold of our detector ranges from $10^4$ to $10^5$ electrons/cm$^2$-sec-ster, depending on proton background and the electron spectrum. With that qualification, we would conclude that all electrons above about 1 MeV in the inner zone were injected by the Starfish event in July 1962. Pfitzer (1968) has observed inner-zone variations only for electrons below 690 keV.

Curves of counting rate versus time, drawn through 10-day averages of the data from our lowest energy electron channel (threshold at 280 keV) are given in Figure 4. Comparison of this data at $L$ = 1.2, 1.3, and 1.5 with that of Figure 3 shows that, whereas the high-energy electrons showed almost no structure, the low-energy electrons are strongly influenced by major magnetic storms throughout the inner zone. The Starfish component at this energy was undoubtedly large at $L$ = 1.2 and 1.3 in 1963, but the intensity, even as low as $L$ = 1.5, may well have been influenced by the September 1963 storm. This is clearly the case at $L$ = 1.8 and 2.2. Storm-time changes show that the inner-zone electrons above 280 keV have been close to their (fluctuating)

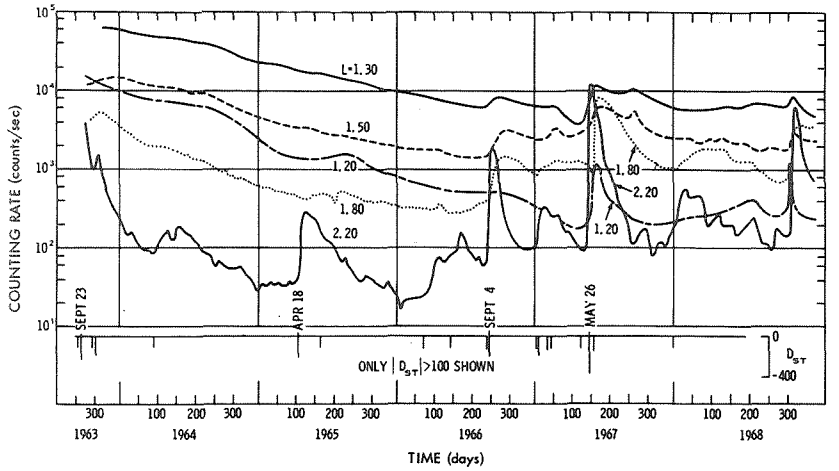


Figure 4—Curves derived from ten-day average counting rates for $C_1$ ($E_e \geqslant 0.28$ MeV) from October 1963 through December 1968 at $L$ = 1.2, 1.3, 1.5, 1.8, and 2.2 $R_e$. The $D_{ST}$ scale indicates times of major magnetic storms.

natural level of intensity since the beginning of 1966. In fact, at $L$ = 1.5, 1.8, and 2.2 a minimum in the intensity occurred in 1966. The minimum for $L$ = 1.2 and 1.3 occurred in 1967 but this may well have been because of the Starfish population at these $L$-values. Note that all data presented here are for $B$-values such that $h_{min} > 600$ km and solar-cycle variations in atmospheric density should not greatly affect the trapped radiation (Blanchard and Hess, 1964). The minimum is rather broad and appears to lag behind the minimum in the sunspot cycle by perhaps one to two years. Both the time lag and its $L$-dependence could be due to the presence of Starfish electrons. During this time period, major magnetic disturbances occurred in September 1966, May 1967, and November 1968 and, in each case, the low-energy electron population increased throughout the entire inner radiation zone. Smaller disturbances produce significant changes in the outer region of the inner zone; they probably produce small changes through the inner zone. This is examined in more detail in a later section.

In the next four figures data on protons in four different energy ranges are presented.

The 10-day average counting rates for protons with energy between 25 and 100 MeV at $L$'s from 1.2- to 2.2-$R_e$ are shown in Figure 5. The maximum intensity in our orbit occurs at $L \approx 1.27$ and the flux ($j_\perp$) during the 1965–1968 period is $8.6 \times 10^3$ per $cm^2$-sec-ster, compared with the value of about $2 \times 10^3$ from the AP 1 map produced by Vette (1966). Time variations are almost negligible. The September 23, 1963 storm produced a decrease in energetic protons at $L \gtrsim 1.8$, as reported by McIlwain (1965). 1963 38C was launched just after this event and the recovery is observed at $L$ = 1.8 and $L$ = 2.2. The only other major perturbation for these protons over this time period was in May 1967 and resulted in a decrease at $L > 2$. At $L$ = 2.2 the flux decreased by a factor of about three and one-half. Note that for a period of 4 years at $L$ = 1.27 and 5 years at $L$ = 1.2, 1.5, and 1.8, the counting rates have remained essentially constant with no obvious long-term trend associated with this period of the solar cycle. Data at $L$ = 1.27 through 1964 and at $L$ = 1.20 and $L$ = 1.50 through 1963 have been found to be contaminated by the intense Starfish electron fluxes and are, therefore, omitted.

The data in Figure 6 are for protons between 8.2 and 25 MeV. Again five $L$-values beginning with 1.2 and extending to 2.6 are shown. The others were chosen to show different regions while minimizing overlap. At this energy, there are very few rapid, large changes, although the September 1963 storm apparently had an effect and the May 1967 storm produced a decrease above $L$ = 2.2 which is clear at $L$ = 2.6. However, in the 8- to 25-MeV range there is a slow but steady decrease over the 4 years, at $L$ between 1.35 and 2.2. The slope of the line through the points at $L$ = 1.35 yields a mean life of 7.1 ± 1.4 years. At $L$ = 1.2 there is essentially no change over this time period.

The next lower energy, 2.2 to 8.2 MeV, where one begins to see considerably more activity is shown in Figure 7. Data for $L$ between 1.5 and 3.0 are shown. The high-energy proton background has been subtracted, and this channel is insensitive to electrons. The major disturbances, when $|D_{ST}|$ exceeded 100 gamma, are shown across the bottom of the figure. There is a long-term decrease at all $L$-values shown and the effect of the September 1963 storm is not known. Except at $L$ = 3, there are no large

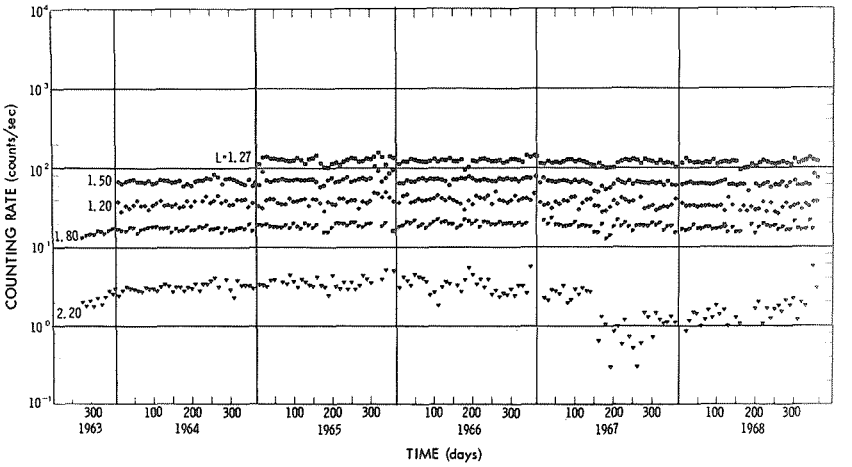


Figure 5—Ten-day average counting rates for P4 ($25 \leqslant E_p \leqslant 100$ MeV) from October 1963 through December 1968 at $L$ = 1.20, 1.27, 1.50, 1.80, and 2.20 $R_e$.

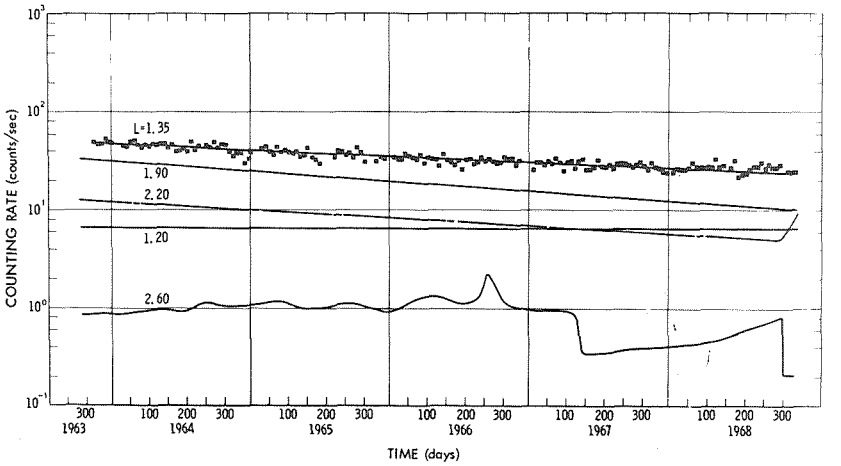


Figure 6—Curves derived from ten-day average counting rates for P3 ($8.2 \leqslant E_p \leqslant 25$ MeV) from October 1963 through December 1968 at $L$ = 1.20, 1.35, 1.90, 2.20, and 2.60 $R_e$. Representative ten-day average points are shown for $L$ = 1.35.

changes associated with magnetic disturbances until May 1967. At $L$ = 3 the response to major events may be a decrease as in April 1965 and May 1967, or an increase as in September 1966. The magnitude of the change is a factor of two to four and it takes place over a period of 20 to 40 days. The May 26, 1967 event obviously stands out as the largest magnetic disturbance in these 5 years, when $D_{ST}$ reached −370 gamma. It had the greatest effect on the inner-zone trapped particles during the period of observation. For these protons the largest enhancement occurred at $L$ = 2.2 (a factor of nine) and this was accompanied by a depletion at $L$ = 1.5 and at $L$ = 2.6 by a factor of two. At $L$ = 1.8 there was no change. These changes are examined further in the next section.

In Figure 8, 1.2- to 2.2-MeV protons at $L \geqslant 1.8$ are shown. The vertical scale is expanded, and the high-energy proton background has been subtracted. Although this channel is sensitive to electrons above 800 keV, the simultaneous data from the electron spectrometer show that background from this source can contribute only at $L \gtrsim 2.6$ and only during the first few days of an

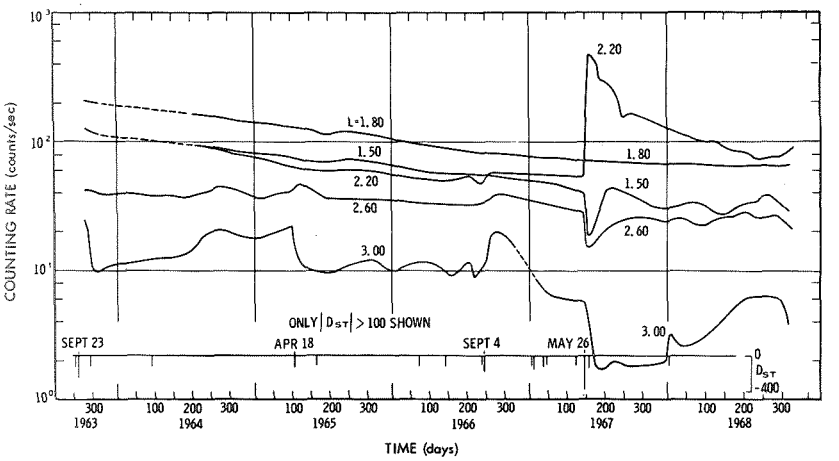


Figure 7—Curves derived from ten-day average counting rates for (P2-P6) ($2.2 \leqslant E_p \leqslant 8.2$ MeV) from October 1963 through December 1968 at $L$ = 1.5, 1.8, 2.2, 2.6, and 3.0 $R_e$. The $D_{ST}$ scale indicates times of major magnetic storms.

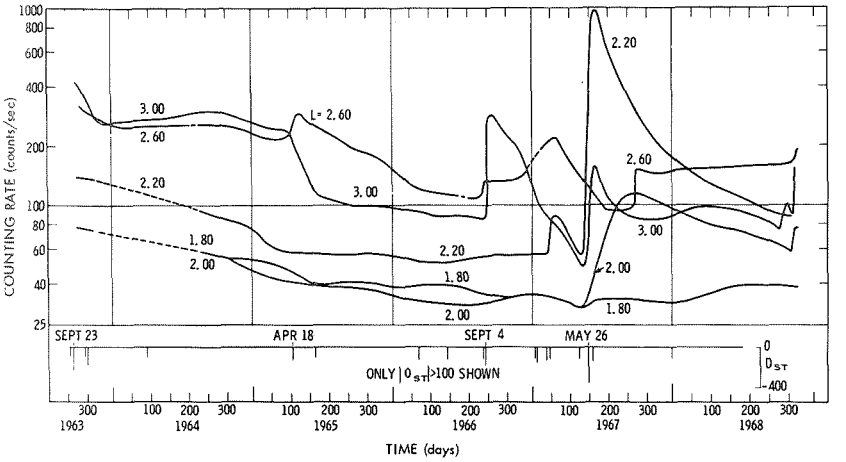


Figure 8—Curves derived from ten-day average counting rates for (P1-P5) ($1.2 \leqslant E_p \leqslant 2.2$ MeV) from October 1963 through December 1968 at $L$ = 1.8, 2.0, 2.2, 2.6, and 3.0 $R_e$. The $D_{ST}$ scale indicates times of major magnetic disturbances.

event. That is, the apparent lifetimes of energetic electrons are much shorter than those of protons and the temporal behavior of energetic electrons is quite different. We conclude, therefore, that at $L$ = 1.8, 2.0, and 2.2, electrons do not contribute and that at $L$ = 2.6 and 3.0 the electron contamination is small and of short duration ($\leqslant$10 days). Here again a variety of responses to magnetic disturbances are seen. In April 1965, there is a 50% increase at $L$ = 2.6 and a decrease at $L$ = 3 to about one-half the pre-storm value. The decrease at $L$ = 3 is rather slow, taking about 75 days, with a further response to the storm on June 15th. In September 1966 the flux increased by a factor of three and one-half at $L$ = 3, and by about 30% at $L$ = 2.6. The response at $L \leqslant 2.2$ was small or nonexistent until the May 1967 event, when the flux at $L$ = 2.2 increased by a factor of about 17. $L$ = 2.6 showed no immediate effect and $L$ = 3, a rapid increase. At $L$ = 2 a gradual increase by about a factor of four occurred over a period of 100 days.

## STORM-TIME VARIATIONS

The primary purpose of this paper is the presentation of long-term observations on the inner-zone trapped particles. Each of the events associated with the major magnetic disturbances requires detailed study and correlation with other observations. However, some aspects of the storm-time changes have been examined in slightly more detail than is shown on the 10-day average graphs. These observations are presented in this section.

The May 1967 event was, of course, the largest and produced major changes in the $E_e \geqslant 0.28$ MeV electron population throughout the inner zone. A sequence of profiles in $L$ of the C1 counting rate is given in Figure 9.

The dashed line shows the situation prior to the September 1966 storm. The Day 130, 1967 profile shows that the long-term effect of the September 1966 storm was to enhance the region between $L = 1.4$ and 2.2. Day 140 is essentially identical with 130 at $L$ below 2.2, but the recovery from an earlier storm on May 3rd is seen at higher $L$. On Day 150, four days after the $D_{ST}$ maximum, we find a large enhancement at higher $L$, 3 decades at $L = 3$, and also at low $L$, an increase by a factor of five at $L = 1.2$. However, at $L = 1.6$, 1.7, and 1.8 the changes were relatively small. By Day 160, the region between $L = 1.5$ and 2.0 has been increased, and the region above $L = 2$ has begun to decrease. Finally, 40 days later on Day 200, $L > 2.4$ had returned to prestorm values; the flux at $L = 1.2$ has returned to about twice its prestorm value; and the region between $L = 1.5$ and 2.4 is still well above prestorm levels by a factor of two to eight. At $L = 1.5$ the increase at lower $L$ appears to be continuing, although the profile still shows a dip at $L = 1.5$.

To examine these changes further, look at the storm-period data in more detail. Figure 10 was derived by means of all of the available data, which have been corrected for the $B$-dependence. The $B$-values to which the data were normalized are for $L = 1.25$ and 1.3, $B = 0.18$; for $L = 1.2$, 1.4, and 1.5, $B = 0.19$; for $L = 1.6$ and 1.7, $B = 0.20$; and for $L = 1.8$, 1.9, and 2.0, $B = 0.21$ gauss. There are two distinct regions of the inner zone in which particle injection and/or acceleration occur: (1) deep in the inner zone ($1.2 \leqslant L \leqslant 1.4$) where immediate and rapid increases are observed, and (2) the region of high $L$ ($L \geqslant 1.9$) where less rapid but larger percentage changes are found. In between is a transition region ($1.5 \leqslant L \leqslant 1.8$) in which the increases are smaller and/or occur later. Although we are unable to determine very precisely the risetimes, it is clear from the data that the increase at $L = 1.2$ to 1.4 occurs in a few hours. This deep inner-zone effect is considerably smaller at $L = 1.5$ and 1.6, while at $L = 1.7$ it is not seen at all. Meanwhile, the much larger enhancement above $L = 2$ appears to move inward gradually. By Day 151 the intensity at $L = 1.6$ has begun to increase but there is no sign of this inward diffusion affecting $L = 1.5$. It is possible that the rapid increase at low $L$ is the result of local acceleration since the detector is a threshold device. The high-$L$ behavior is similar to earlier observations of storm-time effects (Williams et al., 1968) wherein the largest and most rapid increase occurs at a particular value of $L$ depending on the severity of the magnetic disturbance (in this case $L \approx 2.4$) and then the particle disturbance propagates both inward and outward in $L$. It is interesting, for instance, that the May 26, 1967 storm, which had such a marked effect on the inner zone, was not a particularly noteworthy event in the outer zone. At $L \geqslant 3.5$ its effects were less notable than those of a number of much smaller storms.

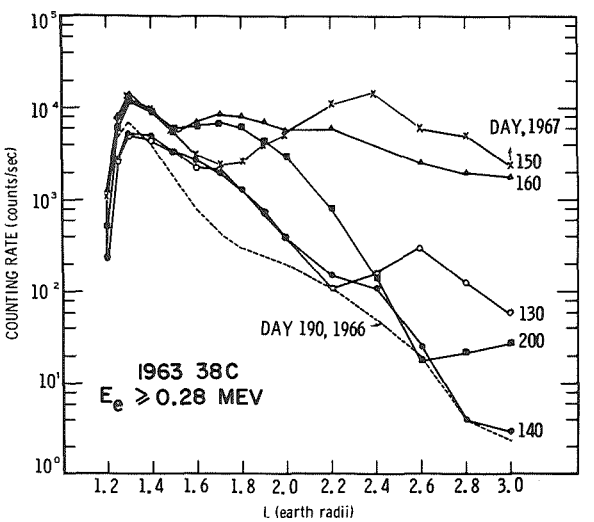


Figure 9—C1 counting rate versus $L$ profiles for Day 190, 1966 (prior to September 1966 event), and for Days 130, 140, 150, 160, and 200, 1967. The May 1967 storm occurred on Days 145 to 146.

Another example of the rapid storm-time increases at low $L$ was seen in November 1968. The clearly recognizable responses at $L = 1.2$ to $L = 1.3$ of electrons ($E_e \geqslant 0.28$ MeV) to geomagnetic activity, as measured by $\Sigma K_p$, are given in Figure 11. Other responses of the electron population might have occurred during periods of increased $\Sigma K_p$ but due to sparse data they are less obvious than those shown. In fact, there seems to be a very close correspondence between $\Sigma K_p$ and the intensity of these electrons, but this topic will require more detailed treatment. Of primary interest here is the electron response to the magnetic disturbance that began on Day 304 and lasted through Day 309. Generally, both the rise and decay are slower at higher $L$. The uncertainty in the initial time of rise and the time of peak enhancement, shown in Figure 11, is ±1 day. The magnitude of the increase has a maximum at

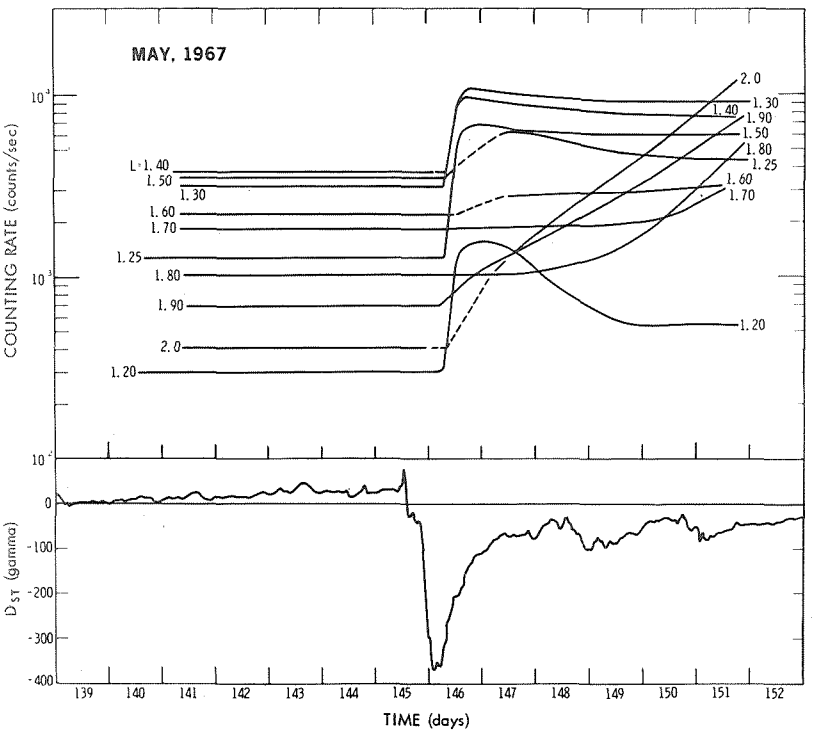


Figure 10–C1 counting rate versus time for $1.20 \leqslant L \leqslant 2.0$ $R_e$ in May 1967. $D_{ST}$ values are plotted below the data.

$L = 1.27$. Our detector does not permit us to determine whether we might be observing an energy-selective redistribution of the type reported by Imhoff et al. (1966) or some other acceleration mechanism.

The May 1967 storm produced some major changes in the proton distribution as well. The magnitude of the changes is much smaller for protons than for electrons and these changes occur only in a limited region of space. The net effect of the storm is shown in Figure 12 where the prestorm and poststorm flux distributions for the four proton-energy ranges are presented. The flux from the AP 5 map produced by King (1967) is given for the 1.2- to 2.2-MeV range for comparison. The protons above 8.2 MeV were depleted at all $L$'s shown, the depletion factor being larger for higher energy and higher $L$. The spectrum of the protons introduced at $L = 2.2$ apparently included some protons above 8.2 MeV, accounting for the small (15%) net loss of 8.2- to 25-MeV protons. For 2.2 to 8.2 MeV, there was little change at $L \leqslant 2$, an increase by a factor of nine at $L = 2.2$, an increase of less than a factor of two at $L = 2.4$, and a decrease at $L > 2.5$. For the lowest energy interval, the increase occurs over a wider range of $L$, but it still peaked at $L = 2.2$ and the only apparent decrease was at $L = 2.6$. If one examines a sequence of these cuts in time, the tendency is for the flux to decay at $L \geqslant 2.2$ and for the peak to broaden and increase at lower $L$.

## SUMMARY

Data on trapped electrons and protons between $L = 1.2$ and 3.0 over a period of 5 years and 3 months, from September 1963 through December 1968 are presented in this paper. These data allow us to make the following statements.

Protons above 25 MeV are extremely stable at $L \leqslant 1.8$. Above $L = 2$ they were depleted during the September 1963 and the May 1967 events.

Protons between 8.2 and 25 MeV also respond only to exceptional magnetic disturbances but show a long-term decrease during this period. The apparent mean lifetime at $L = 1.35$ is $7.1 \pm 1.4$ years.

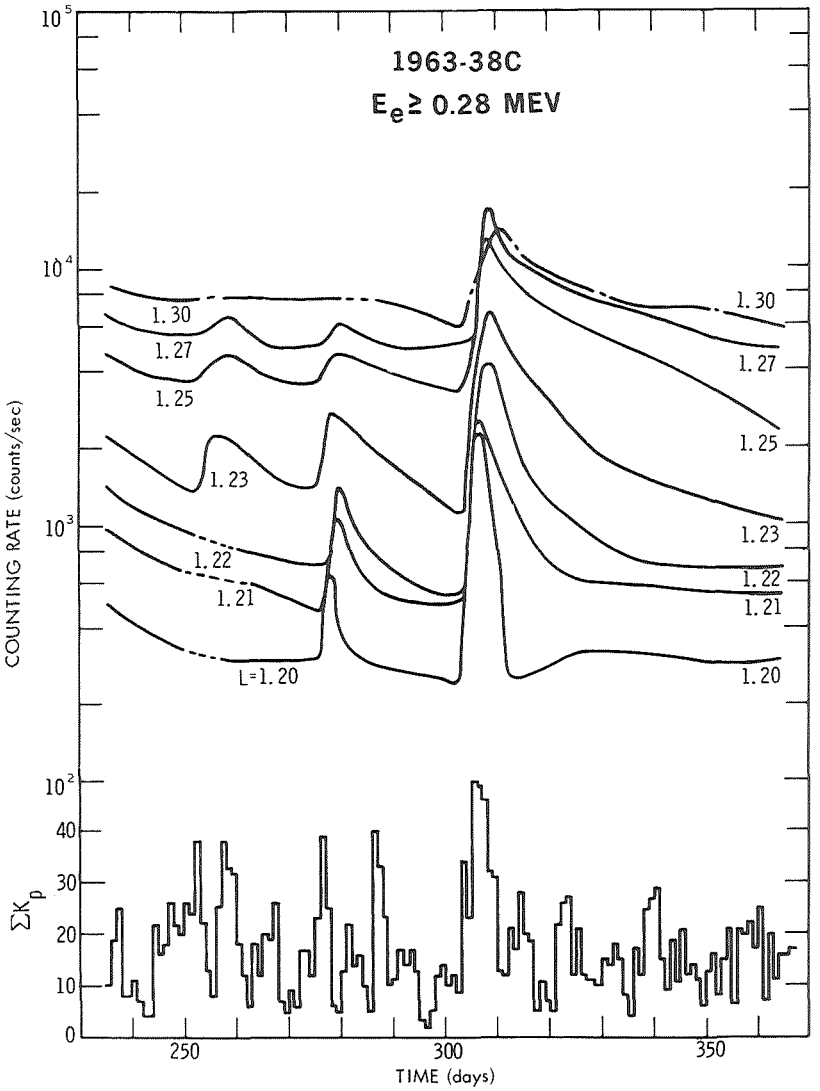


Figure 11—C1 counting rate versus time for $1.20 \leq L \leq 1.30$ $R_e$ showing the low-$L$ response to the November 1968 storm. $K_p$ daily sums are plotted below the data.

Low-energy protons (1.2 to 8.2 MeV) at $L = 3$ may be enhanced or depleted following a magnetic disturbance. The enhancement following the May 1967 storm was sharply peaked at $L = 2.2$ and accompanied by depletion at both higher and lower $L$-values. The proton behavior strongly suggests a resonance phenomenon because the response is restricted in both energy and $L$.

With regard to electrons above 1.2 MeV, in 5 years and 3 months we have seen no indication of response to magnetic perturbations at $L < 2$, there being only a monotonic decrease to a high-energy proton background. We conclude, therefore, that there is no source for 1.2-MeV electrons which can produce a quiescent or transient flux of more than $10^4$ to $10^5$ electrons/cm$^2$-sec-ster. The Starfish component at the end of 1968 was not measurable with our detectors.

Electrons above 280 keV have been at or near their natural level of intensity since the beginning of 1966 for $L > 1.3$. There is some evidence that Starfish electrons persisted into early 1967 for $L \lesssim 1.3$. The response of electrons of this energy to a magnetic disturbance is always an increased intensity. There are two distinct regions of response defined by immediate and rapid increases in electron intensity. The outer-region response is consistent with the previously reported outer-zone electron response to geomagnetic activity except that it is displaced into the outer edge of the inner zone for the very large magnetic disturbances that

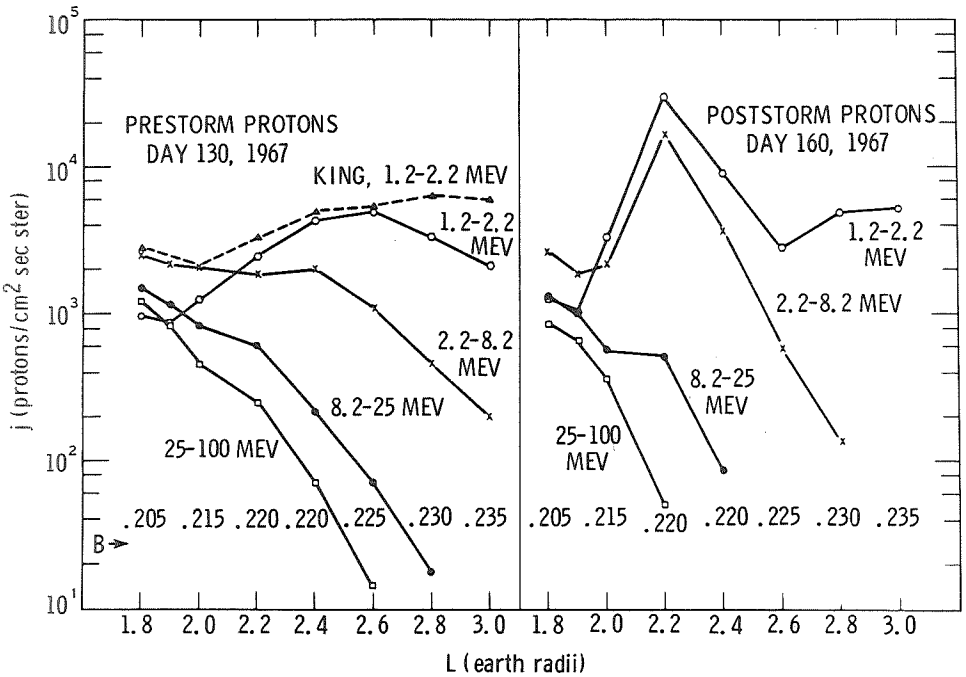


Figure 12—Proton flux versus $L$ for several energies showing the effect of the May 1967 storm on the proton distribution.

were studied (peaking at $L = 2.4$ for the May 1967 event). The inner-region response is believed to be a previously unreported phenomenon. This response would have been masked in experiments prior to 1966 by the Starfish electrons. That it is a real phenomenon is demonstrated by the close correspondence between electron intensity at $L = 1.2$ and $\Sigma K_p$ (not presented in detail in this report) even for times of relatively low geomagnetic activity. These two regions are separated by a transition region, the inner edge of which is marked by an immediate but slow rise in intensity and the outer edge of which is marked by a delayed and slow rise in intensity. The inner edge of this transition region moves outward in $L$ and the outer edge moves inward in $L$ as the severity of the magnetic disturbance increases. As an example, in May 1967 we observed a rapid increase above $L = 1.8$ and below $L = 1.6$. The initial change was followed by an increase between $L = 1.6$ and $L = 1.8$ and subsequent decay at all $L$'s.

## ACKNOWLEDGMENTS

We wish to thank all of the many persons who have contributed to the long and fruitful life of satellite 1963 38C. In particular, we gratefully acknowledge the assistance of Mr. C. J. Monahan, Miss B. A. Dodge, and Mrs. R. L. McQuiney in the analysis and presentation of the data.

This work was supported in part by the National Aeronautics and Space Administration under DPR No. R21-009-004, and in part by the Naval Ordnance Systems Command, Department of the Navy, under contract NOw 62-0604-c.

## REFERENCES


Beall, D. S., "Graphs of Selected Data From Satellite 1963 38C for 1963–1967," The Johns Hopkins Univ. Applied Physics Lab., Tech. Memorandum TG 1050 (5 volumes), April 1969.

Beall, D. S., Bostrom, C. O., and Williams, D. J., "Structure and Decay of the Starfish Radiation Belt, October 1963 to December 1965," *J. Geophys. Res.* 72: 3403–3424, 1967.

Blanchard, R. C., and Hess, W. N., "Solar Cycle Changes in Inner Zone Protons," *J. Geophys. Res.* 69: 3927–3937, 1964.

Bostrom, C. O., "Data User's Guide to Satellite 1963 38C," The Johns Hopkins Univ. Applied Physics Lab., Tech. Memorandum TG 1068, 1969.

Bostrom, C. O., and Armstrong, J. C., "The Effects of the September 20–23, 1963 Magnetic Disturbances on the Inner Zone Protons," *Trans. Am. Geophys. Union* 47: 479, 1966.

Bostrom, C. O., Beall, D. S., and Armstrong, J. C., "Trapped Particles in the Inner Zone, 1963 Through 1967," (abstract) International Symposium on the Physics of the Magnetosphere, Washington, D.C., September 3–13, 1968.

Bostrom, C. O., Kohl, J. W., and Williams, D. J., "The February 5, 1965 Solar Proton Event. 1. Time History and Spectrums Observed at 1100 Kilometers," *J. Geophys. Res.* 72: 4487–4495, 1967.

Brown, W. L., "Observations of Transient Behavior of Electrons in the Artificial Radiation Belts," in *Radiation Trapped in the Earth's Magnetic Field*, ed. by B. M. McCormac, Dordrecht, Holland: D. Reidel Publishing Co., 1966, pp. 610–633.

Fillius, R. W., "Trapped Protons in the Inner Radiation Belt," *J. Geophys. Res.* 71: 97–123, 1966.

Filz, R. C., and Holeman, E., "Time and Altitude Dependence 55-MeV Trapped Protons, August 1961 to June 1964," *J. Geophys. Res.* 70: 5807, 1965.

Heckman, H. H., and Nakano, G. H., "Low-Altitude Trapped Protons During Solar Minimum Period, 1962–1966," *J. Geophys. Res.* 74: 3575–3590, 1969.

Hess, W. N., editor, "Collected Papers on the Artificial Radiation Belt From the July 9, 1962 Nuclear Detonation," *J. Geophys. Res.* 68: 605–758, 1963.

Imhoff, W. L., Cladis, J. B., and Smith, R. V., "Observations of an Energy-Selective Redistribution of Trapped Electrons in the Inner Radiation Belt," *Planet. Space Sci.* 14: 569–577, 1966.

Imhoff, W. L., Reagan, J. B., and Smith, R. V., "Long-Term Study of Electrons Trapped on Low L Shells," *J. Geophys. Res.* 72: 2371–2377, 1967.

King, J. H., "Models of the Trapped Radiation Environment. Vol. IV: Low Energy Protons," NASA SP-3024, 1967.

Krimigis, S. M., and Burns, A. L., "The Time Dependence of Low Energy Protons and Alpha Particles in the Radiation Belts," (abstract) International Symposium on the Physics of the Magnetosphere, Washington, D.C., September 3–13, 1968.

McIlwain, C. E., "Measurements of Trapped Electron Intensities Made by the Explorer XV Satellite," in *Radiation Trapped in the Earth's Magnetic Field*, ed. by B. M. McCormac, Dordrecht, Holland: D. Reidel Publishing Co., 1966, pp. 593–609.

Paulikas, G. A., Blake, J. B., and Freden, S. C., "Inner Zone Electrons in 1964 and 1965," *J. Geophys. Res.* 72: 2011–2020, 1967.

Pfitzer, K. A., "An Experimental Study of Electron Fluxes From 50 keV to 4 MeV in the Inner Radiation Belt," Univ. of Minnesota School of Physics and Astronomy Technical Report CR-123, August 1968.

Pizzella, G., "On the Inner Van Allen Zone of the Earth," *Nuovo Cimento* 19: 867–882, 1963.

Pizzella, G., McIlwain, C. E., and Van Allen, J. A., "Time Variations of Intensity in the Earth's Radiation Zone, October 1959 Through December 1960," *J. Geophys. Res.* 67: 1235–1253, 1962.

Van Allen, J. A., "Spatial Distribution and Time Decay of the Intensities of Geomagnetically Trapped Electrons From the High Altitude Nuclear Burst of July 1962," in *Radiation Trapped in the Earth's Magnetic Field*, ed. by B. M. McCormac, Dordrecht, Holland: D. Reidel Publishing Co., 1966, pp. 575–592.

Vette, J. I., "Models of the Trapped Radiation Environment. Vol. I: Inner Zone Protons and Electrons," NASA SP-3024, 1966.

Williams, D. J., and Smith, A. M., "Daytime Trapped Electron Intensities at High Latitudes of 1100 Kilometers," *J. Geophys. Res.* 70: 541–556, 1965.

Williams, D. J., Arens, J. F., and Lanzerotti, L. J., "Observations of Trapped Electrons at Low and High Altitudes," *J. Geophys. Res.* 73: 5673–5696, 1968.

Zmuda, A. J., Pieper, G. F., and Bostrom, C. O., "Trapped Protons in the South Atlantic Magnetic Anomaly, July Through December 1961," 3. "Magnetic Storms and Solar Proton Events," *J. Geophys. Res.* 70: 2045–2056, 1965.

# LONG-TERM BEHAVIOR OF ENERGETIC INNER-BELT PROTONS

H. H. Heckman
Lawrence Radiation Laboratory, University of California
Berkeley, California

P. J. Lindstrom
Space Sciences Laboratory, University of California
Berkeley, California

and

G. H. Nakano
Research Laboratories, Lockheed Missiles and Space Company
Palo Alto, California

## ABSTRACT

This report summarizes experimental results since late 1962 of the temporal behavior of low-altitude trapped protons, $E \geqslant 57$ MeV. These data are interpreted in terms of the time-dependent continuity equation, using a source function that is empirically deduced from the data. The observed changes in the flux of 63-MeV protons between 1963 and mid-1969 are in agreement with those expected from solar-cycle changes in the atmosphere. Preliminary calculations that include semiannual as well as solar-cycle atmospheric density variations indicate that beginning in 1967 semiannual changes in the 60-MeV proton flux should be observable at altitudes below about 350 km. Our flux measurements are consistent with this computational result.


## INTRODUCTION

Since late 1962, we have monitored the low-altitude trapped protons, $E \geqslant 57$ MeV, using emulsion detectors recovered from oriented, polar-orbiting satellites. The span of nearly 7 years during which these observations have taken place constitutes a significant part of the current 11-year solar cycle. As part of this work, properties of the inner radiation belt protons have been examined in detail for a period concurrent with solar-minimum activity, from September 1962 through June 1966, by Heckman and Nakano (1969). Throughout the solar-minimum period the characteristic feature of the energetic trapped protons was their high degree of stability.

Coincident with increasing solar activity in mid-1966, there is substantial evidence for a diminution in the proton flux at $E = 63$ MeV (Nakano and Heckman, 1968). As of May 1969, the flux levels between 220- and 450-km altitude have decreased by more than a factor of two, relative to the solar-minimum period. It appears that the present solar cycle is very near the maximum. Consequently, the low-altitude proton flux is at, or near, its minimum value for this solar cycle.

This paper reports briefly on the latest results on the solar-cycle variations in the proton flux. The altitude-flux profiles and differential energy spectra of trapped protons during solar minimum are reviewed. The second part of this report presents some preliminary computational results, using the time-dependent continuity equation (Singer, 1958 and Dragt, 1969), which is compared with experimental data.

## PROPERTIES OF TRAPPED PROTONS 220- TO 450-km ALTITUDE

At low satellite altitudes, the inner radiation belt is detected only in the South Atlantic anomaly. This region, centered at approximately 34° S by 34° W, is the site of anomalously low intensities of the geomagnetic field and, hence, high fluxes of trapped radiation. The geometry of the South Atlantic anomaly is given in Figure 1. The solid-line contours are Injun 3 isoflux contours (in particles/cm$^2$-sec) for protons in the energy interval $40 < E < 110$ MeV at an altitude of 400 km (Valerio, 1964). The contours of constant $L$, computed by using the 48-coefficient Jensen and Cain geomagnetic field model (1962), are shown as dashed lines. The northward trajectories traversing the anomaly region are those of a typical 4-day satellite flight at 400-km altitude and 75° orbit inclination. Demonstrated here is the uniform sampling of the particle fluxes in the anomaly, as well as the limited range of the $L$-parameter. The magnetic field intensity, $B$, varies from 0.21 to 0.25 gauss over the range of $L$-values shown.

The inner-belt protons exhibited a high degree of stability during the recent solar-minimum period, September 1962 through June 1966 (Heckman and Nakano, 1969). Some of those temporally stable features of the inner-belt protons referred to in the second part of this report are illustrated in Figures 2 through 5. The altitude dependence of the omnidirectional flux of $E = 63$ MeV protons is presented in Figure 2. We plotted the average daily flux, $J$ (in protons/cm$^2$-day-MeV), normalized to a 90° orbit inclination, observed for each satellite flight, versus the average minimum mirror-point altitude, $\bar{h}_{\min}$. This flux refers only to those protons detected during northward passes of the satellite in the anomaly (see Figure 1). To remarkable precision, the altitude profile of the omnidirectional flux of 63-MeV protons can be fitted by a simple power-law function of the form $J(65\ \text{MeV}) \propto \bar{h}^n_{\min}$.

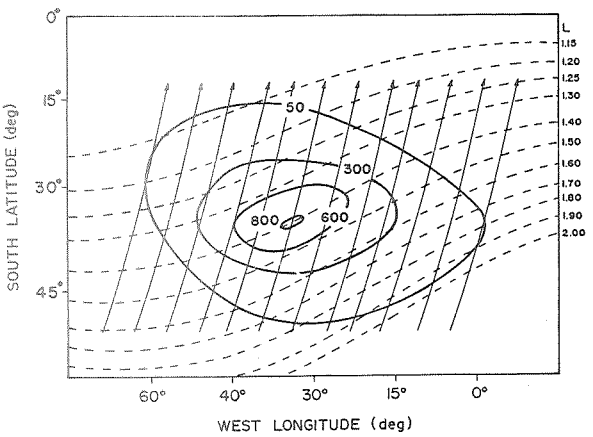


Figure 1—The South Atlantic anomaly. The heavy-line contours are Injun 3 isoflux contours for protons, $40 < E < 110$ MeV, at 400-km altitude. Dashed lines are contours of $L$ from the Jensen and Cain 48-coefficient field model. The northward traversals of a satellite, 75° orbit inclination, during a 4-day flight are shown as arrows.

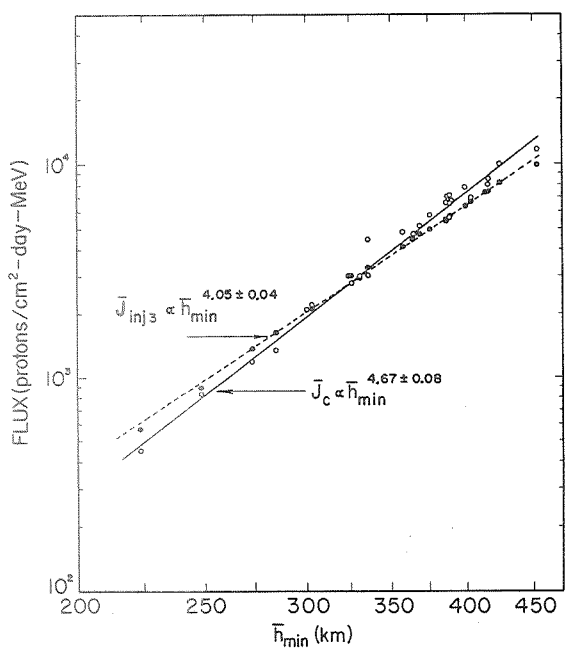


Figure 2—Omnidirectional flux of 63-MeV protons versus average minimum-mirror-point altitude during solar minimum, November 1962 to June 1966. Experimental data are shown as open circles; the least-squares fit to these is denoted by $J_c$. Computed Injun 3 daily fluxes and least-squares fit are shown by the solid points and dashed line.

The experimental data are shown as open circles and are fitted to a least-squares power law, $J_c \propto \bar{h}_{min}^{4.67\pm0.08}$, to an accuracy of ±7.6% (SD). The computed daily fluxes for each flight, derived from the Injun 3 $B$-, $L$-proton-flux contours and the satellite ephemerides, are shown as dark circles. The least-squares fit to these data yields an exponent $n = 4.05 \pm 0.04$. Although the differences between the slopes of the observed and computed altitude-flux profiles are statistically significant, we believe the Injun 3 data (recorded between December 24, 1962 and September 28, 1963) reproduce well our solar-minimum data, clearly within the stated accuracy (20%) of the Injun 3 data.

Five measurements of the differential energy spectra for protons, $E > 57$ MeV, between June 1963 and June 1966, are given in Figure 3. The data are normalized to an altitude $\bar{h}_{min} = 375$ km, assuming the omnidirectional flux varies as $\bar{h}_{min}^{4.67}$, independent of energy. The errors of measurement are consistent with the spread in the data points. There is, therefore, no evidence for a change in the spectral shape of the protons during the solar-minimum period. In fact, the energy spectrum obtained by Heckman and Armstrong (1960) (shown as a dashed line, normalized at $E = 63$ MeV) also exhibits the same spectral shape. Thus, within the observational errors, the proton energy spectrum has been invariant for almost a complete solar cycle.

In what follows, the spectral shape of the spectrum between 50 and 90 MeV is needed. For this energy interval, we take the spectrum to be $dJ(E)/dE \propto E^{-0.72}$. This energy spectrum was first derived by Freden and White (1960) and is in agreement with the observed spectrum for $50 < E < 90$ MeV.

The temporal behavior of the omnidirectional proton flux at 63 MeV, between September 1962 and May 1969, is presented in Figure 4. Plotted as a function of time is the quantity $J(t)/J_c$, the ratio of the 63-MeV omnidirectional proton flux at time, $t$, to the least-squares flux, observed during the solar-minimum period (Figure 2). The data are grouped into three altitude ranges: (a) $220 < \bar{h}_{min} < 300$ km, (b) $300 < \bar{h}_{min} < 400$ km, and (c) $400 < \bar{h}_{min} < 455$ km. Within the experimental errors (the 5% statistical errors are indicated for the 300- to 400-km interval) we conclude that the flux of 63-MeV protons was, for all practical purposes, in a steady state at all altitudes between 220 and 455 km during the period November 1962 to June 1966.

Variations in the proton flux before and after the quiescent period are readily apparent. The high value of the flux observed in September 1962, the first measurement, can be attributed to the effects on the inner-belt protons of the Starfish nuclear detonation in July 1962 (Filz and Holeman, 1965). Near mid-1966, the proton flux began to decline and as of May 1969, had decreased to about 0.40 of its solar minimum value.

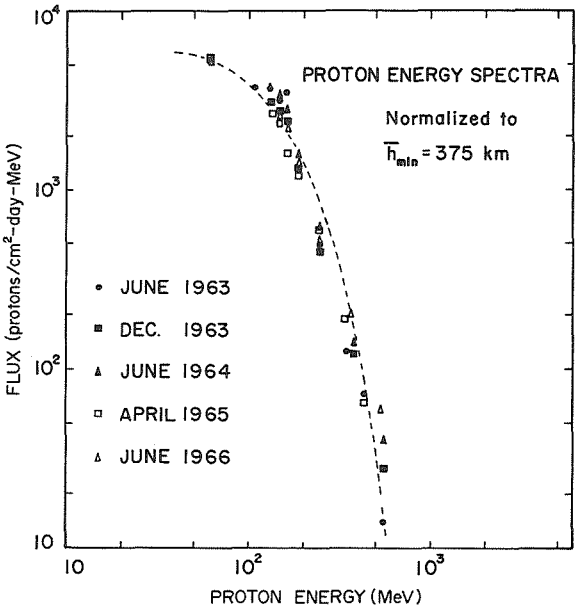


Figure 3—Differential energy spectrum for protons, $E > 57$ MeV, 1963 to 1966. Dashed curve is a smoothed fit to the spectrum measured in 1960 by Heckman and Armstrong.

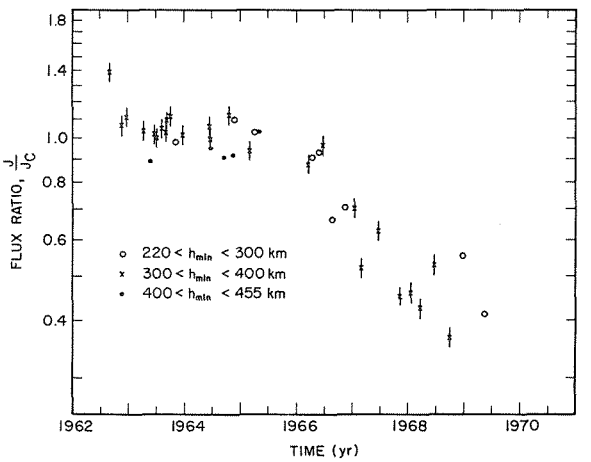


Figure 4—Temporal behavior of the 63-MeV omnidirectional proton flux, September 1962 to May 1969. Plotted are the ratios $J(t)/J_c$ versus time, where $J_c$ is the least-squares fit to the data for the period November 1962 to June 1966.

# CONTINUITY EQUATION: COMPUTATIONS

## Solar Cycle Variations

It is these experimental results that we wish to discuss in terms of the time-dependent continuity equation (Singer, 1958 and Freden and White, 1960)

$$\frac{dN}{dt} = S - \frac{d}{dE}\,\nu N(E)\frac{dE}{dx} - \rho\sigma\nu N\,, \qquad (1)$$

where

$N$ = particle density in particles/cm$^3$-MeV

and

$S$ = source strength in particles/cm$^3$-MeV-sec.

The second and third terms on the right are, respectively, the rates of particle loss due to energy loss by ionization and nuclear interactions in the residual atmosphere. For the atmospheric density averaged over the particles' trajectory, $\rho$, we used the results of Heckman and Brady (1966). In our present calculations, the results of Heckman and Brady, which are based on the Harris and Priester (1962 and 1963) model atmosphere, are reformulated in terms of $F_{10.7}$ (in $10^{-22}$ W/m$^2$-cps), the 10.7 solar flux. Furthermore, we have augmented the atmospheric density calculation to permit the evaluation of the effective atmospheric densities as a function of $F_{10.7}$ as well as $E$, the proton energy. The latter correction enters because the atmosphere traversed by a trapped particle is dependent on its cyclotron radius, hence energy, for a given minimum mirror-point altitude of the particle's guiding center (Heckman and Brady, 1966).

The experimental data cited above, when incorporated into solutions of Equation 1, should give some insight as to the source strength, altitude dependence, and the temporal behavior of the trapped protons. Explicitly, the data state that, in the energy interval $50 < E < 90$ MeV,

$$\frac{dN}{dt} \approx 0 \text{ (between 1963.0 and 1966.0)}\,,$$

$$N(h_{\min}) \propto h_{\min}^{4.67}\,(250 < h_{\min} < 450 \text{ km})\,,$$

and

$$N(E) \propto E^{-0.72}\,.$$

Given the time-dependent effective atmospheric density, $\rho(h_{\min}, E, F_{10.7}(t))$, where $F_{10.7}(t)$ is the monthly averaged 10.7-cm solar flux, our objective is to solve for the energy and altitude dependence of the source function, $S(E, h)$, from which the particle density $N(E)$ can be computed as a function of time and altitude.

To prepare Equation 1 for integration, we follow Freden and White (1960) and express the velocity, $v$, and rate of energy loss, $dE/dx$, in terms of power-law relationships in energy, $E$, for the interval $50 < E < 90$ MeV. Given a source strength, $S$, and a proton density at time $t$, $N(E, t)$, then, at time $t + \Delta t$,

$$N(E, t + \Delta t) = N(E, t) + \frac{dN(E, t)}{dt} \Delta t \,. \qquad (2)$$

Integration errors in Equation 2 are less than 0.1% for step size $\Delta t$ of 1 to 2 hours.

Is there an $S(E, h)$ such that an approximate steady-state solution is given by Equation 1 between 1963.0 and 1966.0, independent of $E$ and $h$? Yes, there is. As a particular example, $S(h)_{obs}$, for 60-MeV protons, that yields flux values that are practically constant during the solar-minimum period, $250 \leqslant h_{min} \leqslant 450$ km, are given in Figure 5. The errors assigned to $S(h)_{obs}$ represent the uncertainty in the source function that arises from the approximate scatter of ±10% in the flux measurements about their mean value for the period 1963.0 to 1966.0.

The significant result is that, between 250- and 450-km altitude, the source function is not constant (as one might expect were the proton source solely due to albedo-neutron decay), but decreases with increasing altitude according to $S(h)_{obs} \propto h_{min}^{-2.4}$. Also presented are the altitude dependences of $N$ (at 60 MeV) $\propto h_{min}^{4.7}$ (observed) and $\rho \propto h^{-7.0}$ (computed). As noted by Cornwall et al. (1965) the quantity $S/N\rho$ is a constant under equilibrium conditions. Our results are in good agreement with this condition. The numerical values of $S$ and $N$ need be relative only, because it is the ratio $S/N$ that is important here. However, to be somewhat realistic, we have adopted for $N$ (at 60 MeV) at 1963.0 the proton density obtained from the Injun 3 data for $h_{min}$ = 350 km, $L$ = 1.40 earth radii.

In their examination of the changes in $B$-, $L$-space with time, Lindstrom and Heckman (1968) pointed out that the minimum mirror-point altitudes in the South Atlantic anomaly are decreasing at a rate of $\dot{h} \approx 7$ km/year owing to the secular change of the earth's magnetic field. Such a drift in the minimum mirror-point trajectories in the anomaly produces an apparent source of protons of the amount $S_B = \dot{h}(dN/dh)$, where $\dot{h}$ is the inward drift velocity and $dN/dh$ is the altitude gradient of the proton flux. This apparent source is also shown. We note that its magnitude does not significantly contribute as a proton source at the lower altitudes, comprising only about 2% of $S_{obs}$ at 250 km. However, because of its strong dependence on altitude (that is, $S_B$ varies as $h^{3.7}$) the $S_B$ source becomes quite significant for higher altitudes, and can account for nearly one-half of $S_{obs}$ for altitudes above 450 km. It should be stressed that the apparent source, $S_B$, arises solely from the dynamic behavior of the geomagnetic field and is independent of any assumptions as to nonadiabatic behavior in the particle motion.

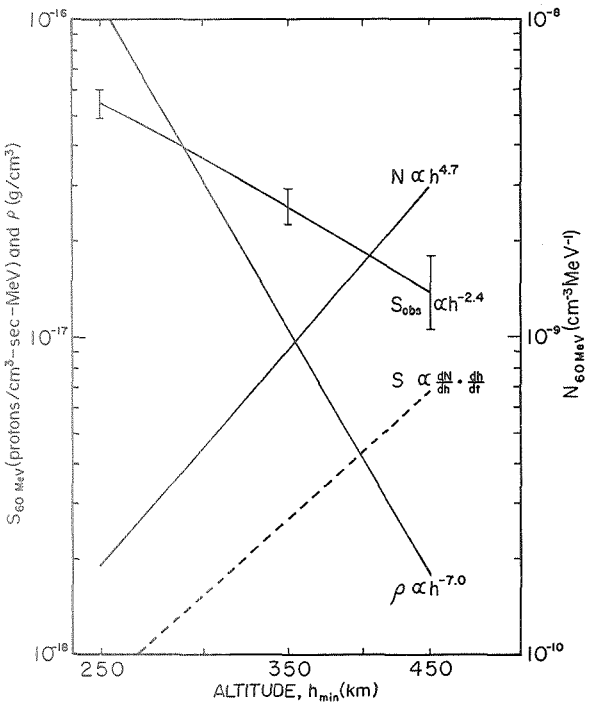


Figure 5—Altitude dependence of source function of 60-MeV protons, $S_{obs}$, required to account for a constant flux level observed between 1963.0 and 1966.0. The altitude dependence of the measured proton density, $N(h)$, and computed effective atmospheric density, $\rho(h)$, for 1963.0 are also shown. The source $S_B$ is the apparent source of 60-MeV protons arising from the lowering of the mirror-point trajectories owing to the secular variation of the geomagnetic field.

The results of computations on the solar-cycle variations in the flux of 60-MeV protons are presented in Figures 6 and 7. Figure 6 shows the temporal behavior at 250, 350, and 450 km at $L$ = 1.40 between January 1963 and May 1969. Plotted versus time are the computed ratios $j(t)/j(1963.0)$. The experimental data (Figure 4) are superimposed on the computed curves for comparison.

The good agreement between the solutions of the continuity equation and our experimental data is most encouraging. Between 1963.0 and 1966.0, the empirical source function, $S_{obs}$, reproduces well the observed constancy of the proton flux. As solar activity developed after 1966, the computations show the characteristic differences in the behavior of 60-MeV protons as the altitude and, hence, lifetimes, increase. Since mid-1967, the calculations indicate that the proton flux at 250 km has sustained a nearly constant minimum value, coincident with the plateau in activity during solar maximum. That is in contrast to the fluxes at 350 and 450 km, which were still decreasing in early 1969. Such an effect accounts for the apparently high values of $J/J_c$ observed in our last two flights ($\bar{h}_{min}$ = 224 and 299 km).

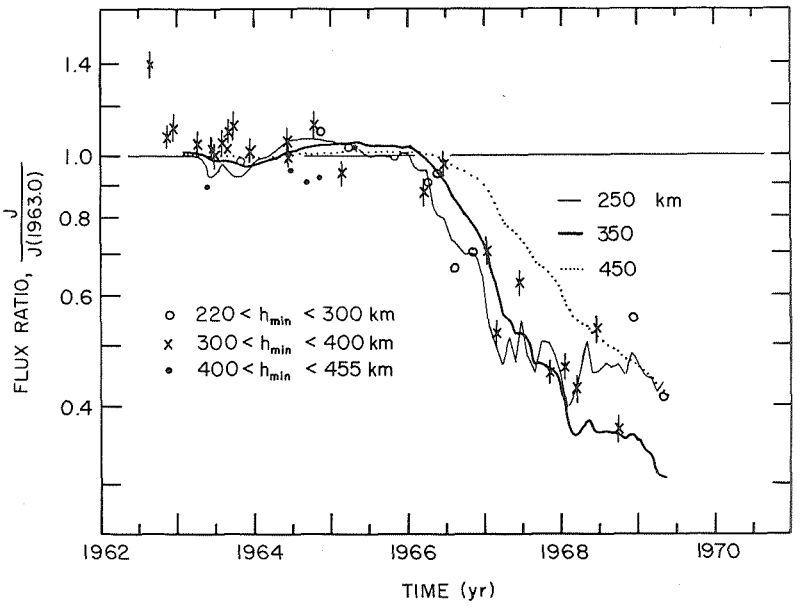


Figure 6—Computed ratios of $J(t)/J(1963.0)$ at 60 MeV and minimum-mirror point altitudes of 250, 350, and 450 km, $L$ = 1.40, between January 1963 and May 1969, given source $S_{obs}$. Flux data from Figure 4 are also shown.

## Starfish Redistribution

Filz and Holeman (1965) have reported that an abrupt increase in the low-altitude proton flux followed the Starfish nuclear detonation on July 9, 1962. At 350 ± 50 km, their data indicate the proton flux was increased by about seven times over its prebomb level by this event, owing to a nonadiabatic redistribution of the low-altitude protons. On the basis of Filz and Holeman's work (1965) we would conclude that the proton flux decayed within 1 year to a constant level, which was some two and one-half times the prebomb level. It is evident, therefore, that the temporal behavior of the inner belt, which we have been studying, has likewise been artificially perturbed. To examine this further, we have carried out the integration of Equation 1 for the flux $J(t)_{60\ MeV}$ at $h_{min}$ = 350 km beginning 1953.0, under the assumption that $S_{obs}$ is time independent. Two initial arbitrary flux values were assumed: (a) $J(1953.0)$ = 9.2 protons/cm$^2$-sec-MeV, equal to the 60-MeV flux observed in 1964, one full solar cycle later, and (b) $J(1953.0)$ = 3.2 protons/cm$^2$-sec-MeV.

The results of this computation are presented in Figure 7. Solutions (a) and (b) converge to a unique solution after 1958.5, yielding a $J(t)$ that is independent of initial conditions. The anticorrelation of the proton flux with the atmospheric density, the latter shown by the dashed line is well illustrated. The computed curves of $J(t)$ from 1958 through 1968 display how flux changes at 60 MeV would have occurred had there been no Starfish detonation and, hence, proton redistribution. Our interpretation of the sequence of events portrayed is that, on July 9, 1962, the Starfish detonation caused a rapid increase in the proton flux, and, after an apparently short-lived transient period, settled down to a 3-year, steady-state condition. This steady-state phenomenon was fortuitously produced when the natural solar-cycle increase in the proton flux was just compensated by the decay of the Starfish perturbation. The difference between the Starfish and no-Starfish calculations is, in fact, an exponential decay curve. The particle data denoted by circles are from Filz and Holeman (1965); the data of this experiment are shown as $X$'s. All the data are restricted to $\bar{h}_{min}$ = 350 ± 50 km. The two sets of data points are independently normalized to the computed, steady-state condition for 1963.0 to 1966.0. We believe it is significant that the relative changes in the (57-MeV) proton flux observed by Filz and Holeman at 350-km altitude, before and after the Starfish detonation, are in agreement with calculations that were, in turn, based on our independently measured post-Starfish data. Finally, we note that the effects of Starfish have now virtually disappeared for altitudes of 350 km and less. Henceforth, the inner-proton belt will be (one hopes) in its natural state at these low altitudes.

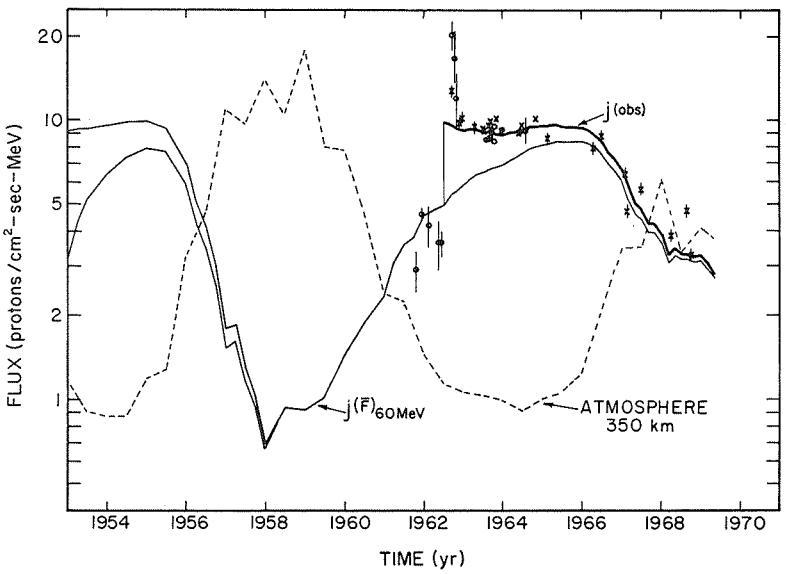


Figure 7—Computed proton flux $J(t)_{60\ MeV}$ at $h_{min}$ = 350 km, beginning 1953.0, assuming source $S_{obs}$ is constant, and initial flux values $J(1953)$ = 9.2 and 3.2 $cm^{-2}$ $sec^{-1}$ $MeV^{-1}$. Unique solution is obtained at this altitude after 1958.5. The Starfish redistribution on July 9, 1962, the 3-year steady-state, 1963 to 1966, and the abrupt solar-cycle decrease in the proton flux after mid-1966 are reproduced in these calculations. The data denoted by open circles are from Filz and Holeman; the x's, this experiment. The data points are limited to $\bar{h}_{min}$ = 350 ± 50 km. Solar-cycle behavior of atmosphere at 350-km altitude is given by the dashed curve.

## Semiannual Variations

Recent satellite atmospheric-drag results have revealed that during the course of our particle measurements, the semiannual and solar-cycle density variations in the atmosphere have been comparable in magnitude at altitudes between 191 and 1030 km (King-Nele et al., 1968 and 1969 and Cook and Scott, 1967). The semiannual variation has yet to be explained, although the effect has been well documented. It is adequate for our purposes that, to the extent it has been studied over an 8-year period, the semiannual effect is a highly stable, global phenomenon (Jacchia et al., 1969). Irrespective of altitude and local time, the atmosphere exhibits in-phase world-wide density variations, the minima occurring on about January 26 and July 25, and the maxima on April 1 and November 1. Although the periods between minima and maxima are not equal, the dates on which they occur have been determined to within an accuracy of several days. The minimum-to-maximum density ratios affected by the semiannual variation are typically 1:2. The observed amplitudes of the density variations appear to be related to temperature variations in the thermosphere, the latter being correlated with the intensity of the 10.7-cm solar flux.

It is quite obvious, then, that when proton lifetimes are less than about 6 months, observable semiannual changes in the flux of inner-belt protons should occur. To investigate this statement quantitatively, we have attempted to include in our atmosphere model a realistic description of the semiannual density variations. To do so, we have referred to the works of King-Hele et al. (1968 and 1969) and Cook et al. (1967), who have, since 1964, examined the semiannual variations at altitudes 191, 470, 480, and 1130 km. We have collected these data and presented them in Figure 8. To reveal the semiannual variation, diurnal and solar-activity effects have been removed from the data. The residual semiannual variations were then reduced to an $\bar{F}_{10.7}$ that was characteristic of the time during which the atmospheric density measurements were made. The dashed lines through the data are the analytical functions we use to represent the semiannual effect.

We now have a description of a (bounce- and drift-averaged) Harris and Priester atmospheric model that includes both solar-cycle and empirical semiannual time variations. The flux changes for 60-MeV protons predicted by the continuity equation with this model atmosphere are given in Figure 9. Upon comparing this figure with Figure 6, we see that the semiannual density changes

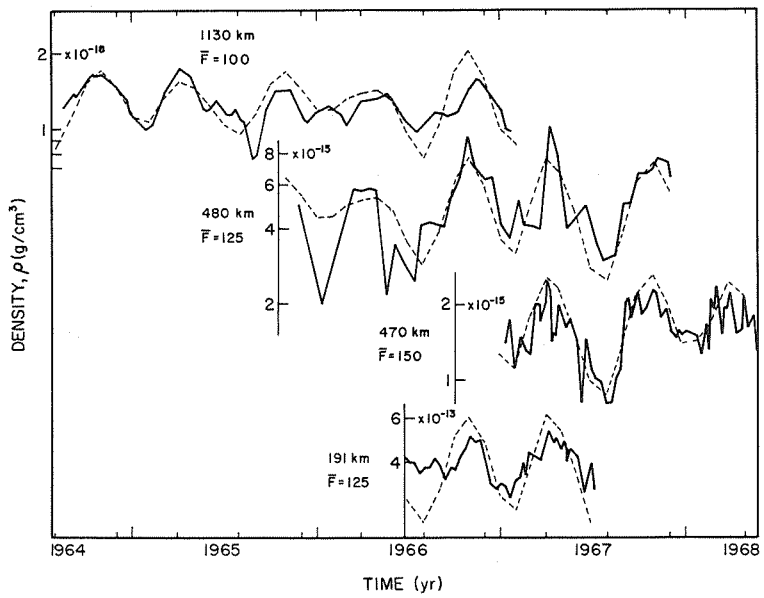


Figure 8—Semiannual density variations in the atmosphere, reproduced from King-Hele et al. and Cook and Scott. Dashed curves are analytic functions used to represent the semiannual density changes in the computations.

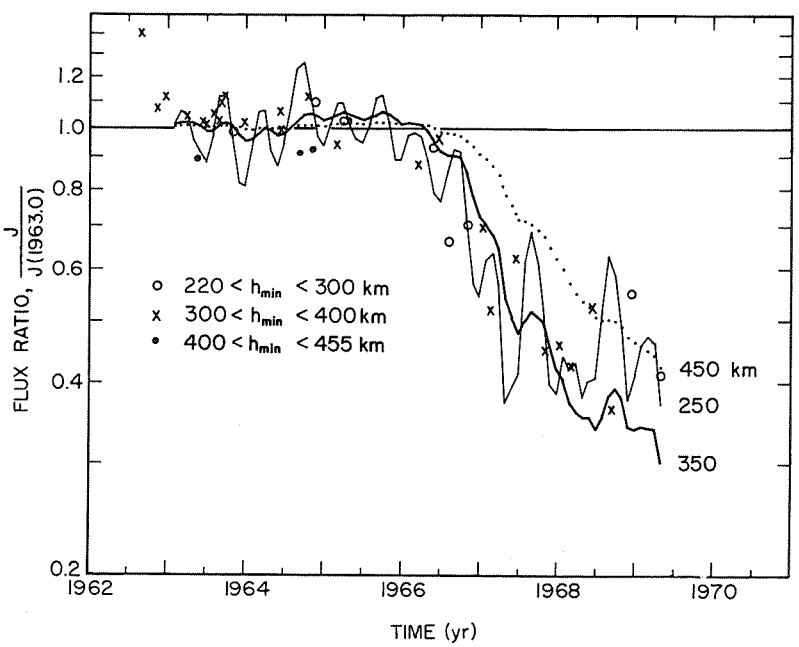


Figure 9—Calculated $J(t)/J(1963.0)$ at 60 MeV at $h_{min}$ = 250, 350, and 450 km when both solar-cycle and semiannual density changes are incorporated into the continuity equation. Again, the experimental data are shown for comparison with the theory.

are clearly present at 250 km, but not so at 350 and 450 km. There are two salient features of these computations that are in accord with the experimental data.

First, between 1963.0 and 1966.0, the semiannual changes in the proton fluxes are small; that is, they are typically equal to or less than the experimental errors. The computed results continue to exhibit a very stable flux level during solar minimum.

Second, as solar activity increases, the average density of the atmosphere increases and the proton lifetimes decrease. Consequently, the response of the trapped protons to changes in the atmosphere becomes more pronounced. This is exemplified by the increasing semiannual oscillations in the proton flux since 1967. The observed amplitudes of the fluctuations in the proton-flux measurements since 1967 are consistent with this interpretation.

Because of the preliminary and sensitive nature of the calculations to our atmospheric and magnetic field models, we do not attribute any significance to the fact that the variations in the 350 ± 50-km data appear to be characteristic of an altitude slightly less than 350 km.

Thus far, a number of instances in which the experimental data are accounted for by theory have been discussed. In contrast to this, an interesting, and perhaps quite important, observation can be made by closely examining Figure 9. It is that the observed flux changes are not in phase with the computed semiannual flux variations. Taken at face value, the flux changes appear to be out of phase with the solutions of the continuity equation by about 5 weeks. Surprisingly, this phase difference is such that the proton-flux variations are nearly in phase with the semiannual density changes in the atmosphere. The significance of this observation is certainly not clear at this time. We wish, however, to make the following observation. The principal unknown in the theory of the energetic, inner-belt protons is the source. We have treated the source $S(E, h)$, therefore, as an empirical quantity to be determined by experiment. Using this approach, we find that this empirical source, $S_{obs}$, decreases with increasing altitude. The only other physical entity that decreases with altitude is the density of the atmosphere. The implication, then, is that there is an effective source of trapped protons related somehow to the atmosphere, indicative of pitch-angle scattering.

## SUMMARY

On the basis of our experimental studies on the temporal behavior of low-altitude, inner-belt protons, and their interpretation in terms of solutions of the time-dependent continuity equation, using an empirically determined source function, we make the following conclusions.

The observed temporal changes in the flux of 63-MeV protons since 1963, $220 < \bar{h}_{min} < 450$ km, are in agreement with those expected from the solar-cycle changes in the atmosphere.

The computed time-history of the proton flux at 60 MeV before and after the Starfish detonation is in excellent agreement with the observations of Filz and Holeman, as well as with our post-Starfish data.

For altitudes of about 250 km, semiannual density changes in the atmosphere should be observable in flux changes of protons, $E \leqslant 60$ MeV. That a phase difference may exist between the observed and computed semiannual changes in the proton flux is unexpected and needs to be explained.

Pitch-angle diffusion, which may be an effective source strongly correlated with the atmospheric density, must now be included in the theory in order to see whether or not it can account for the altitude dependence of the source function implicated by our experimental observations.

## ACKNOWLEDGMENT

This work was done under the auspices of the U.S. Atomic Energy Commission, the National Aeronautics and Space Administration, Contract NAS 9-5249, and the Lockheed Missiles and Space Company, Independent Research.

## REFERENCES


Blanchard, R. C., and Hess, W. N., "Solar Cycle Changes in Inner-Zone Protons," *J. Geophys. Res.* 69: 3927, 1964.

Cook, G. E., and Scott, D. W., "Variations in Exospheric Density at Heights Near 1100 km, Derived From Satellite Orbits," *Planet. Space Sci.* 15: 1933, 1967.

Cornwall, J. M., Sims, A. R., and White, R. S., "Atmospheric Density Experienced by Radiation Belt Protons," *J. Geophys. Res.* 70: 3099, 1965.

Dragt, A. J., "Solar-Cycle Modulation of the Radiation Belt Proton Flux," University of Maryland Technical Report 938, Feb. 1969.

Filz, R., and Holeman E., "Time and Altitude Dependence of 55-MeV Trapped Protons, August 1961 to June 1964," *J. Geophys. Res.* 70: 5807, 1965.

Freden, S. C., and White, R. S., "Particle Fluxes in the Inner Radiation Belt," *J. Geophys. Res.* 65: 1377, 1960.

Harris, I., and Priester, W., "Theoretical Models for the Solar-Cycle Variation of the Upper Atmosphere," *J. Geophys. Res.* 67: 4585, 1962; also NASA Technical Note D-1444, 1962.

Harris, I., and Priester, W., "Relation Between Theoretical and Observational Models of the Upper Atmosphere," *J. Geophys. Res.* 68: 5891, 1963.

Heckman, H. H., and Armstrong, A. H., "Energy Spectrum of Geomagnetically Trapped Protons," *J. Geophys. Res.* 67: 1255, 1962.

Heckman, H. H., and Brady, V., "Effective Atmospheric Losses for 125-MeV Protons in South Atlantic Anomaly," *J. Geophys. Res.* 71: 2791, 1966.

Heckman, H. H., and Nakano, G. H., "Low-Altitude Trapped Protons During Solar Minimum Period, 1962–1966," *J. Geophys. Res.* 74: 3575, 1969.

Jacchia, L. G., Slowey, J. W., and Campbell, I. G., "A Study of the Semi-Annual Density Variation in the Upper Atmosphere From 1958 to 1966, Based on Satellite Drag Analysis," *Planet. Space Sci.* 17: 49, 1969.

Jensen, D. C., and Cain, J. C., "An Interim Geomagnetic Field," (abstract), *J. Geophys. Res.* 67: 3568, 1962.

King-Hele, D. G., and Hingston, J., "Air Density at Heights Near 190 km in 1966–7, From the Orbit of Secor 6," *Planet. Space Sci.* 16: 675, 1968.

King-Hele, D. G., and Hingston, J., "Variations in Air Density at 480 km, From the Orbit of Midas 2," *Planet. Space Sci.* 16: 937, 1968.

King-Hele, D. G., and Walker, D. M. C., "Air Density at a Height of 470 km Between January 1967 and May 1968, From the Orbit of the Satellite 1966-118A," *Planet. Space Sci.* 17: 197, 1969.

Lindstrom, P. J., and Heckman, H. H., "B-L Space and Geomagnetic Field Models," *J. Geophys. Res.* 73: 3441, 1968.

Nakano, G. H., and Heckman, H. H., "Evidence for Solar-Cycle Changes in the Inner-Belt Protons," *Phys. Rev. Lett.* 20: 806, 1968.

Singer, S. F., "Trapped Albedo Theory of the Radiation Belt," *Phys. Rev. Lett.* 1: 181, 1958.

Valerio, J., "Protons From 40 to 110 MeV Observed on Injun 3," *J. Geophys. Res.* 69: 4949, 1964.

# THE PARTICLE ENVIRONMENT AT THE SYNCHRONOUS ALTITUDE

G. A. Paulikas
and
J. B. Blake
Space Physics Laboratory
The Aerospace Corporation
El Segundo, California

# INTRODUCTION

The synchronous orbit is now perhaps the region of space most densely populated by satellites. The obvious advantages obtained by communications and meteorological instrumentation placed in this orbit have resulted in a satellite population explosion at the synchronous altitude. More than 50 satellites had been placed into synchronous or nearly synchronous orbit as of late 1969.*

The requirements for engineering data about the synchronous radiation environment were realized at an early date and the now historic electron flux compilation by Vette and Lucero (1967) resulted. It is interesting to note that no data from satellites in a truly synchronous orbit were used in the Vette/Lucero compilation since no synchronous satellite was instrumented with particle radiation detectors prior to 1966. Data obtained at or near the synchronous orbit from satellites in elliptical orbits were used to construct the model electron environment. In a subsequent study, King (1967) presented a model of the low-energy trapped proton environment for the outer zone, including the synchronous orbit.

The first satellite, in synchronous orbit, equipped with an array of radiation detectors was the ATS 1 launched in December 1966. Subsequently, other satellites with complements of particle instrumentation have been placed into this orbit. A picture of the synchronous particle population and the changes that this population undergoes with changing magnetic activity can now be constructed, based on data from geostationary satellites. Table 1 lists the satellites which are now in orbit and have contributed (or will, hopefully, contribute) to the picture of the particle environment at synchronous altitude. The amount of available data regarding the particle environment at this altitude is now immense; the present report will consider, in the main, data obtained by the Aerospace Corporation omnidirectional spectrometer on ATS 1.

The synchronous orbit is also very interesting from the point of view of radiation belt physics. Some separation of spatial variation from temporal effects can be obtained because the satellite samples only a limited range of the magnetic field. Field lines connect the synchronous region with the auroral zone and experiments correlating measurements on the magnetic equator with the foot of the field line can be readily done (Parks et al., 1968). Solar protons penetrate readily to this altitude and the question of access of solar particles to the polar regions is intimately connected with solar particle access to the synchronous altitude.

Because the synchronous orbit coincides approximately with the center of the ring current (Frank, 1968), the particle population exhibits extremely dynamic behavior and construction of an average picture of the environment requires an almost statistical approach. Such an approach was initially used by Vette and Lucero to order the energetic electron data and this approach, where possible, has been adopted in this paper.

While most of the time a synchronous satellite is comfortably within the domain of closed field lines, the synchronous orbit approaches the trapping boundary on the night side. During magnetically active periods, plasma intruding from the tail of the magnetosphere may reach down to these altitudes (Freeman, 1968 and Freeman and Maguire, 1967). This causes perturbations of the field lines on the night side of the earth (the field may sometimes become almost radial) and, therefore, very significantly modifies the trapped particle population.

In several instances on record, changes in the solar wind momentum were sufficiently large to compress the boundary of the earth's magnetic field to a radius $<6.6$ earth radii. At those times, of course, the energetic particles disappeared and were replaced by low-energy particles characteristic of the magnetosheath.

Solar protons have surprisingly free access to the synchronous region even during times of magnetic calm (Lanzerotti, 1969). During magnetically active periods, solar protons well below 1 MeV can enter the synchronous region with essentially full efficiency. Thus, solar particles also form an important constituent of the particle environment.

In the subsequent sections of this paper, the behavior of the population of trapped energetic electrons and the penetration of solar protons to the synchronous orbit will be discussed in detail. Although present only temporarily at the synchronous altitude following solar proton events, solar protons are an important element in the total radiation picture near the period of maximum solar activity (Lanzerotti, 1969).

*TRW Space Log.

Table 1
Scientific Satellites at Synchronous Altitude.

| Satellite | Launch |
|---|---|
| ATS 1 | December 1966 |
| OV2 5 | September 1968 |
| ATS 5 | August 1969 |

The limitations of the subject matter of the present report (high-energy electrons and protons) should not obscure the underlying unity and interrelation of the behavior of the trapped particle population. It is particularly important to remember that the bulk of the particle energy density resides in the low-energy (approximately tens of keV) population of trapped protons and electrons. The behavior of the trapped energetic electrons and solar protons merely reflects the interaction of the low-energy ring-current particles and the geomagnetic field; energetic electrons and solar protons do not contribute much energy to this particle-field interaction.

## THE MAGNETIC CONTAINER*

Central to the discussions of the particle population and the spatial and temporal variations of these particles is an understanding of the configuration of the geomagnetic field which confines and guides the motion of the charged particles. Figure 1 is a qualitative picture of the magnetosphere and shows the location of the synchronous orbit (at 6.6 $R_e$) in relation to the main features of the magnetosphere. As can be seen, the earth's magnetic field at high altitudes loses cylindrical symmetry and dipolelike character because of the distortion of the terrestrial field caused by the solar wind. A satellite at the synchronous orbit sees a diurnal variation (in the absence of temporal variation) in the strength and orientation of the magnetic field as well as in the trapped particle population. The loss of cylindrical symmetry has an important effect upon trapped particle motion in that the parameter $L$ becomes a function of pitch angle, so that the longitudinal drift path is now pitch-angle dependent. The families of drift paths for two extremes of equatorial pitch angle are shown in Figure 2 in relation to the synchronous orbit. A satellite at 6.6 $R_e$ samples a range of particle-drift shells which, for the particular magnetospheric parameters used in the calculation of the curves of Figure 2, have equatorial crossings from 6.1 to 7.6 $R_e$. Measurements of omnidirectional flux such as form the bulk of this compilation, therefore, are representative of a range of radial distance (Roederer, 1967, 1968, and 1969).

An important consequence of the asymmetry of the magnetosphere is that particles can be locally trapped yet be unable to execute a complete longitudinal drift period. Such particles are called quasi-trapped, and their mirror points are located in the quasi-trapping regions of Figure 1. Particles mirroring at high latitudes near local noon are connected with open lines in the tail. Conversely, particles mirroring at low latitudes near the midnight meridian will drift out the flanks of the magnetosphere and fail to complete a longitudinal circuit. The particle angular distribution which results is illustrated (in a qualitative manner) in Figure 3. A drift loss cone appears, in addition to the usual bounce loss cone associated with particle loss into the atmosphere. In general, the drift loss cone can be much larger than the small (about 3°) bounce loss cone and thus modify the angular distributions in an important way. Since the synchronous orbit often enters the region of quasi-trapping, the existence of the drift loss cones must be explicitly considered. White et al. (1969) have experimentally confirmed the theoretical predictions by detecting the existence of a proton drift loss cone.

The model of Mead and Williams (1965) used to calculate Figure 2, has proved to be a good representation of the quiet-time magnetic field at the synchronous orbit. Roederer et al. (1968) using ATS 1 magnetometer data have devised a procedure to adjust the parameters contained in the Mead-Williams model and in this way analytically reproduce the observed field components and the diurnal variation in these field components. The quiet-time magnetic field can thus be reasonably well related to a field model. (This model neglects such refinements as the diurnal and seasonal variation of the aspect of the earth's magnetic field axis with respect to the solar wind.) In effect, then, extended measurements of magnetic field components at the synchronous altitude amount to synoptic monitoring of the shape and configuration of the entire magnetosphere (Roederer, 1969).

## ENERGETIC ELECTRONS AT THE SYNCHRONOUS ALTITUDE

### Typical Data

To set the background for subsequent discussions, we present in this section several sequences of data that illustrate the variability of the electron fluxes at synchronous altitude. The data show the transition from magnetically quiet to disturbed conditions

* An extensive review of the properties of the magnetic field at the synchronous altitude can be found in a report by Coleman (1968).

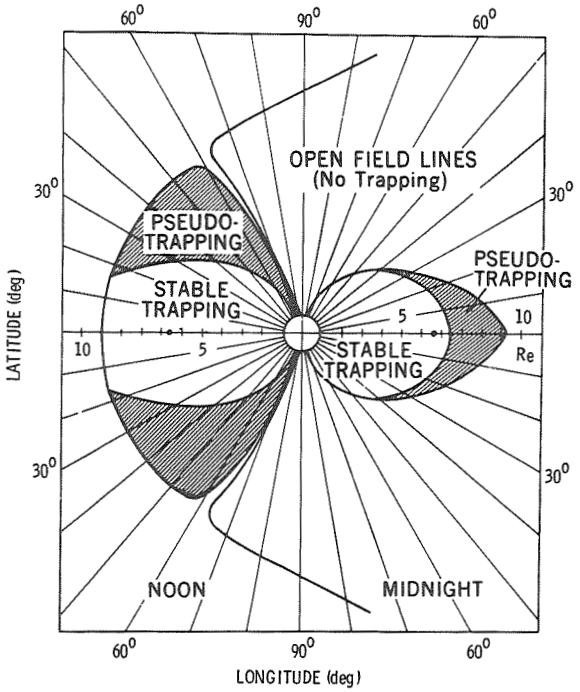


Figure 1—Location of synchronous orbit (dot at 6.6 $R_e$) in a Mead-Williams model of the magnetosphere. Particles mirroring in pseudo-trapping regions cannot complete a longitudinal drift and are lost from the magnetosphere (Roederer, 1967 and 1968).

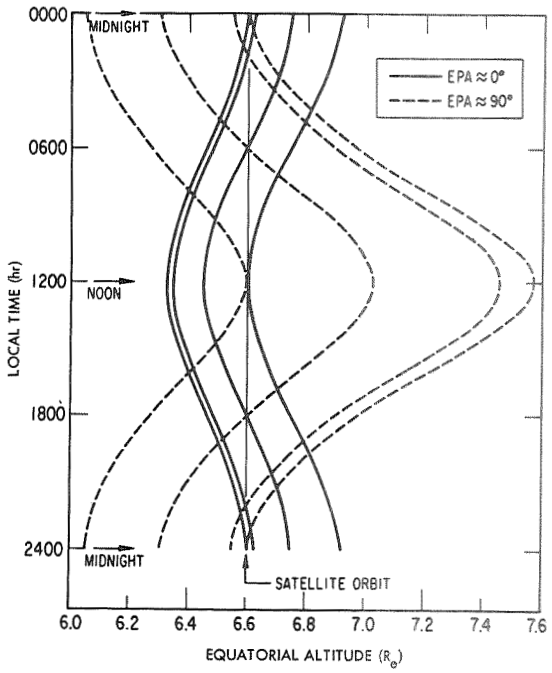


Figure 2—Drift paths (equatorial-crossing altitudes) of electrons for particles mirroring near equator (EPA = 90°) and those mirroring at high latitudes (EPA = 0). Computations were performed assuming a magnetosphere termination at 10 $R_e$ on the noon meridian and a neutral sheet extending from 8 to 200 $R_e$ on the midnight meridian. Tail field of 15$\gamma$ was assumed.

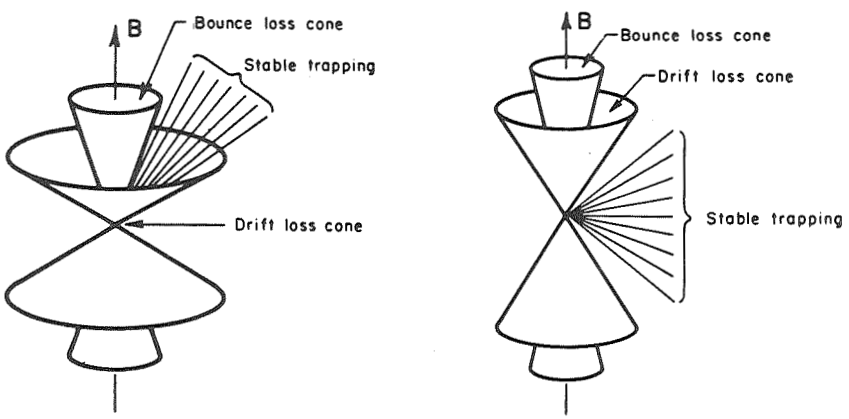


Figure 3—Schematic representation of angular distributions on the magnetic equator for: (a) local midnight and (b) local noon (Roederer, 1967 and 1968).

and the characteristics of the electron fluxes associated with varying degrees of magnetic activity. Inspection of all data available to us (December 6, 1966 to January 1, 1969) indicates that such sequences of quiet and disturbed electron fluxes are typical and can serve as a model for the discussion below.

Figure 4 illustrates a decrease in the energetic electron flux associated with a moderate magnetic disturbance. Typical diurnal variations in the electron fluxes are found on December 31 ($K_p$ = 6−) and January 2 ($K_p$ = 14−). The small disturbance occurring on January 1 ($K_p$ = 24−) created a very different curve of flux versus local time, one rich in short time-scale fluctuations and with energetic ($E_e$ > 1.9 MeV) electron flux depressed by about an order of magnitude.

The data for January 6, ($K_p$ = 11o), presents a striking example of transition from very smooth count rates to a profile of count rate versus time containing a wealth of fine structure (Figure 5). Here there clearly is a pronounced diurnal variation, ranging from about a factor of two for electrons >300 keV (top trace) to a factor of 10 for electrons >1.9 MeV (bottom trace).

The small-scale fluctuations are real and represent drift periodic echoes. Small changes in the position of the magnetopause result in motion of the electron flux distribution past the satellite, repeating with a period characteristic of the longitudinal drift. A complete analysis of this effect has been made by Brewer et al. (1969) using the data of Lanzerotti et al. (1967). An excellent example of drift periodic echoes for the day 351, 1966 is represented in Figure 6.

A very disturbed period starts on January 7 ($K_p$ = 27+). Subsequent days (Figure 7) show the postdisturbance period and the gradual return to quiet magnetic conditions. Recoveries (and depressions) of particle fluxes appear to contain adiabatic as well as nonadiabatic phases.

Examination of the data for several years obtained by this experiment shows that a more or less smooth diurnal variation persists during magnetically quiet times with the maxima in the electron flux occurring near local noon and the minima near local midnight. Magnetic storms introduce large changes in the electron fluxes at all local times and disrupt the diurnal variation found during quiet and moderately disturbed times. As viewed by the satellite, the fluxes of energetic electrons (>300 keV) are depressed and fluctuate irregularly during a storm. Another signature of a magnetic storm is a depressed and irregularly fluctuating magnetic field. The fluxes recover to prestorm levels with time constants that are of the order of days and appear to depend, among other things, on the energy of the particle. During a magnetic storm the omnidirectional electron fluxes show a great deal of fine temporal structure on time scales of minutes. The storm-time behavior of energetic electrons is illustrated in Figure 8.

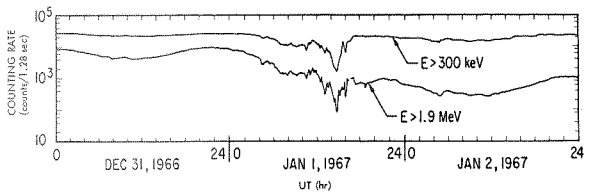


Figure 4—Counting rates of energetic electrons above two thresholds from December 31, 1966 through January 2, 1967. To convert from UT to local time for all ATS 1 data, subtract 10 hours.

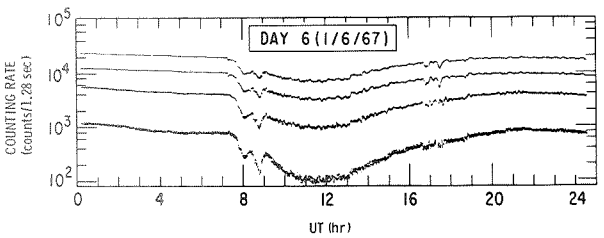


Figure 5—Electron counting rates for January 6, 1967 versus universal time. Traces, from top to bottom, represent electrons >300 keV, >450 keV, >1.05 MeV, and >1.9 MeV. To convert from UT to local time for all ATS 1 data, subtract 10 hours.

The unusual feature of the storm of January 13 and 14 is that the energetic electrons vanished for a time period of the order of half an hour, that is, the counting rates dropped to what might be expected from cosmic ray background (Figure 9) and reappeared (Figure 10) in a manner that suggests that the satellite moved in and out of the region of trapping of energetic electrons (see compilation, 1968). This observation was confirmed by the UCLA magnetometer data from ATS 1. The field reversed direction and became somewhat disordered in association with the disappearance of energetic electrons. This phenomenon occurred at local times from 1400 to about 1500; previous measurements by other satellites have shown that the domain of energetic electrons extends to >8 $R_e$ on the sunward side of the magnetosphere.

This magnetic storm does not differ from the previous disturbed period (January 7–8, 1967) or from other magnetic storms that were observed during the first part of 1967 as far as surface magnetograms and ATS 1 energetic electron data are concerned. Typical behavior of energetic electrons during disturbed times is characterized by the following features: (a) transition from smooth flux-versus-time profiles to those containing much temporal structure in all integral electron channels, (b) general depressions of energetic electron fluxes during the storm, with all local times affected, and (c) a poststorm recovery period without any diurnal variation during which the electron fluxes gradually recover to the prestorm levels. The complete disappearance of energetic electron count rates near 0007 UT on January 14 (Figure 9) and the subsequent appearance and disappearance of these particles (Figure 10) suggest that the satellite was moving in and out of the region of trapping.

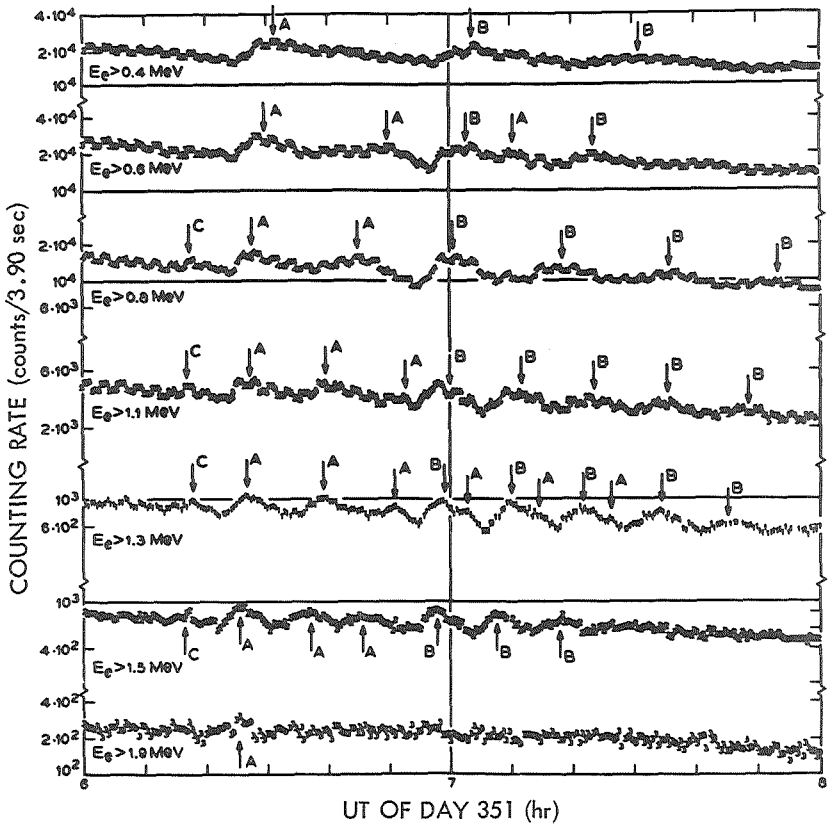


Figure 6—Drift periodic electron echoes observed by the Bell Telephone Laboratories experiment aboard ATS 1. Each repeated letter represents the same group of electrons making repeated transits past the satellite as they drift in longitude (Brewer et al., 1969).

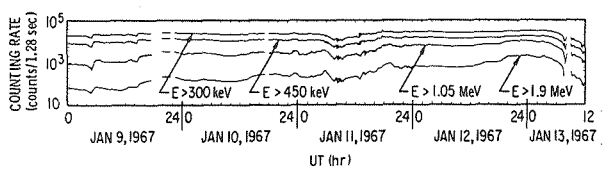


Figure 7—Counting rates of energetic electrons from January 9, 1967 through January 13, 1967. This sequence of data illustrates the recovery of the electron fluxes after the magnetic storm of January 7 and 8, 1967.

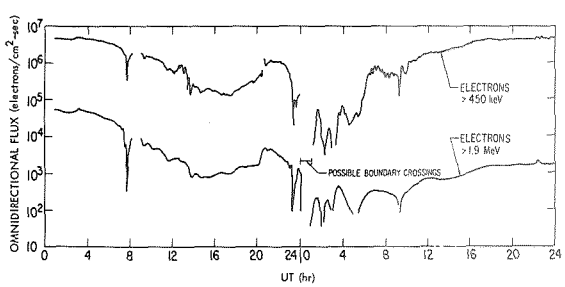


Figure 8—Omnidirectional electron fluxes above two integral thresholds during the magnetic storm of January 13 and 14, 1967. Possible crossings of the boundary of the magnetosphere occurred between 0008 and 0105 on January 14, 1967.

## Data Reduction

It is clear from a consideration of the few samples of data discussed above, that enormous variations in electron fluxes are typical of the synchronous orbit. In order to prepare a representative picture of the energetic electron environment at the synchronous altitude, it was necessary to reduce a great body of data and present the results in a simple parametric format.

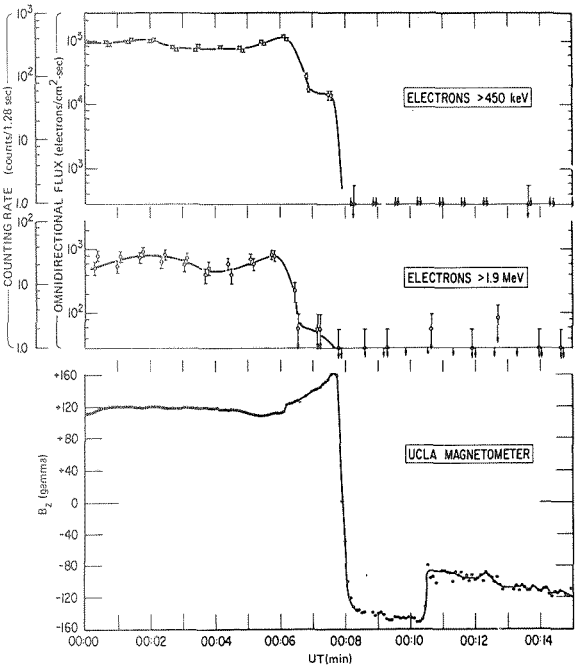


Figure 9—Details of the rapid electron-flux changes above two thresholds together with field components from the UCLA magnetometer data for 0000 UT to 0010 UT on January 14, 1967. The $H(z)$ component of the magnetometer data is shown.

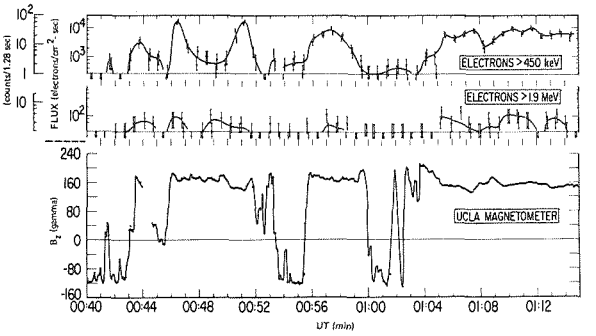


Figure 10—Details of the rapid electron-flux changes above two thresholds together with field components from the UCLA magnetometer data for 0040 UT to 0115 UT on January 14, 1967. The $H(z)$ component of the magnetometer data is shown.

The data were reduced by computer and presented as plots of flux versus universal time for a given day. The averages of the flux for each hour centered on the (UT) hour were also computed and ordered versus day number. An example of such a plot of hourly flux averages versus day number is given in Figure 11. This figure very clearly displays the large temporal flux variations and suggests that a model environment is best cast as a probabilistic model. These hourly averages are the basis of the average energetic-electron environment presented in this report. Averaging tends to mask the short-term fluctuations in electron fluxes that are often observed, especially during magnetically disturbed periods. But since we are concerned with a long-term semiprobabilistic interpretation of this data, the treatment of data on an hourly average basis does considerably simplify data reduction.

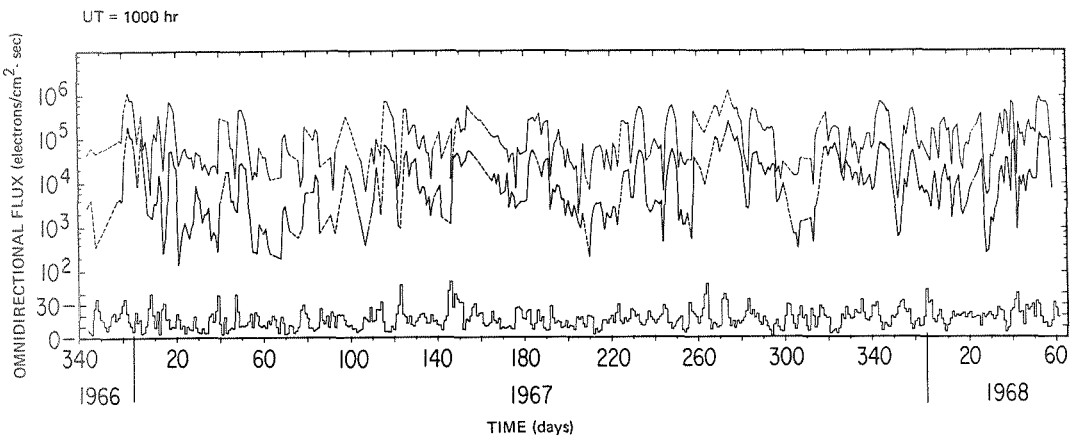


Figure 11—Plot of hourly averages of omnidirectional electron (upper trace >1.05 MeV, and lower trace >1.9 MeV) for time span considered in this report. Local time of all data is midnight. Daily sum of $K_p$ is plotted at the bottom of the figure.

Data were then ordered in local time and in terms of magnetic activity, as indicated by the $K_p$ index. Daily sums of $K_p > 24$ were considered indicative of magnetic disturbance. The threshold of $\Sigma K_p > 24$ was chosen because inspection of a large subset of the data revealed that at about this level of magnetic disturbance the diurnal variation in the electron flux levels was not visible above the large temporal variations. The data were analyzed in a manner first employed by Vette and Lucero (1967). We calculated from the experimental data the probability $P(F > F_x)$ of observing a flux greater than $F_x$ for an integral energy threshold $F_j$ (Figure 12). A more complete set of $P(F > F_x)$ compilations can be found in Paulikas et al. (1969). The mean of the logarithm of the flux ($\mu$) and the standard deviation ($\sigma$) are calculated and the $P(F > F_x)$ data are fitted, assuming a gaussian distribution with parameters $\mu$ and $\sigma$. The relevant formulas are

$$P(F > F_x) = \frac{\text{number of data points with } F > F_x}{\text{total points in sample}},$$

$$\mu = \frac{1}{n}\sum_i \log_{10} F_i = \frac{1}{n}\sum_i Z_i,$$

$$\sigma^2 = \frac{1}{n-1}\sum_i (\log_{10} F_i - \mu)^2,$$

$$P(F > F_x) = \int_{F_x}^{\infty} \frac{1}{\sqrt{2\pi\sigma^2}} \exp\left[-\frac{(Z-\mu)^2}{2\sigma^2}\right] dZ,$$

and

$$P(F) = \frac{1}{\sqrt{2\pi\sigma^2}} \exp\left[-\frac{(Z-\mu)^2}{2\sigma^2}\right].$$

The fits to the data are quite satisfactory (Figure 13), so that it is possible to characterize the electron flux distribution by the parameters $\mu$ and $\sigma$, which are, of course, functions of local time, electron energy, magnetic activity, and so forth.

## Local Time Variation of Electron Fluxes

The data shown in Figures 12 and 13 summarize all the data available. We have separately computed $\mu$ and $\sigma$ for each local time. Figures 14 through 21 present plots of $\mu$ and $\sigma$ as functions of local time. Figure 22 summarizes the data and explicitly displays the larger diurnal variation for the more energetic electrons (Paulikas et al., 1968). The figures in this section clearly show that the maxima and minima in the electron flux do not occur precisely at local noon and local midnight, respectively. At the

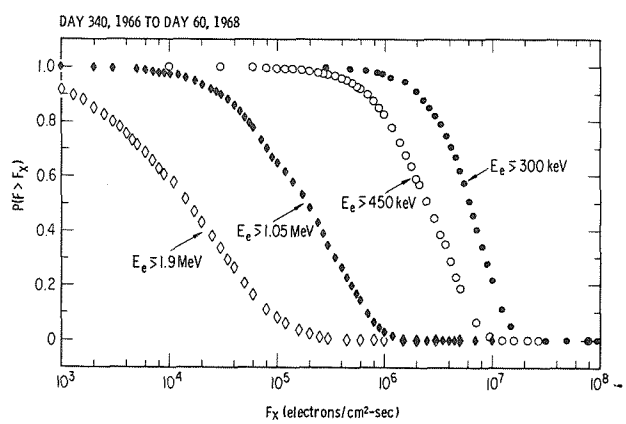


Figure 12—Plot of $P(F > F_x)$ (the probability of observing an omnidirectional flux $F$ greater than $F_x$) versus $F_x$ for four integral energy thresholds.

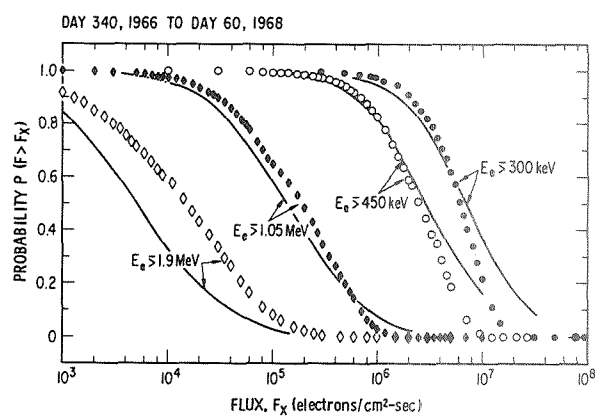


Figure 13—Fits to data presented in Figure 12. A fit has been made to the integral probability $P(F > F_x)$; in addition, the probability density $P(F)$ has also been plotted.

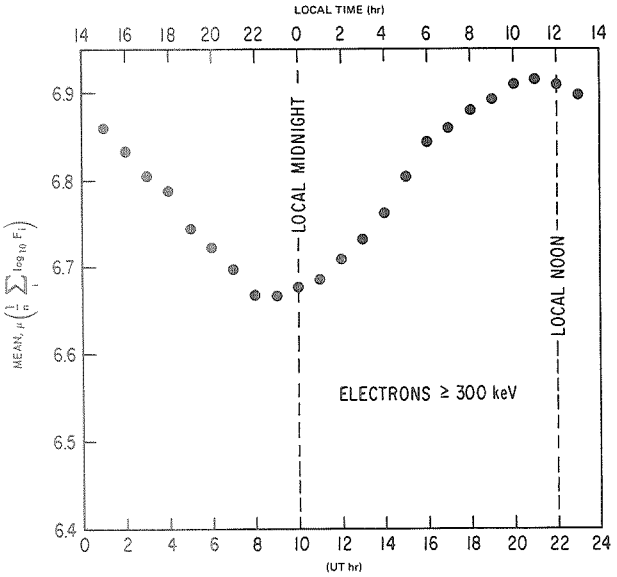


Figure 14—Mean of the logarithm of the flux for electrons, >300 keV, versus time. Data covers Day 340, 1966 through Day 60, 1968.

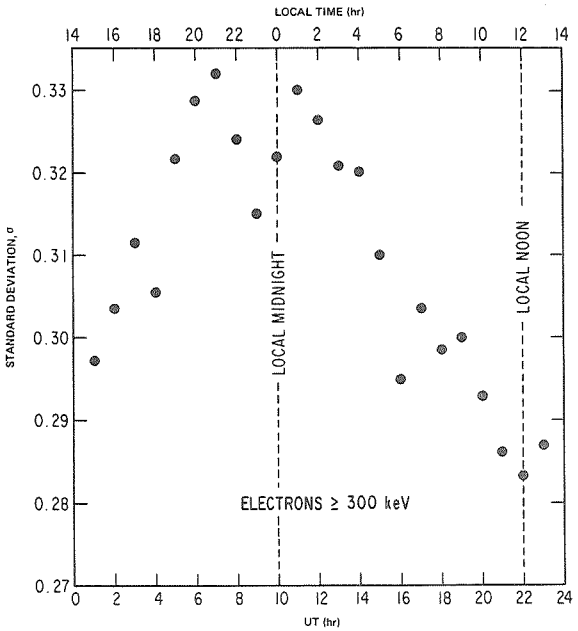


Figure 15—Standard deviation ($\sigma$) of logarithm of electron flux for electrons, >300 keV, versus time. Data covers Day 340, 1966 through Day 60, 1968.

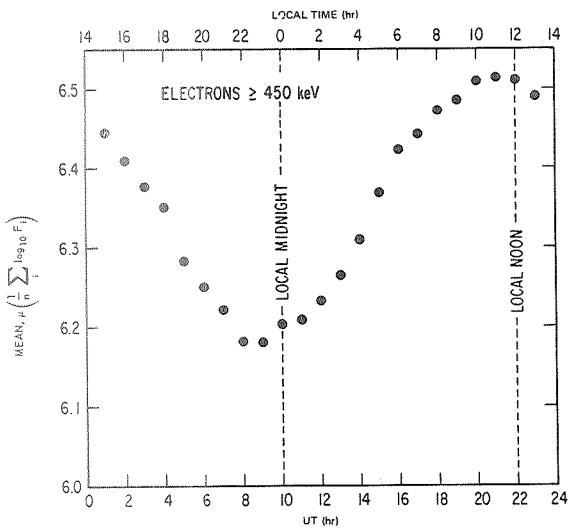


Figure 16—Mean of the logarithm of the flux for electrons, >450 keV, versus time. Data covers Day 340, 1966 through Day 60, 1968.

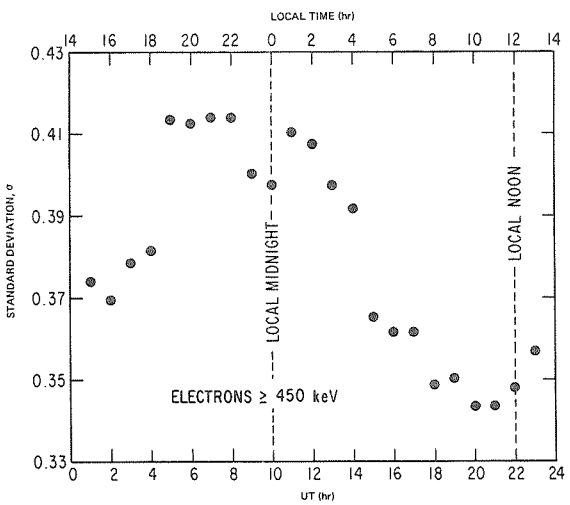


Figure 17—Standard deviation ($\sigma$) of logarithm of electron flux for electrons, >450 keV, versus time. Data covers Day 340, 1966 through Day 60, 1968.

synchronous orbit the magnetosphere is no longer symmetric about the sun-earth line, but displays about a 15° twist in the westward direction. The cause of this twist may be the draping of the interplanetary field (arriving at 1 AU at an angle of 45° to 55° with respect to the sun-earth line) over the magnetopause (Walters, 1964) or an effect internal to the magnetosphere caused by partial ring currents (Frank, private communication). Note also that $\sigma$ reaches a maximum near local midnight reflecting the greater variability of the electron fluxes on higher field lines.

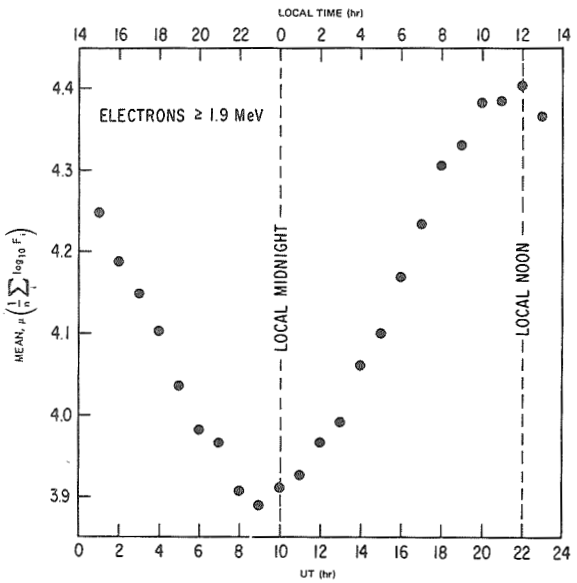


Figure 18—Mean of the logarithm of the flux for electrons, >1050 keV, versus time. Data covers Day 340, 1966 through Day 60, 1968.

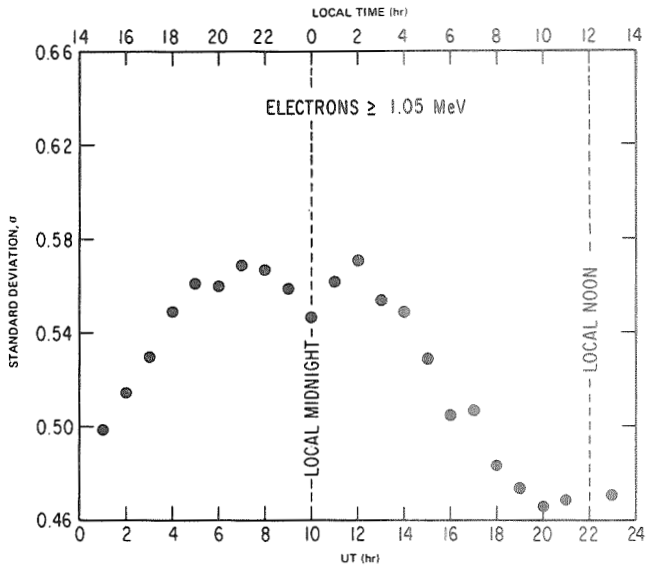


Figure 19—Standard deviation ($\sigma$) of logarithm of electron flux for electrons, >1050 keV, versus time. Data covers Day 340, 1966 through Day 60, 1968.

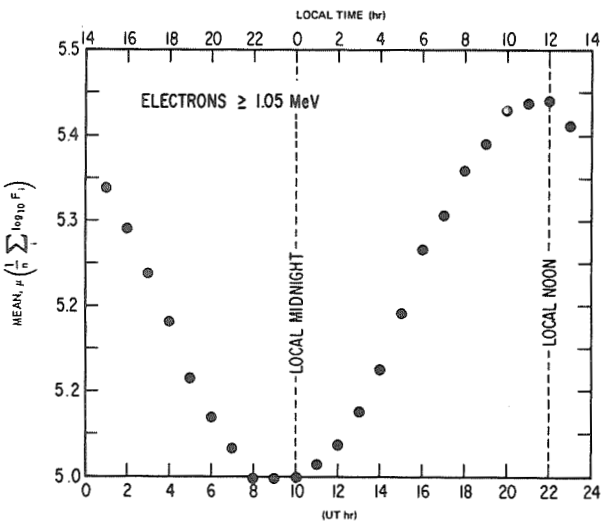


Figure 20—Mean of the logarithm of the flux for electrons, >1900 keV, versus time. Data covers Day 340, 1966 through Day 60, 1968.

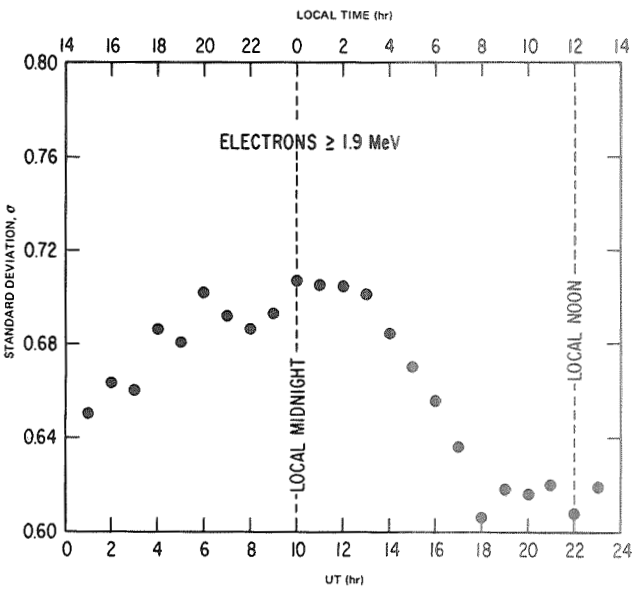


Figure 21—Standard deviation ($\sigma$) of logarithm of electron flux for electrons, >1900 keV, versus time. Data covers Day 340, 1966 through Day 60, 1968.

All data obtained by ATS 1 in the time interval of December 1966 to March 1968 are summarized in Figure 23 in the usual presentation of $P(F > F_x)$ versus $F_x$. The curves in the figure are the result of the synchronous environment compilation (AE3) of Vette and Lucero (1967). The agreement is quite satisfactory, considering the uncertainties in the absolute geometric factors of the different instruments. Table 2 summarizes the means and standard deviations for the AE3 model and the ATS 1 data.

There does not appear to be a truly major difference between the AE3 compilation (characteristic of near solar-minimum condition) and the ATS 1 data obtained primarily during 1967 (during the increasing phase of solar activity).

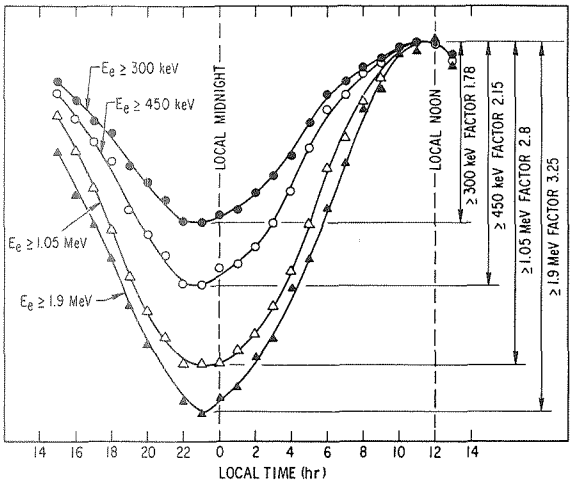


Figure 22—Summary of diurnal variation of mean of logarithm of flux for electrons. Data are normalized to 1100 local time.

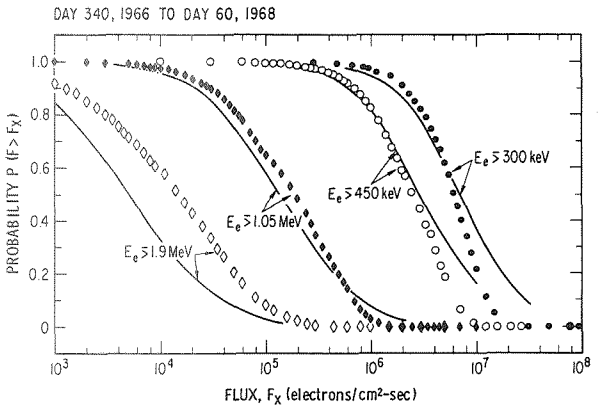


Figure 23—Comparison of ATS 1 data compilation (symbols) with Vette-Lucero AE3 model (solid lines). AE3 data for electrons, >1.9 MeV, is modified from information published in Vette and Lucero (1967), per private communication from Dr. Vette.

Table 2
ATS 1, AE3 Comparison.

| Minimum energy | Mean (log flux) | | Sigma (log flux) | |
|---|---|---|---|---|
| | AE3 | ATS 1 | AE3 | ATS 1 |
| $E_e \geq 300$ keV | 6.84 | 6.795 | 0.49 | 0.319 |
| $E_e \geq 450$ keV | 6.47 | 6.358 | 0.53 | 0.396 |
| $E_e \geq 1.05$ MeV | 5.12 | 5.204 | 0.615 | 0.549 |
| $E_e \geq 1.9$ MeV | 3.71 | 4.138 | 0.71 | 0.680 |

## Correlation of Trapped Electron Fluxes with Sector Structure of Interplanetary Magnetic Field

We have also ordered the data (for a given local time) in terms of solar rotations, attempting to correlate changes in the trapped particle population with changes in the sector structure of the interplanetary field. Such a correlation was demonstrated for lower $L$-values using data from the low-altitude near-polar satellite 1963 38C (Williams, 1966) and was also presented by Vette and Lucero (1967). No such correlation is obvious in our data when we compare the trapped electron fluxes with the sector structure as reported by Wilcox and Colburn (1969). There are several reasons for such a lack of correlation.

The rapid succession of storms during the time period of high solar-activity affects the particle population drastically through generation of new particles and loss of old particles on a time scale (days) that masks the long-term (about 7-day) variation which might be expected from the effects of changing interplanetary field orientation. The evolving nature of the sector structure during the time period under consideration also helps to obscure any recurrence tendencies in the electron fluxes.

While the field geometry of low-lying ($L \approx 4$) drift shells is relatively stable, we have seen earlier that storms may totally alter the magnetic field from its dipolelike configuration, especially on the nightside quadrant. Thus, the field geometry is not constant.

## Effect of Substorms

The compilation of electron data presented in Figure 23 represents a group of particle fluxes which change in a correlated fashion; that is, an increase in the >300-keV flux is accompanied by an increase in the >1.9-MeV electron flux. For electron energies below about 150 keV such correlation need no longer obtain and flux changes of low-energy electrons may be anticorrelated with flux changes occurring among relativistic electron groups.

An important effect at the synchronous orbit is the injection of 50 to 150 keV electrons into this region by magnetic substorms. The Minnesota group has presented a great body of results dealing with the effects of substorms on the electron population at the synchronous orbit (Parks et al., 1968; Arnoldy and Chan, 1964; Pfitzer and Winckler, 1969; and Parks and Winckler, 1968). The magnetospheric substorm is most often interpreted in terms of an instability which developed in the sector of dusk to midnight in the magnetosphere with a time scale of several hours. A general extension of the field in the anti-solar direction is

observed, and concurrently a loss of trapping, that is, the particle population decreases during a substorm. Recovery consists of a rapid relaxation of the magnetic field to its quiet-day configuration, with a concurrent recovery in the trapped particle fluxes.

At this time a rapid increase of the 50- to 150-keV electron flux occurs and can be interpreted as injection of particles from the magnetotail. This pulse of new electrons is observed to propagate in longitude (Pfitzer and Winckler, 1969) in a manner analogous to the drift periodic echoes observed for relativistic electrons.

During such injection of 50- to 150-keV electrons associated with a substorm, the relativistic electron fluxes do not increase and may even decrease. Considering the spectrum in Figure 24, one might recognize this effect as a rocking of the spectrum about a fulcrum at about 200 keV. The behavior of low-energy electrons thus differs in a fundamental way from that of the relativistic electrons. It has been suggested that the substorm injections of electrons are sufficiently frequent and powerful to provide the source from which the relativistic electron fluxes may be generated (Arnoldy and Chan, 1969).

A complete description of the electron environment will thus also involve a correlation between low-energy and relativistic electron fluxes, that is, a probabilistic analysis of the electron spectrum.

## PENETRATION OF SOLAR PROTONS TO SYNCHRONOUS ALTITUDE

One of the surprises contained in the initial ATS 1 observations was the fact that low-energy solar protons penetrated to the synchronous altitude. Cursory analysis of data obtained during the solar-proton event which began on January 28, 1967 showed that protons with energies greater than about 20 MeV had essentially free access to synchronous altitude at all local times. More detailed analysis has confirmed this result and has also shown that during disturbed times solar protons down to less than 1 MeV in energy can reach synchronous altitude without attenuation (Lanzerotti, 1968 and 1969 and Paulikas and Blake, 1969).

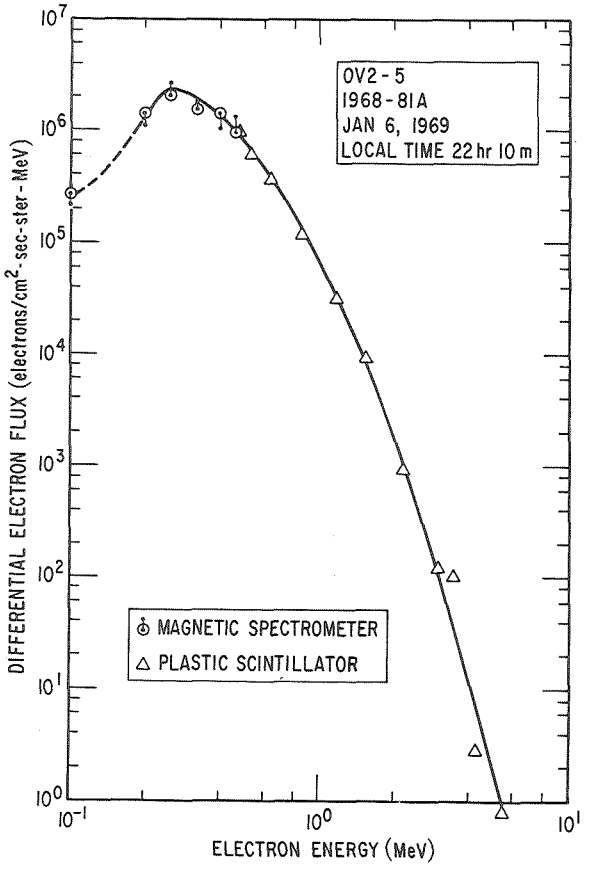


Figure 24—Spectrum of electrons at synchronous altitude obtained aboard OV2 5 (J. R. Stevens and A. L. Vampola, private communication). Substorms primarily affect particle fluxes with energies below 200 keV.

Measurements of the transmission efficiency are most directly and unambiguously performed by comparing the flux outside the magnetosphere with measurements of the synchronous orbit. Because a synchronous satellite by definition covers all local times within one 24-hour period, the transmission efficiency as a function of local time is easily computed. Solar longitude gradients in the solar-particle fluxes are assumed not to be important if comparisons are made with satellites which are outside the earth's magnetosphere but still in earth orbit. A series of results which demonstrate the access of solar protons to the synchronous orbit is presented in Figures 25 through 28.

The phenomena of access of solar protons to the synchronous altitude increases in complexity as one examines successively lower energy particles. The problem is being actively pursued by several groups at this time, but it seems useful to summarize the current (fall 1969) state of knowledge for the purpose of this report.

Protons with energies $\gtrsim$20 MeV reach synchronous altitude without significant attenuation when compared with fluxes above the same threshold outside the magnetosphere. Thus, observation of protons at this energy, carried out at the synchronous altitude are equivalent to measurements of the interplanetary flux and it is possible to derive such results as source spectra, source strengths, and interplanetary diffusion coefficients from these data. This result adds energetic solar-proton monitoring to the already numerous useful tasks which can be performed by satellites at the synchronous orbit.

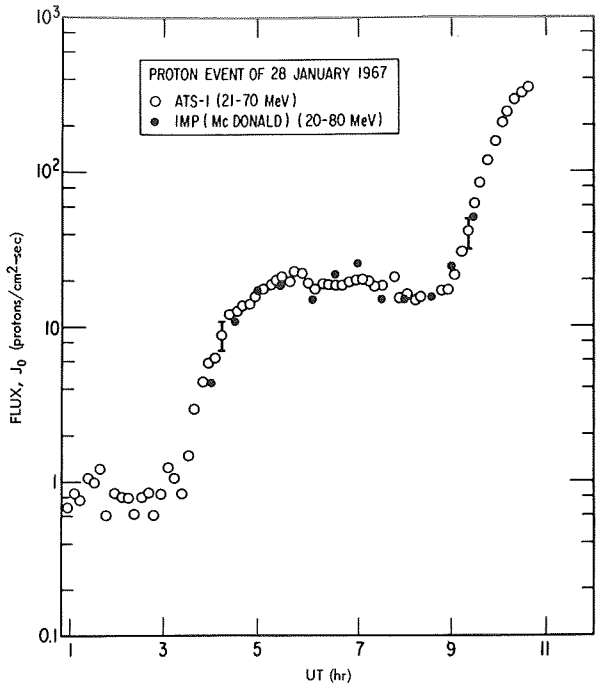


Figure 25—Comparison of ATS 1 and IMP 3 data obtained during initial phase of January 28, 1967 solar proton event. IMP 3 directional fluxes have been converted to omnidirectional fluxes assuming isotropy. The assumption of isotropy is reasonable since the source region of particles was on back side of the sun.

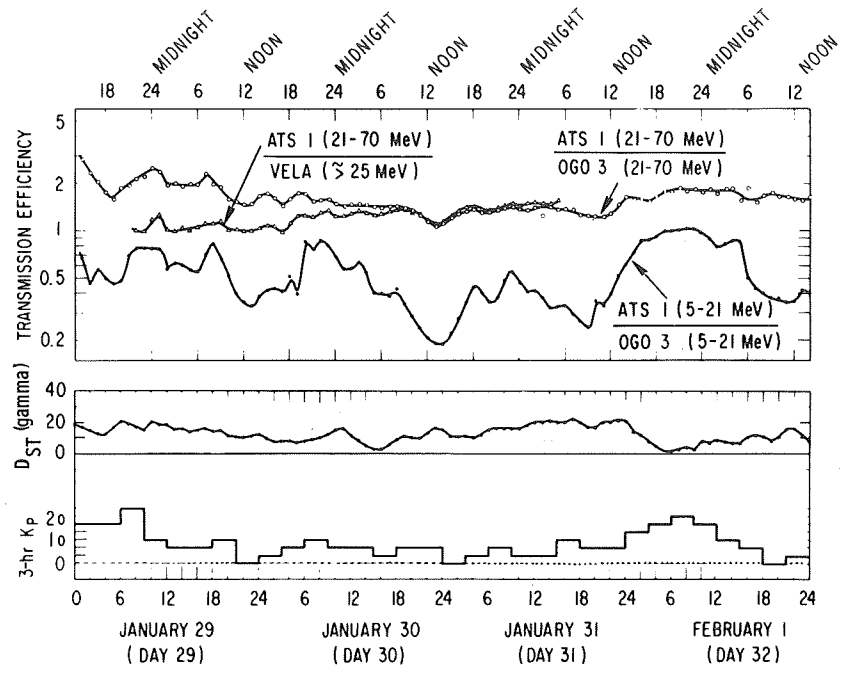


Figure 26—Transmission coefficient for 5- to 21-MeV and 21- to 70-MeV protons for January 29 through February 1, 1967. Uncertainties in geometric factors are the main source of error in computations of transmission efficiencies and amount to ±30% for the 5- to 21-MeV channel and ±50% for the 21- to 70-MeV channel. Also shown are the 3-hour $K_p$ indices and hourly DST values (M. Sugiura and S. Cain, private communication).

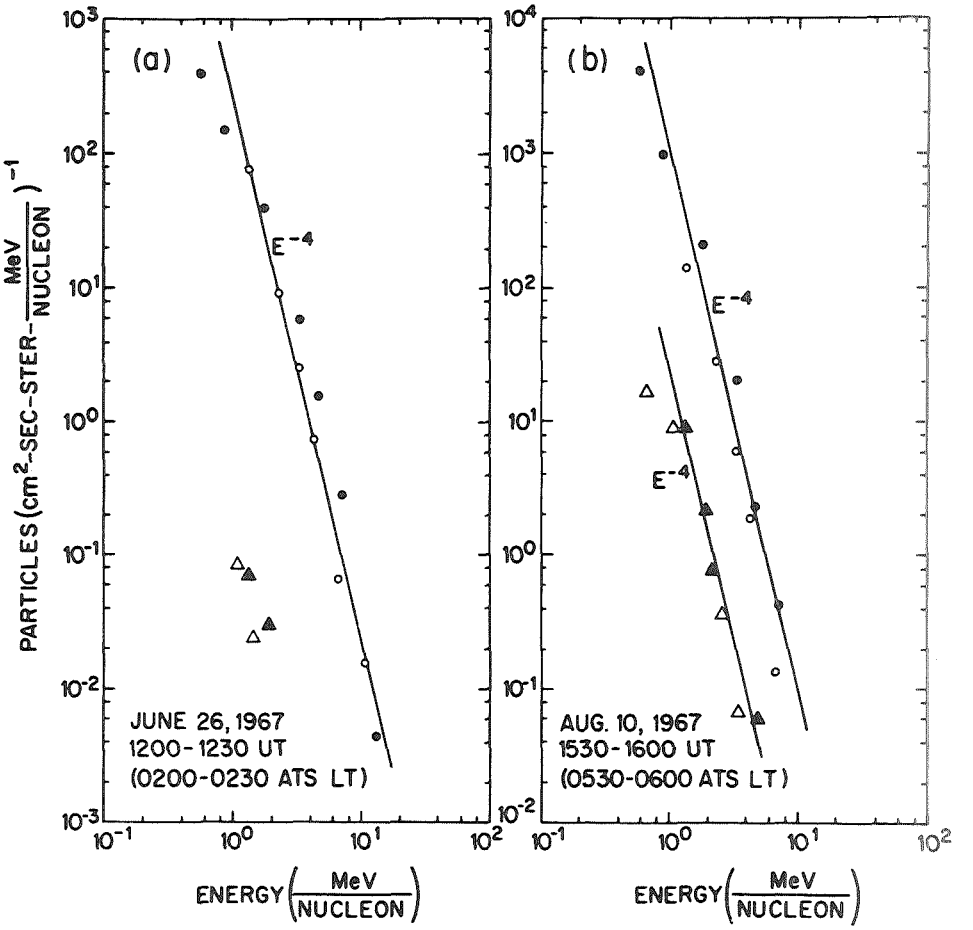


Figure 27—Comparison of low-energy solar protons (dots) and alphas (triangles) measured inside the magnetosphere aboard ATS 1 (open symbols) and aboard Explorer 34 outside the magnetosphere (solid symbols) by the BTL experimenters (Lanzerotti, 1968).

Protons with energies below about 20 MeV are affected by the magnetosphere. This interaction manifests itself as a diurnal variation in the solar-proton flux caused by the asymmetric nature of the magnetosphere. The solar-proton diurnal variation is inverted with respect to the trapped electron variation. More solar protons are observed near local midnight than near local noon. During magnetic quiet and near local noon, the flux at the synchronous altitude of 5- to 21-MeV protons is decreased by a factor of five to ten with respect to interplanetary levels. However, at night or during disturbed times the attenuation is less than a factor of two. Direct and indirect evidence indicates that solar protons below about 20 MeV are temporarily trapped in the geomagnetic field. The trapping lifetime is of the order of half an hour or less. Because the particles are trapped, they may be locally accelerated by changes in the geomagnetic field, and the flux (in a given energy interval) may temporarily increase to exceed the interplanetary flux (Figure 29).

Protons of a few MeV energy are still able to reach the synchronous altitude. The ease of access appears to depend in a complicated way upon particle energy and the state of agitation of the magnetosphere. Occasionally, significant temporal delays (hours) are observed between arrival of solar particles in interplanetary space near the earth and arrival of those particles at the synchronous altitude (Lanzerotti, 1969a).

The behavior of various energy groups of solar protons during the event of January 28, 1967 is illustrated in Figure 30. Note that diurnal variation is most pronounced for particles of intermediate energy; the diurnal variation is absent for protons $E_p > 20$ MeV and also for protons with $E_p \leqslant 3$ MeV.

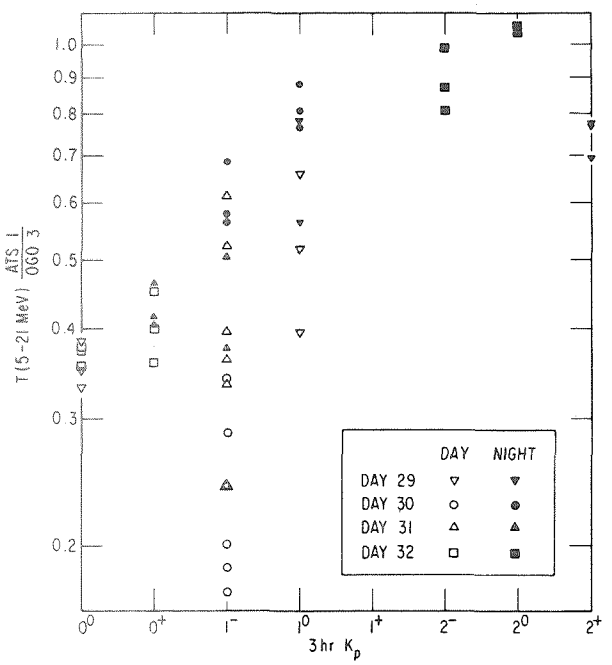


Figure 28—Transmission coefficient for 5- to 21-MeV protons as a function of 3-hour $K_p$. Data in the 0900 to 1500 local time quadrant (day) and the 2100 to 0300 local time quadrant (night) are separately identified.

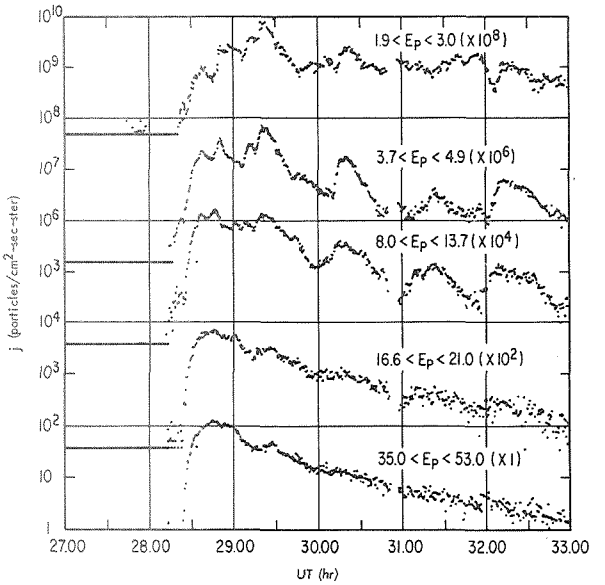


Figure 30—Behavior of solar proton fluxes in five energy intervals at the synchronous altitude. Data were obtained by the BTL experiment aboard ATS 1 during the solar proton event of January 28, 1967. Factor in parentheses is scale factor appropriate for each plot (Roberts et al., 1968).

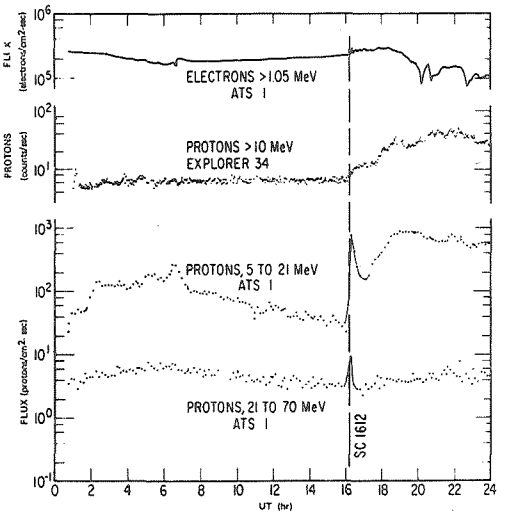


Figure 29—Effect of sudden commencement on solar proton fluxes. Solar proton flux on July 13, 1968 (Day 195). Shown are the ATS 1 proton flux 10-minute averages in two energy intervals (5- to 21-MeV and 21- to 70-MeV) and the Explorer 34 (>10 MeV) counting rate. (Explorer 34 was outside the magnetosphere.) Also shown (as an indicator of the state of the magnetic field fluctuations) is the trapped flux of electrons >1.05 MeV. The proton flux enhancement following the sudden commencement is followed by a flux increase associated with energetic storm particles (Paulikas and Blake, 1969).

It is important to note that orbit tracing in realistic, but static, models of the magnetosphere does not predict the observed situation regarding solar-proton access to the synchronous altitude (Lanzerotti, 1969a and Paulikas and Blake, 1969). Only by making extreme assumptions regarding the distance to the magnetopause or the strength of the tail field in, for example, a Williams-Mead model can protons of about 10 MeV mirroring near the equator reach 6.6 $R_e$ according to such calculations. It is necessary to invoke a diffusion mechanism, as yet unspecified, which transports particles radially deeper into the magnetosphere than predicted by orbit tracing alone. Direct diffusion into the flanks of the magnetosphere has been proposed by Lanzerotti (1968). An alternative mode of rapid access can be visualized by noting that (Figure 1) the quasi-trapped regions on the night side, at somewhat larger geocentric distances than the synchronous orbit, are accessible from the flanks of the magnetosphere by drift alone. If pitch-angle scattering of the particles is added, radial diffusion will occur because of the dependence of drift path on pitch angle.

Solar-proton observations aboard ATS 1 during 1967 are summarized in Figure 31. The data have been ordered in terms of solar rotations. Note that solar proton fluxes above background are present a significant fraction of the time; however, the major contributions to the integrated flux for 1967 were made by the events of January 28 and May 23.

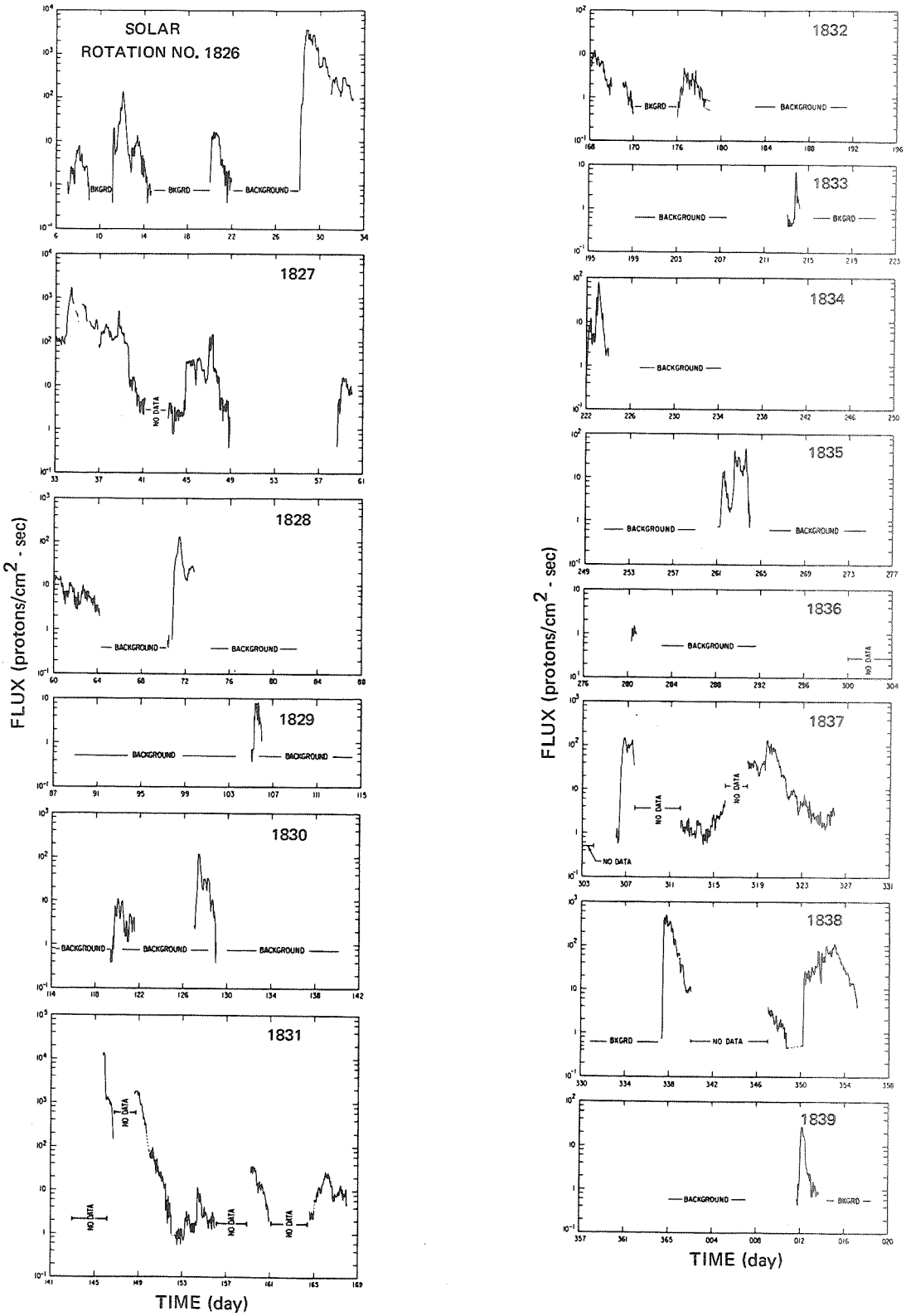


Figure 31—Compilation of (5- to 21-MeV) solar proton fluxes observed aboard ATS 1 during 1967. Data are ordered in terms of solar rotations (Paulikas and Blake, 1968).

## SUMMARY

This paper has presented a state-of-knowledge report on the trapped energetic electrons and energetic solar-protons observed at the synchronous altitude. Important progress has been made in understanding the behavior of the particle population at this altitude, although large gaps still exist in our knowledge. The increase in knowledge has been exceptionally rapid because of the availability of a large volume of high-quality (nearly continuous) data from ATS 1 and other satellites. An important ingredient in this progress is the relative ease of data analysis for experiments operating at the synchronous altitude.

There exists still only fragmentary data regarding pitch-angle distributions of energetic particles. Interesting new results can be expected from analysis of pitch-angle data.

Some progress is also being made in quantitative understanding of the particle-field interactions which operate in this region of the magnetosphere. It is this kind of work that promises to unravel the fundamental processes in the radiation belt and build a sound theoretical basis for the phenomena presented in this report.

## ACKNOWLEDGMENTS

This report owes much to the ATS 1 experimenters who shared with us their ideas, speculations, preliminary data, and results. We are particularly grateful to Dr. P. Coleman (UCLA) for magnetometer data and Dr. L. Lanzerotti (Bell Telephone Laboratories) for many stimulating discussions.

We were assisted in various phases of ATS 1 instrument construction and calibration by Mr. S. Imamoto and Mr. S. Solow. The massive job of data reduction was performed by Miss J. Palmer, Mr. D. Griffin, and Mr. J. Pauley. Dr. S. C. Freden, now at NASA in Houston, participated in the early phases of this work.

This research was supported under USAF Space and Missile Organization Contract F04701-69-C-0066; the integration of the experiment into ATS 1 as well as the operations, data acquisitions, and initial data reduction was supported by NASA. We are grateful to both organizations for their continued support.

### REFERENCES

Arnoldy, R. L., and Chan, K. W., "Particle Substorms Observed at the Geostationary Orbit," *J. Geophys. Res.* 74: 5019, 1969.

Brewer, H. R., Schulz, M., and Eviatar, A., "Origin of Drift-Periodic Echoes in Outer Zone Electron Flux," *J. Geophys. Res.* 74: 159, 1969.

Coleman, P. J., "Final Report for the ATS-1 Magnetometer," Publication No. 725, Institute of Geophysics and Planetary Physics, UCLA, 1968.

Frank, L. A., "On the Distribution of Low Energy Protons and Electrons in the Earth's Magnetosphere," *Earth's Particles and Fields*, ed. by B. M. McCormac, New York: Reinhold Publishing Corp., 1968.

Freeman, J. W., "Observation of Flow at Low-Energy Ions at Synchronous Altitudes and Implications for Magnetospheric Convection," *J. Geophys. Res.* 73: 4151, 1968.

Freeman, J. W., and Maquire, J. J., "Gross Local-Time Particle Asymmetries at the Synchronous Orbit Altitude," *J. Geophys. Res.* 72: 5257, 1967.

King, J. H., "Models of the Trapped Radiation Environment. Vol. IV: Low Energy Protons," NASA SP-3024, 1967.

Lanzerotti, L. J., "Penetration of Solar Protons and Alphas to the Geomagnetic Equator," *Phys. Rev. Lett.* 21: 929, 1968.

Lanzerotti, L. J., "Solar Proton Radiation Damage of Solar Cells at Synchronous Altitudes," *J. Spacecr. Rockets* 6: 1086, 1969b.

Lanzerotti, L. J., "Access of Solar Particles to Synchronous Altitudes," Paper presented at Third ESLAB/ESRIN Symposium, Noordwijk, Holland, September 1969. To be published in *Proceedings of the Third ESLAB/ESRIN Symposium—Intercorrelated Satellite Observations Related to Solar Events*, Dordrecht, Holland: D. Reidel Publishing Co., 1970.

Lanzerotti, L. J., Roberts, C. S., and Brown, W. L., "Temporal Variations in the Electron Flux at Synchronous Altitudes," *J. Geophys. Res.* 72: 5893, 1967.

Opp, A. G., "Penetration of Magnetopause Beyond 6.6 $R_e$ During the Magnetic Storm of January 13–14, 1967": Introduction, *J. Geophys. Res.* 73: 5697–5755, 1968.

Parks, G. K., Arnoldy, R. L., Lezniak, T. W., and Winckler, J. R., "Correlated Effects of Energetic Electrons at the 6.6 $R_e$ Equator and the Auroral Zone During Magnetospheric Substorms," *Radio Sci.* 3: 715, 1968.

Parks, G. K., and Winckler, J. R., "Acceleration of Energetic Electrons Observed at the Synchronous Altitude During Magnetic Substorms," *J. Geophys. Res.* 73: 5786, 1968.

Paulikas, G. A., and Blake, J. B., *Solar Proton Observations at Synchronous Altitude During 1967*, Aerospace Corporation Report TR-0200(4260-20)-2, September 1968.

Paulikas, G. A., and Blake, J. B., "Penetration of Solar Protons to Synchronous Altitude," *J. Geophys. Res.* 74: 2161, 1969.

Paulikas, G. A., and Blake, J. B., "Effects of Sudden Commencement on Solar Protons at the Synchronous Orbit," *J. Geophys. Res.* 75: 734, 1970.

Paulikas, G. A., Blake, J. B., Freden, S. C., and Imamoto, S. S., "Observations of Energetic Electrons at Synchronous Altitude. 1. General Features and Diurnal Variations," *J. Geophys. Res.* 73: 4915–4925, 1968.

Paulikas, G. A., Blake, J. B., and Palmer, J. A., "Energetic Electrons at the Synchronous Altitude: A Compilation of Data," Aerospace Corporation Report TR-0200(4260-20)-5, October 1969.

Pfitzer, K. A., and Winckler, J. R., "Intensity Correlation and Substorm Electron Drift Effects in the Outer Radiation Belt Measured With the OGO3 and ATS-1 Satellites," *J. Geophys. Res.* 74: 5005, 1969.

Roberts, C. S., Brown, W. L., Lanzerotti, L. J., and Gleckner, E. J., "Synchronous Altitude Observation of Energetic Proton During the Solar Proton Event of January 28, 1967," *Trans. Amer. Geophys. Union* 42: 275, 1968.

Roederer, J. G., "On the Adiabatic Motion of Energetic Particles in a Model Magnetosphere," *J. Geophys. Res.* 72: 981–992, 1967.

Roederer, J. G., "Shell Splitting and Radial Diffusion of Geomagnetically Trapped Particles," *Earth's Particles and Fields*, ed. by B. M. McCormac, New York: Reinhold Publishing Corp., 1968.

Roederer, J. G., "Quantitative Models of the Magnetosphere," *Rev. Geophys.* 7: 77, 1969.

Roederer, J. G., Cummings, W. D., Coleman, P. J., and Robbins, M. F., "Determination of Magnetosphere Parameters From Magnetic Field Measurements at Synchronous Altitudes," *Trans. Amer. Geophys. Union* 49: 227, 1968.

Vette, J. I., and Lucero, A. B., "Models of the Trapped Radiation Environment. Vol. III: Electrons at Synchronous Altitude," NASA SP-3024, 1967.

Walters, G. K., "Effect of Oblique Interplanetary Magnetic Field on Shape and Behavior of Magnetosphere," *J. Geophys. Res.* 69: 1769, 1964.

White, R. S., Wilson, J., Martina, F., and Stevens, J. R., "Proton Energy Distributions From 0.060 to 3.45 MeV at 6.6 Earth Radii," Paper presented at IAGA General Assembly, Madrid, Spain, September 1969.

Wilcox, J. M., and Colburn, D. S., "Interplanetary Sector Structure in the Rising Portion of the Sunspot Cycle," *J. Geophys. Res.* 74: 2388, 1969.

Williams, D. J., "A 27-Day Periodicity in Outer Zone Trapped Electron Intensities," *J. Geophys. Res.* 71: 1815, 1966.

Williams, D. J., and Mead, G. D., "Nightside Magnetosphere Configuration as Obtained From Trapped Electrons at 1100 Kilometers," *J. Geophys. Res.* 70: 3017, 1965.

04U 001 54 51 3DS 71147 00903
AIR FORCE WEAPONS LABORATORY /WLOL/
KIRTLAND AFB, NEW MEXICO 87117

ATT E. LOU BOWMAN, CHIEF,TECH. LIBRARY



*"The aeronautical and space activities of the United States shall be conducted so as to contribute . . . to the expansion of human knowledge of phenomena in the atmosphere and space. The Administration shall provide for the widest practicable and appropriate dissemination of information concerning its activities and the results thereof."*

—NATIONAL AERONAUTICS AND SPACE ACT OF 1958

# NASA SCIENTIFIC AND TECHNICAL PUBLICATIONS

TECHNICAL REPORTS: Scientific and technical information considered important, complete, and a lasting contribution to existing knowledge.

TECHNICAL NOTES: Information less broad in scope but nevertheless of importance as a contribution to existing knowledge.

TECHNICAL MEMORANDUMS: Information receiving limited distribution because of preliminary data, security classification, or other reasons.

CONTRACTOR REPORTS: Scientific and technical information generated under a NASA contract or grant and considered an important contribution to existing knowledge.

TECHNICAL TRANSLATIONS: Information published in a foreign language considered to merit NASA distribution in English.

SPECIAL PUBLICATIONS: Information derived from or of value to NASA activities. Publications include conference proceedings, monographs, data compilations, handbooks, sourcebooks, and special bibliographies.

TECHNOLOGY UTILIZATION PUBLICATIONS: Information on technology used by NASA that may be of particular interest in commercial and other non-aerospace applications. Publications include Tech Briefs, Technology Utilization Reports and Technology Surveys.

*Details on the availability of these publications may be obtained from:*

**SCIENTIFIC AND TECHNICAL INFORMATION OFFICE**

**NATIONAL AERONAUTICS AND SPACE ADMINISTRATION**

**Washington, D.C. 20546**